OPTICAL INVESTIGATION OF THE ENERGY LEVELS OF MANGANESE IN ZINC SELENIDE, ZINC SULPHIDE, AND ZINC SELENO-SULPHIDE

Thomas Coutts Leslie

A Thesis Submitted for the Degree of PhD
at the
University of St Andrews

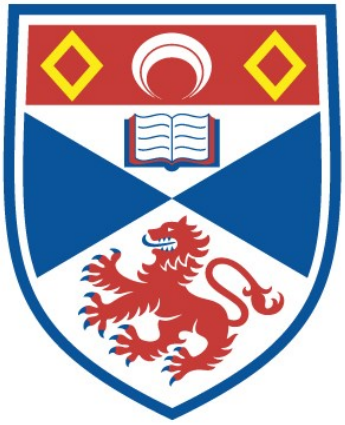

1980

OPTICAL INVESTIGATION OF THE ENERGY LEVELS OF MANGANESE IN ZINC SELENIDE, ZINC SULPHIDE, AND ZINC SELENO-SULPHIDE

A Thesis

presented by

Thomas Leslie

to the

University of St Andrews

in application for the Degree

of Doctor of Philosophy

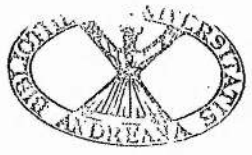

DECLARATION

I hereby certify that this thesis has been composed by me, and is a record of work done by me, and has not previously been presented for a higher degree.

The research was carried out in the Wolfson Institute of Luminescence, within the School of Physical Sciences in the University of St Andrews, under the supervision of Mr J.W. Allen.

T.C. Leslie

CERTIFICATE

I certify that Thomas Leslie has spent nine terms at research work in the Wolfson Institute of Luminescence within the School of Physical Sciences in the University of St Andrews under my direction, that he has fulfilled the conditions of the Resolution of the University Court, 1967, No. 1, and that he is qualified to submit the accompanying thesis in application for the Degree of Doctor of Philosophy.

J.W. Allen
Research Supervisor

CAREER

I first matriculated in the University of St Andrews in October 1971. In 1974 I obtained the James Brodie prize in physics and in 1975 I graduated with First Class Honours.

In October 1975 I was enrolled as a research student under Resolution of the University Court, 1967, No. 1 as a candidate for the Degree of Doctor of Philosophy.

ACKNOWLEDGEMENTS

I wish to thank the Science Research Council for the grant enabling me to undertake this project.

I would also like to thank Mr M D Ryall and Dr J M Noras for general help and advice, and Dr E J Lisher for assistance with computing.

Most of all, I wish to convey my gratitude to my supervisor, Mr J W Allen, for his guidance throughout this project.

CONTENTS

CHAPTER 1

Introduction

This thesis describes the results of a course of experimental research into the optical properties of manganese impurities in the II-VI host lattices ZnSe, ZnS, and $ZnSe_xS_{1-x}$.

These materials are of some commercial importance, since they exhibit electroluminescence when appropriately prepared. For this reason it is desirable to ascertain which inherent properties of the materials would determine device performance, and to try to distinguish these from apparently limiting criteria which are in fact caused by unknown and unwanted defects. Removal of such undesirable impurities may substantially benefit device performance.

These materials are also of interest in that they exhibit some of the more complex properties of solids, which can only be studied by the selection of a material which manifests the effects in question. That is, although the effects are studied in these compounds, it is to be expected that they will also occur more generally, although not perhaps as obviously.

In order to fully appreciate some of the more complex effects which are studied, it is necessary to provide a substantial theoretical background. This is the function of chapters two, three, and four in this work. Chapter two is an introduction to the fundamental problem of transition metal impurities in solids, together with an indication of the approaches which have been made, and the approximations invoked. In chapter three the general problem of electron-lattice interactions is discussed, with the aim being to offer an insight into

the Jahn-Teller and Ham effects. Chapter four deals more specifically with zero-phonon lines, the medium through which the experimental investigation of chapter six is undertaken. Also included in chapter four is an account of the thermal broadening of zero-phonon lines, including a mechanism which had hitherto received scant attention in this context.

The details of the experimental apparatus and techniques are given in chapter five, together with computational methods. Also included in this chapter is a method of determining mixed crystal composition, applicable to the $ZnSe_xS_{1-x}$ system which is much simpler than other techniques which have been employed.

Chapter six reports the results of investigations into the zero-phonon lines in ZnSe:Mn. These results are interpreted in terms of the Jahn-Teller and Ham effects, and from the type of broadening mechanism invoked to explain the temperature dependence of the lines, a more accurate assignation of the energies of states split by spin-orbit and Jahn-Teller interactions is made. The broadening mechanism invoked is of some importance, since it appears to have been largely ignored in studies on zero-phonon lines, although it is well known in those on spin-lattice relaxation.

In chapter seven, the problem of non-radiative transitions in all three materials is studied, with the emphasis being on the limitations which they inflict on possible devices. Radiationless processes are considered first of all by investigating the thermal dependence of emission intensity, and secondly by examining the effects of temperature on the lifetime of the excited state involved in the transition. It is demonstrated that the thermal quenching of

luminescence is not an inherent property of the materials used, which had previously been suggested, but is dependent on the existence of some unidentified defect.

Those chapters (i.e. six and seven) are essentially complete in themselves, including conclusions. In chapter eight, a brief, general summing-up is given, together with suggestions for some further work.

CHAPTER 2

Basic Concepts

2.1 Introduction

The incorporation of impurity atoms into a crystal can introduce localised energy levels into the energy band structure of that crystal. The existence of such localised levels can radically alter the bulk properties of the crystal, and it is for this reason that the study of impurity atoms in crystals is of such importance.

These localised energy levels may be usefully subdivided into two broad categories, namely deep levels and shallow levels. Shallow levels are those whose energy is very close to some host crystal energy band, and so may be thermally emptied of any charged particles which they contain; for example P, As, or Sb impurities in Ge or Si release electrons to the conduction band whilst B, Al, or Ga in the same host materials release holes to the valence band. In consequence, impurities with shallow levels provide charge carriers in the bulk crystal and these can dominate the bulk electrical properties. This phenomenon is best considered as the bulk crystal being perturbed by the presence of the impurity atoms.

Deep levels, on the other hand, are those whose energy is so far removed from any host energy band that they cannot be thermally emptied. Thus any charged particle on the impurity remains bound: such an impurity may have more than one available energy level within the energy gap of the host material and transitions within the impurity energy level structure become important. The interesting phenomena in this case may best be considered as properties of the impurity perturbed by its host crystal environment.

2.2 Theoretical Methods

Despite the importance of impurity centres in crystals our knowledge of them is largely empirical. An exception to this general truth is provided by impurities producing shallow levels, with loosely-bound electrons or holes which can be described by a 'hydrogen-like' model. The wavefunctions of such impurities can be expanded as a sum of a limited number of the Bloch (or Wannier) functions used to describe the band structure of the host material. A very good review of shallow impurity states in elementary semiconductors is given by Kohn[1].

For impurities (such as transition and rare earth metals) which produce deep levels the approach outlined above cannot readily be used. The electron orbitals for such an impurity can be subdivided into three groups - inner core, bonding and d- or f- orbitals. The inner core electrons have little effect on observed phenomena except for providing a contribution to the potential 'seen' by the outer electrons. The bonding orbitals are considered to be merged in the valence band of the host crystal, leaving the d- or f-orbitals essentially similar to those of the free ion. The band structure of the host crystal is essentially derived from s- and p-functions and so large numbers of these would have to be considered in order to give a reasonable description of the d- or f-orbitals of the impurity electrons.

A different method has already been implicitly suggested above, namely to consider the whole system of impurity and host as an ion (the impurity) surrounded by some modifying environment. From this starting point a number of theoretical methods may be used and these are discussed in many standard textbooks[2,3,4].

Chronologically, the first method to be used was crystal-field theory, originally developed by Bethe[5], who proposed that the energy level structure of an impurity is caused by the coulomb interaction of the impurity with the electrical field arising from its neighbours included in the Hamiltonian for the free ion. The neighbouring atoms were treated as point charges. This model implies that the crystal fields would be greater in the more ionic II-VI compounds than in the more covalent III-V ones. This model can be improved by incorporating the charge distribution of the bonding orbitals[6].

Historically the development of ligand-field theory uses a more phenomenological approach. The ligands (neighbouring atoms) of an impurity ion are regarded solely as a means of providing a crystal potential, the exact origin of which (point-ion or bonding charge distribution) is ignored except that it is required to reflect the symmetry of these ligands.

The difference between the two theories is perhaps more readily conveyed by considering the one-electron orbitals of the impurity ion which each employs. In crystal field theory, these are modified versions of the free ion one-electron orbitals, where no account is taken of electron transfer (i.e. covalency) between the impurity and its ligands. In ligand field theory the one-electron orbitals are formally bases of the irreducible representations of the point symmetry group of the system. Unfortunately this difference is often obscured by the fact that suitable basis functions are often chosen to be linear combinations of the free ion one-electron orbitals. However these basis functions should not be regarded as representing anything other than the symmetry of the true orbital wavefunctions.

Attempts to relate these basis functions to actual electron orbitals are embodied in the molecular-orbital and Heitler-London theories.

It should be noted that, in practice, very little distinction is drawn between crystal- and ligand-field theories, especially by experimentalists.

Making the static lattice approximation, the Hamiltonian for an impurity ion in a crystal is

$$H = -\frac{\hbar^2}{2m}\sum_i \nabla_i^2 - \sum_i \frac{Ze^2}{r_i} + \tfrac{1}{2}\sum_{i\neq j}\frac{e^2}{r_{ij}} + \sum_i \xi_i(r)\,\underline{l}_i\cdot\underline{s}_i + V \qquad (2.1)$$

which is the Hamiltonian for the free ion (assuming only first order spin-orbit coupling) with an additional term V due to the crystal potential. Screening effects are also neglected. The problem is then the standard one in quantum-mechanical treatments, namely diagonalising the Hamiltonian given in eq (2.1). Although the final results are the same in each case, the detailed calculation and degree of difficulty of the calculation depends on the order in which the last three terms of eq (2.1) are treated.

There are six possibilities, of which three may conveniently be ignored, because they require $\sum_i \xi_i(r)\underline{l}_i\cdot\underline{s}_i$ to be diagonalised before $\frac{1}{2}\sum_{i\neq j} e^2/r_{ij}$, which for a free ion would be synonymous with j-j coupling. Since studies of the free ions in the transition and rare earth series show that LS-coupling is the more appropriate choice, then in ligand-field theory only those coupling schemes where the electron-electron interaction is treated before the spin-orbit interaction need be considered. This leaves three coupling schemes, each of which has some practical importance

(i) $V < \xi_i(r)\underline{l}_i \cdot \underline{s}_i < e^2/r_{ij}$

(ii) $\xi_i(r)\underline{l}_i \cdot \underline{s}_i < V < e^2/r_{ij}$

(iii) $\xi_i(r)\underline{l}_i \cdot \underline{s}_i < e^2/r_{ij} < V$

The first of these is known as the rare-earth coupling scheme, and, as its name implies, it is appropriate for the rare-earth series and possibly the actinides. The second is known as the weak-field coupling scheme and is most useful normally for ions of the first transition series. The third is the strong-field coupling scheme (occasionally referred to as covalent coupling) and is of most use with ions of the second and third transition series, although it applies to ions of the first transition series in some of their compounds.

The simplest application of eq (2.1) to systems of interest, is to that of a single 3d-electron, since for this case there are no electron-electron interactions. It can then be shown[2,3] that the five-fold orbital degeneracy of the free ion is split (assuming a cubic crystalline field) into two levels, conventionally labelled e_g and t_{2g} which are respectively doubly and triply degenerate. The magnitude of this splitting is conventionally labelled as 10Dq or Δ and in crystal-field theory it is treated as a parameter characterising the strength of the crystal field. Strictly, this splitting is calculable in ligand-field theory provided the exact form, and not just the symmetry properties of the one-electron orbitals is known.

For systems with more than one electron, the problem becomes more complicated because the electron-electron interaction can only be characterised through coulomb and exchange integrals in the formal solution. There are ten such integrals. In crystal-field theory, by making the approximation that the one electron orbitals are d-functions,

then the number of independent integrals reduces to three, which are treated as parameters (conventionally A, B and C) known as Racah's parameters. Again, within the formalism of ligand -field theory, these ten integrals could be calculated, given the precise form of the one electron orbitals. In practice, since this has not been achieved, and since ten parameters is too large a number to be obtained from experiment, it is customary for experimental purposes to use crystal-field theory where only four parameters (A, B, C and 10Dq) are required.

2.3 Molecular Orbital Theories[3]

From the previous section, it can be seen that the major drawback of using strict ligand-field theory is that the number of empirical parameters becomes unmanageably large. This could be overcome if the 'one-electron orbitals' used in theory could be obtained in an explicit form, rather than merely requiring them to have the same symmetry properties as the bases or appropriate irreducible representations of the point group of the system. Also it is only by giving an explicit form to these one-electron orbitals that ligand-field theory could be understood more intuitively.

Attempts have been made at providing such a connection between 'actual' one-electron orbitals and irreducible representation bases, and these are embodied in the Molecular-Orbital and Heitler-London theories. The Molecular-Orbital theory applies in the strong-field (covalent) coupling scheme, where a large amount of charge transfer between the impurity and its ligands is postulated. In the weak-field coupling scheme, with little charge transfer the Heitler-London theory is appropriate. In both cases, the derived orbitals should be the one-electron orbitals of the t_{2g} and e_g levels mentioned in the previous section.

2.4 Interpretation of Racah Parmaeters

Energy levels are most often given as some linear combination of Racah parameters and Dq.

$$\text{e.g.} \quad E = wA + xB + yC + zDq$$

The Racah parameter A comes from electrostatic interactions within the d-shell which shift the energy of the shell as a whole. B and C arise from electrostatic interactions within the shell which split the degeneracy of the d-electrons. Dq measures the crystal-field splitting. In principle B, C and Dq can be obtained by spectroscopic investigation of the excited states of an impurity in a crystal although they vary depending on the charge state of the impurity and the exact nature of the host crystal.

It is however difficult to obtain the parameter A by experiment. In order to do so it is necessary to obtain the energy of the ground state of the impurity relative to one of the host crystal energy bands. Attempts have been made[7,8] to relate the parameter A to the free-ion ionisation potential, with some degree of success, and this gives a means of predicting the position of the impurity energy levels with respect to the crystal energy bands.

2.5 Representation of Energy Levels

Having obtained impurity energy levels by using crystal field theory with experimentally determined parameters, the problem of representing them and representing transitions between them remains. Two energy levels of an impurity which both lie between the valence and conduction band of the host may be represented as in Fig. 2.1, where an internal transition between the level is shown schematically. Implicitly this type of diagram regards the charge state of the impurity

as being unaltered. However difficulties arise in any processes (for example photoionisation) where the charge state of the impurity does change. Such processes, on this type of diagram, are most often shown as in Fig. 2.2. E_T is used to determine the difference in energy between the impurity and the conduction band. Such a representation however is based on a fundamental misunderstanding of Koopmans' theorem[9]. Koopmans' theorem however is based on the assumption that the energy of an impurity level, related to that of the conduction band, is the energy required to remove an electron from that level to the bottom of the conduction band, at a point far removed in real space from the impurity, provided that other energy levels remain unaffected by the removal. This is tantamount to stating the following

(i) the energy of the impurity is independent of its charge state

(ii) the energy of the conduction band does not change with the addition of an electron.

The correct procedure for defining such an ionisation energy is to evaluate the energy of the system when there are n electrons on the impurity and also when there are n-1 electrons on the impurity and one in the conduction band, and then take the difference between the two. Realisation of this fact can best be expressed by an energy level diagram of the form shown in Fig. 2.3 where the charge state of the impurity is explicitly labelled. (In this context n, n-1, n+1 are shortened forms of d^n, d^{n-1}, d^{n+1} respectively.)

On such a diagram, an internal transition, without change of charge state is represented by a vertical line. Transitions such as those labelled (b), (c), (d) represent ionisation of the impurity, and (e) represents electron capture.

Using this definition for ionisation energy, or indeed any process where the impurity charge state changes, two charge states of the impurity should be specified for a full description of the transition, i.e. a process such as (b) in Fig. 2.3 should be labelled E(n,n-1).

Hence for a full description of an energy level, not only is the energy separation between the level and some reference point required but also the charge state of the impurity must be specified.

2.6 Summary

In this chapter the theoretical methods of calculating the energy level structures of impurities have been discussed and their relationship to the host crystal energy bands has been considered. The approximations involved have been outlined - most significantly that if the energy levels are discussed in terms of Racah parameters then crystal field and not ligand-field theory is being employed.

Throughout this chapter, the host lattice is assumed to be static and its only role in the theories outlined is to provide a contribution to the potential which the impurity electrons experience. Subsequent chapters will relax the assumption of the static lattice and investigate phenomena arising from the interaction of the impurity electrons with lattice vibrations.

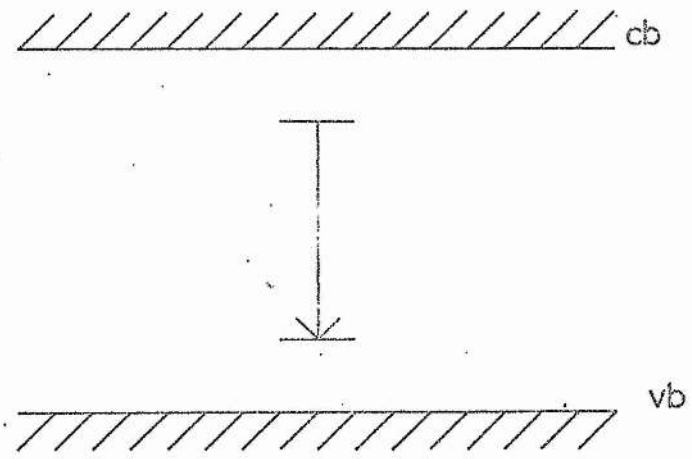

Fig 2·1

Representation of an impurity internal transition

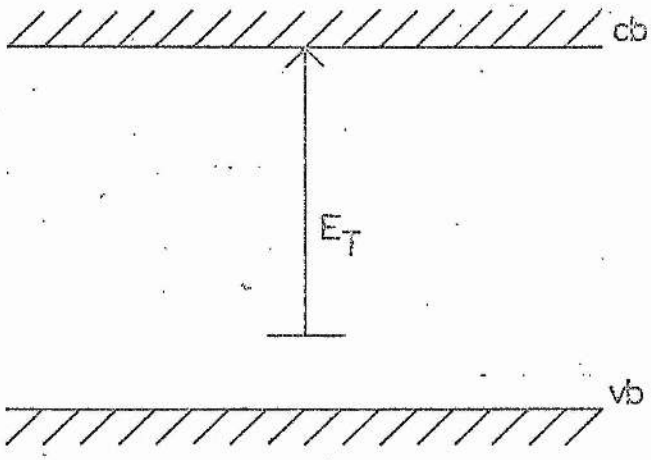

Fig 2.2

Representation of a photoionisation process

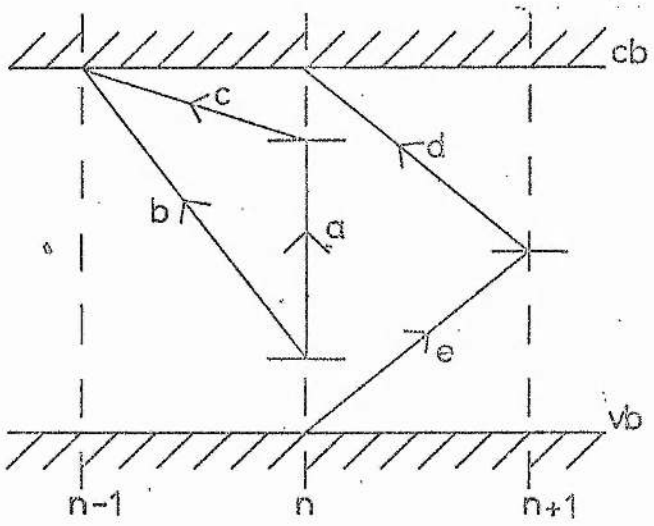

Fig 2·3

(a) internal transition

(b) (c) (d) impurity ionisation

(e) electron capture

CHAPTER 3

Electron-Lattice Interactions

3.1 Introduction

In the previous chapter, methods of calculating the energy level structure of an impurity ion in a crystal were discussed under the assumption that both the impurity and the atoms of the host crystal were static. However as a consequence of their thermal energy, the atoms in a crystal are constantly in motion. Even at absolute zero of temperature, the atoms cannot be stationary, since otherwise the Heisenberg uncertainty principle would be violated. The motion of the atoms at $T = 0^{o}K$ is referred to as the zero-point vibration.

The interaction of these vibrations with the electrons of an impurity ion has significant effects on the electronic energy levels. Most obviously, there is a range of energies available for a given electronic state because of the range of possible vibrational energies. Such a mixed electronic-vibrational state is known as a vibronic state.

3.2 Born-Oppenheimer and Adiabatic Approximations[10]

In the Born-Oppenheimer approximation it is noted that the electron mass is very much less than the nuclear mass, and hence that the nuclei move much more slowly than the electrons. This has two consequences

(i) the electrons adjust to the instantaneous nuclear positions, so that the electronic wavefunction $|\phi\rangle$ is a function of all the electron positions $\underline{r} = (\underline{r}_1, \underline{r}_2 \ldots.)$ and of all the nuclear positions $\underline{R} = (\underline{R}_1, \underline{R}_2, \ldots..)$.

(ii) the nuclei experience an average potential due to the electrons, so that the nuclear wavefunction $|\psi\rangle$ does not depend explicitly on the coordinates of the electrons.

These conditions imply that the total vibronic wavefunction can be written

$$|\phi(\underline{r}, \underline{R})> = |\phi(\underline{r}, \underline{R})> \, |\psi(\underline{R})> \qquad (3.1)$$

The vibronic Hamiltonian can be written as

$$H_v = T_e + T_v + V(\underline{r},\underline{R}) \qquad (3.2)$$

where $T_e \equiv$ electronic kinetic energy,

$T_v \equiv$ nuclear kinetic energy,

$V(\underline{r},\underline{R}) \equiv$ all potential energy terms.

With wavefunctions of the form of eq (3.1), the resultant Schrödinger equation is separable, yielding

$$\{T_e + V(\underline{r},\underline{R})\} \, |\phi(\underline{r},\underline{R})> = U(\underline{R}) |\phi(\underline{r},\underline{R})> \qquad (3.3)$$

and

$$\{T_v + U(\underline{R})\} \, |\psi(\underline{R})> = E|\psi(\underline{R})> \qquad (3.4)$$

where $U(\underline{R})$ is the separation parameter. In obtaining eqs (3.3), (3.4) the adiabatic approximation has been made, namely that terms arising from the action of the nuclear kinetic operator T_v on the electronic wavefunction have been ignored. This is synonymous with the statement that the electrons follow the nuclear positions adiabatically. Within the adiabatic approximation, $U(\underline{R})$ and E are stationary values in eqs (3.3) and (3.4) respectively, so that there areno transitions between vibronic states in the absence of external perturbations. (The non-adiabatic terms neglected in obtaining eqs (3.3) and (3.4) can be regarded as just such a perturbation, coupling electronic and vibrational states and permitting the conversion of electronic energy to vibrational energy and vice versa.)

3.3 The Harmonic Approximation[11]

From eq (3.4) it is clear that the separation parameter $U(\underline{R})$ is

effectively a potential energy for the vibrating nuclei. In order to solve eq (3.4) it is necessary to obtain an explicit form for $U(\underline{R})$. This can be done by expanding the potential energy of the nuclei as a function of their relative positions. Thus,

$$U(\underline{R}) = U(\underline{R}_o) + \sum_i A_i (R_i - R_{io}) + \tfrac{1}{2} \sum_{i,k} A_{ik} (R_i - R_{io})(R_k - R_{ko}) + \ldots \qquad (3.5)$$

where R_i is a typical cartesian coordinate of an atom, and the subscript o denotes an equilibrium value.

The harmonic approximation consists of neglecting terms of order three and higher in the relative displacements. The system is assumed to be in equilibrium when $R_i = R_{io}$, hence the forces $\partial U(\underline{R})/\partial R_i$ must be zero, and so the terms linear in the relative displacements in eq (3.5) must vanish. (This is strictly only valid for non-degenerate states - see 3.5.) The quantity $U(\underline{R}_o)$ can be incorporated in the energy zero to yield, with $U_i = R_i - R_{io}$

$$U(\underline{R}) = \tfrac{1}{2} \sum_{i,k} A_{ik} U_i U_k \qquad (3.6)$$

which is of the form of the potential energy for a set of coupled harmonic oscillators. Thus the vibration Hamiltonian becomes

$$H = T_v + U(\underline{R}) = \sum_i \tfrac{1}{2} M_i \dot{U}_i^2 + \sum_{i,k} \tfrac{1}{2} A_{ik} U_i U_k \qquad (3.7)$$

The relative displacements are thus seen to be coupled - the motion of one nucleus affecting all the others. This coupling can be removed by an appropriate choice of coordinates, the normal coordinates. The dependence of these normal coordinates is found to be that of standing waves in the crystal, known as phonons. The fact that eq (3.7) can be written in a decoupled form implies that these phonons (or normal modes) can coexist without interacting.

Thus the Schrödinger equation (3.4) for the nuclei has eigenvalues and eigenvectors

$$\sum_j \hbar\omega_j(n_j + \tfrac{1}{2}) \quad \text{and} \quad \prod_j |\chi(n_j,q_j)\rangle$$

where n_j is the vibrational quantum number of the j-th mode, q_j is the normal coordinate characterising the j-th mode and the sum and product are to be taken over all modes j: $|\chi(n_j,q_j)\rangle$ is a simple harmonic oscillator wavefunction consisting of the product of a gaussian function with a Hermite polynomial.

From the electronic Schrödinger equation (3.3), the energy of a vibronic state coupled to only one mode can be written,

$$E_v = E_e + (n + \tfrac{1}{2})\hbar\omega \qquad (3.8)$$

where E_e is the energy of the purely electronic state.

3.4 Configuration Coordinates[12,13,14]

In certain instances (outlined below) it is possible for a pictorial representation of vibronic energy levels to be given. Strictly this is valid if and only if

either (i) one local mode is highly predominant, eg the 'breathing' mode in which case the configuration coordinate is simply related to the interatomic spacing. A local mode exists for an impurity if the crystal does not respond appreciably to the vibration of the impurity ion. The wavefunction of a local mode decreases rapidly in going away from the impurity.

or (ii) no local mode occurs, but the impurity is only coupled to certain of the lattice modes (eg in a polar crystal to the LO modes). In the simplest approximation, where these modes all have the same energy and polarisation the configuration coordinate is the normal coordinate associated with this mode.

The energy of the vibronic states arising from two electronic levels can thus be drawn as a function of the configuration coordinate as shown in Fig. 3.1.

In general the two electronic states g and x correspond to different interactions between the impurity and the crystal, so that the minima of the two curves need not occur for the same value of q: nor need the coupling constants be the same so that the curvatures (and also the vibrational energy quantum) of $U_g(q)$ and $U_x(q)$ need not be the same. In some cases it may be that the set of normal coordinates for two vibronic states may differ so that it is not possible to represent both states on the same diagram. Despite the drawbacks mentioned such diagrams are often useful in giving a visual representation to phenomena which otherwise might be rather difficult to grasp.

Because the nuclei move much more slowly than the electrons in a crystal, it is a reasonable approximation to assume that a nucleus is stationary during an electronic transition; this is known as the classical Franck-Condon principle and its significance is that electronic transitions such as optical absorption or emission may be represented by vertical lines on a configuration-coordinate diagram.

Quantum-mechanically a similar (although not equivalent - see[15]) approximation can be made, namely that the electronic transition probability is independent of the nuclear coordinates. To be specific, for an optical absorption, the matrix element for a dipole transition is T_{gx} where

$$\begin{aligned} T_{gx} &\propto \langle \Phi_x(\underline{r},q) | \underline{r} | \Phi_g(\underline{r},q) \rangle \\ &= \langle \psi_x(q) | \psi_g(q) \rangle \langle \phi_x(\underline{r},q) | \underline{r} | \phi_g(\underline{r},q) \rangle \qquad (3.9) \\ &= \text{overlap integral of vibrational states} \times \text{electronic transition matrix element} \end{aligned}$$

This is known as the Condon approximation.

The peak position of the emission (absorption) band of an impurity transition in a crystal between two given electronic states is determined by which vibrational state in the lower (upper) vibronic level in Fig. 3.1 has the greatest overlap integral with the ground vibrational state of the upper (lower) vibronic level .

From these considerations it is possible to define two useful quantities - the Huang-Rhys factors[16] (S_x and S_g) and the dominant phonon energy. For example, in an optical absorption transition, the absorption peak is at an energy $h\nu_a$ where the ground vibrational state of the lower vibronic level overlaps most with some vibrational state of the upper vibronic level, so that

$$\begin{aligned} h\nu_a &= \{E_x + (S_x + \tfrac{1}{2})\hbar\omega_x\} - \{E_g + \tfrac{1}{2}\hbar\omega_g\} \\ &= E_x - E_g + (S_x + \tfrac{1}{2})\hbar\omega_x - \tfrac{1}{2}\hbar\omega_g \\ &\doteq E_{xg} + S_x\hbar\omega_x \end{aligned} \qquad (3.10)$$

where $E_{xg} = E_x - E_g$, S_x is the Huang-Rhys factor for the excited state and is interpreted as the mean number of phonons emitted as the excited vibrational state relaxes to the ground vibrational state of the excited vibronic state; $\hbar\omega_x$ is known as the dominant phonon energy. Similar considerations of an emission process lead to definitions of S_g and $\hbar\omega_g$.

It should be stressed that this configurational coordinate method is not an essential one, and any effects explicable within it can also be treated in more rigorous ways. (see for instance[17,18,19])

3.5 The Jahn-Teller Effect

It would be impracticable to give a comprehensive treatment of this effect or even an exhaustive bibliography. Excellent reviews

are available by Sturge[20] and Englmann[21]. An interesting variational approach is given by Longuet-Higgins[22] and a useful compilation of the more important features by Stoneham[23].

The Jahn-Teller theorem may be stated as follows[24]: An orbitally degenerate state of a non-linear molecule or crystal defect is unstable against at least one asymmetric distortion which lowers the energy and reduces the symmetry of the system. This is an existence theorem derived from group theory and consequently no mention is made of the size or physical origin or the effect. The basic theorem has been extended[25] to argue that spin degeneracy, excepting Kramers degeneracy, will also be lifted, although this is a small effect, and for practical purposes only orbital degeneracy need be considered. This theorem is often misquoted as stating that electronic degeneracy is removed whereas it in fact means that orbital degeneracy is removed only to be replaced by a complicated vibronic degeneracy of at least the same order.

Formally, this theorem can be proved[26] more readily than by the original arguments of Jahn and Teller. By invoking the Hellmann-Feynmann theorem[27,28], the force F_j acting on a nucleus in a potential $U(\underline{q})$ in such a manner as to increase the coordinate q_j is given by

$$F_j = - \langle i | \partial U/\partial q_j | i \rangle \qquad (3.11)$$

where $|i\rangle$ is the electronic state. (This is the quantum-mechanical analogue of the classical $F_j = - \partial U/\partial q_j$.) To prove the Jahn-Teller theorem it suffices to show that $F_j \neq 0$ for all j, because in this case the system will spontaneously distort until all the F_j are zero. Using group theory, it can be shown that[2], if q_j and hence $\partial U/\partial q_j$ transform

as one of the bases of an irreducible representation Γ_j of the point group of the system, and the electronic state $|i\rangle$ transforms as one of the bases of another irreducible representation Γ_i, then the condition for $F_j \neq 0$ is that Γ_j be contained in the reduction of the symmetric product (Γ_i^2). The argument is then identical to that of the original authors[24] who have shown that for all but linear molecules, there is at least one non-totally symmetric q_j for which (Γ_i^2) contains Γ_j.

To be specific, for the case of cubic symmetry, the matrix elements of eq (3.11) are non-vanishing for the cases shown in Table (3.1). Table (3.2) lists those representations appearing in the symmetric products (E^2), (T_1^2) and (T_2^2) for cubic symmetry. The notation is that of Mulliken[29].

The main advantage of this proof is that it illustrates clearly that the Jahn-Teller interaction arises from those terms, linear in the relative nuclear displacements, of eq (3.5) which were taken to be zero for non-degenerate states, in making the harmonic approximation. The disadvantage of using the Hellmann-Feynmann theorem as a starting-point to describe the Jahn-Teller effect is that eq (3.11) is only valid for exact electronic wavefunctions which are in general unknown. (In principle such eigenfunctions would be the exact molecular orbitals discussed in 2.3). This has meant that the Jahn-Teller effect has been considered mainly by perturbation theories (for an exception see[22]).

The problem of an electronic state coupled to many phonon modes has not yet been solved, the most common approximation being that the total interaction with a large number of modes of the same symmetry, but different frequencies and individual coupling constants, can be represented by interaction with a single mode having an 'effective'

frequency and an 'effective' coupling constant. Attempts have been made on the problem of coupling to many modes of the same symmetry and different frequencies[30,31,32] and they can be most easily interpreted as coupling to a single effective mode with the effect of phonon dispersion being introduced as a second order perturbation on the energy level structure obtained with the effective mode approximation. A second problem is that although an orbital doublet (E-state) will couple only to E-modes (Table (3.1)), orbital triplets (T_1 - and T_2-states) can couple to both E- and T_2-modes. This problem has been studied by O'Brien[33,34], for the special case of equal coupling to modes of each symmetry where each symmetry is represented by a single effective frequency and coupling constant.

The approximation that a Jahn-Teller effect can be represented by coupling to a single effective mode means that the effect can be described without further assumptions on a configurational coordinate diagram. This diagram will not in general be two-dimensional, because there will be more than one distortion of the system giving rise to the same Jahn-Teller effect. Examples of such diagrams are given in Figs (3.2) and (3.3) for electronic doublets (E-states) and electronic triplets (T-states) respectively coupled to E-vibrational modes. (These diagrams are adapted from Liehr[35]). From Fig (3.2) the number of equivalent minimum energy configurations is infinite, whilst from Fig (3.3) there are three equivalent minimum energy configurations. Thus although the electronic degeneracy has been removed a more complicated vibronic degeneracy still exists. There are three types of higher order interaction which remove the vibronic degeneracies. These are, anharmonic lattice terms (higher powers of eq (3.5)).

coupling to non-degenerate electronic states and coupling connecting the degenerate electronic states which is of quadratic or higher order. In these cases, the potential energy surfaces such as those illustrated in Figs (3.2) and (3.3) become very complicated. However it is often sufficient just to calculate the minima of such surfaces, and this can be done using methods given by Öpik and Price[36] and Stoneham and Lannoo[37]. These higher-order coupling terms can be neglected except in those cases where linear coupling leaves a vibronic degeneracy.

Study of diagrams of the type Figs (3.2) and (3.3) enables a distinction to be drawn between two cases of the Jahn-Teller effect - the static and the dynamic. The static Jahn-Teller effect occurs when the lattice distortion is permanent, that is when one of the degenerate configurations is selected in preference to the others because higher order coupling terms have removed the vibronic degeneracy so that one configuration is of lower energy than the others. The dynamic Jahn-Teller effect occurs when the system moves from one degenerate configuration to another so that no permanent distortion occurs. The distinction between the two is sometimes drawn by stating that if the energy difference between configurations is greater than the zero-point vibration energy, then the effect is a static one. A better operating definition would be that a static Jahn-Teller effect occurs when the transition time between configurations is slow compared with the characteristic time of an experiment being performed on the system. This is however a semantic difference since quantum-mechanically there will always be a finite transition probability of moving from one configuration to another so that the effect is always dynamic.

It should also be noted that linear electron-lattice coupling between electronic states which are nearly degenerate can also give rise to a Jahn-Teller effect (sometimes known as the Pseudo-Jahn-Teller effect). This is just another illustration of the fact that sharp discontinuities do not occur very often in physics, and the existence of a pseudo-Jahn-Teller effect might have been intuitively expected. This Jahn-Teller effect will disappear if there is a sufficiently large splitting of the nearly-degenerate levels by some means. This is how, for example, spin-orbit splitting may quench the Jahn-Teller effect[36].

3.6 The Ham Effect

This is an example of a phenomenon which was implicitly recognised before Ham[38] placed it on a secure theoretical basis. The Ham effect is concerned with the relationship between the matrix elements of an electronic operator between purely electronic wavefunctions and those of the same operator between vibronic wavefunctions.

The matrix element of an electronic operator $\gamma(\underline{r})$ between the vibronic wavefunctions $|\phi_1(\underline{r},\underline{q})\psi_1(\underline{q})\rangle$ and $|\phi_2(\underline{r},\underline{q})\psi_2(\underline{q})\rangle$ is

$$\gamma_{12}^{vib} = \langle\phi_1(\underline{r},\underline{q})\psi_1(\underline{q})|\gamma(\underline{r})|\phi_2(\underline{r},\underline{q})\psi_2(\underline{q})\rangle \qquad (3.12)$$

and making the Condon approximation

$$\gamma_{12}^{vib} = \langle\psi_1(\underline{q})|\psi_2(\underline{q})\rangle\langle\phi_1(\underline{r},\underline{q})|\gamma(\underline{r})|\phi_2(\underline{r},\underline{q})\rangle$$

$$= \langle\psi_1(\underline{q})|\psi_2(\underline{q})\rangle\ \gamma_{12}^{electronic} \qquad (3.13)$$

If the vibrational wavefunctions are normalised then $\langle\psi_1(\underline{q})|\psi_2(\underline{q})\rangle \leq 1$ by the Schwartz inequality. Thus the vibronic matrix elements are reduced with respect to the electronic ones, with the exception of those

on the diagonal. Considered in this manner, the dipole transition matrix element eq (3.9) is essentially an instance of Ham reduction.

The Jahn-Teller effect provides a means whereby the vibrational parts of different vibronic wavefunctions can be quite far displaced (cf. Fig (3.3)) so that reduction of electronic matrix elements may be especially pronounced. It should be noted however that the Born-Oppenheimer approximation breaks down in the presence of the Jahn-Teller effect because the nuclear motion mixes the electronic states. The appropriate vibronic wavefunction is in fact a linear combination of Born-Oppenheimer products of the form of eq (3.1). The basic proof of the Ham effect is however still similar to that given above.

The case of most significance for present purposes is when the electronic operator is the orbital angular momentum, since this affects spin-orbit coupling. The orbital angular momentum operator only has matrix elements between different states - i.e. only off-diagonal matrix elements between electronic states. From eq (3.13) these will obviously be reduced by the Ham effect. Because the spin angular momentum operator does not operate on Born-Oppenheimer products, the matrix elements of spin-orbit coupling are reduced by the same factor as those of the orbital angular momentum.

In 3.5 it was observed that sufficiently strong spin-orbit coupling could quench the Jahn-Teller effect. In this section the possibility of the opposite process occurring has been outlined. The strength of the spin-orbit coupling is essentially a property of the impurity and the strength of the Jahn-Teller effect is a property of the impurity-lattice interaction so that it is impossible to be general about which effect will quench the other. This can only be determined by experiment for specific cases.

3.7 Summary

The treatment of the electron-lattice interaction has been outlined for the case where the lattice is allowed to vibrate. The approximations relevant to discussions in subsequent chapters have been given, and two important effects - the Jahn-Teller and Ham effects - have been treated in more detail. These are of some importance because of the interplay between the Jahn-Teller effect and spin-orbit coupling where either may quench the other.

Table (3.1) from (2)

Γ_j	Γ_i
E	any of E, T_1, T_2
T_2	any of T_1, T_2

Note: a complete list of possible vibrational modes for cubic systems is given in Appendix II of Englmann[21].
Table (3.2) lists the irreducible representations obtained by reduction of the symmetric products (E^2), (T_1^2) and (T_2^2) in cubic symmetry.

Table (3.2) from (2)

Symmetric Product	Irreducible Representations in Reduction
(E^2)	A_1, A_2, E
(T_1^2)	A_1, E, T_1, T_2
(T_2^2)	A_1, E, T_1, T_2

The notation of the various irreducible representations is that of Mulliken[29].

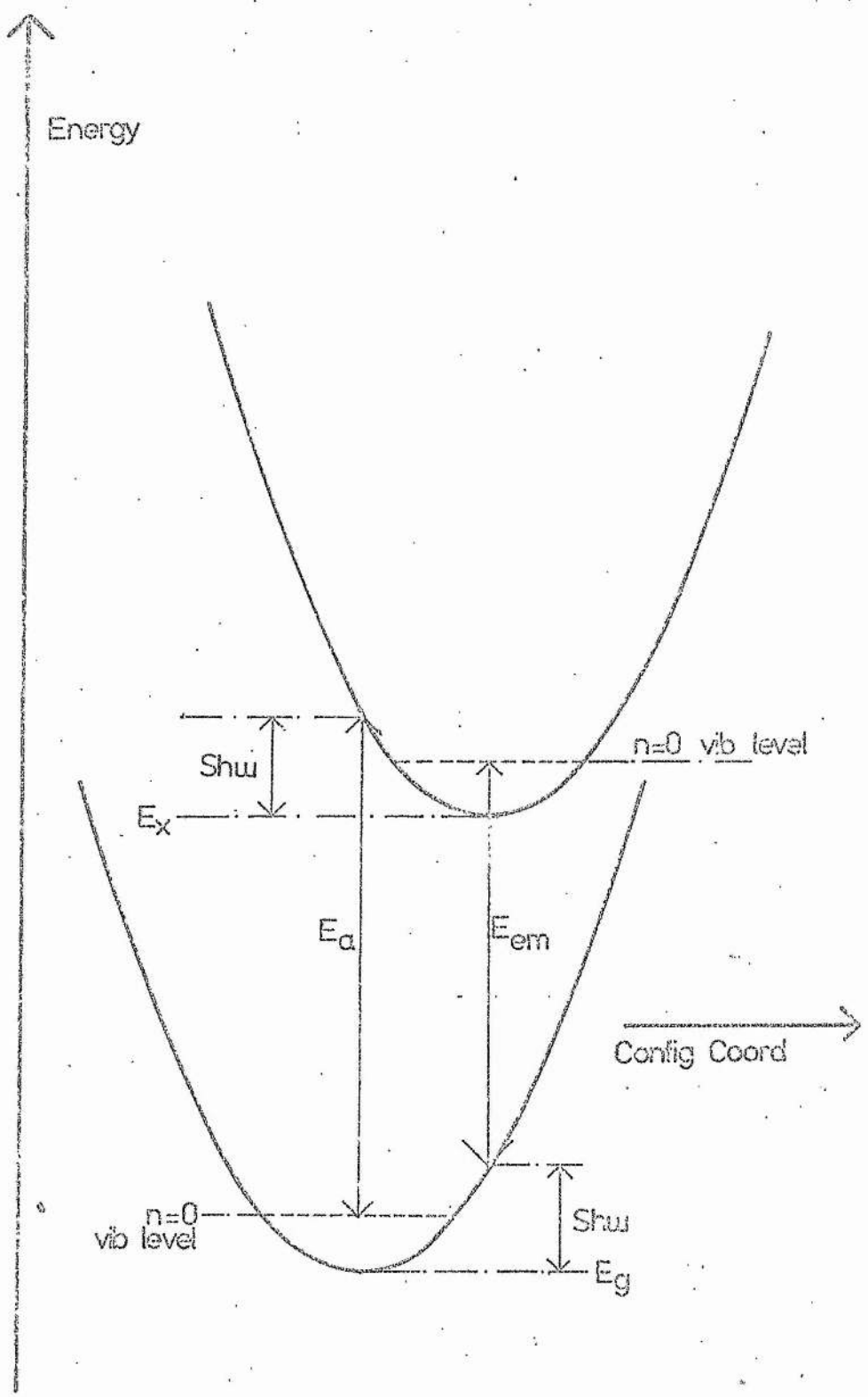

Fig 3-1

One dimensional configuration coordinate diagram

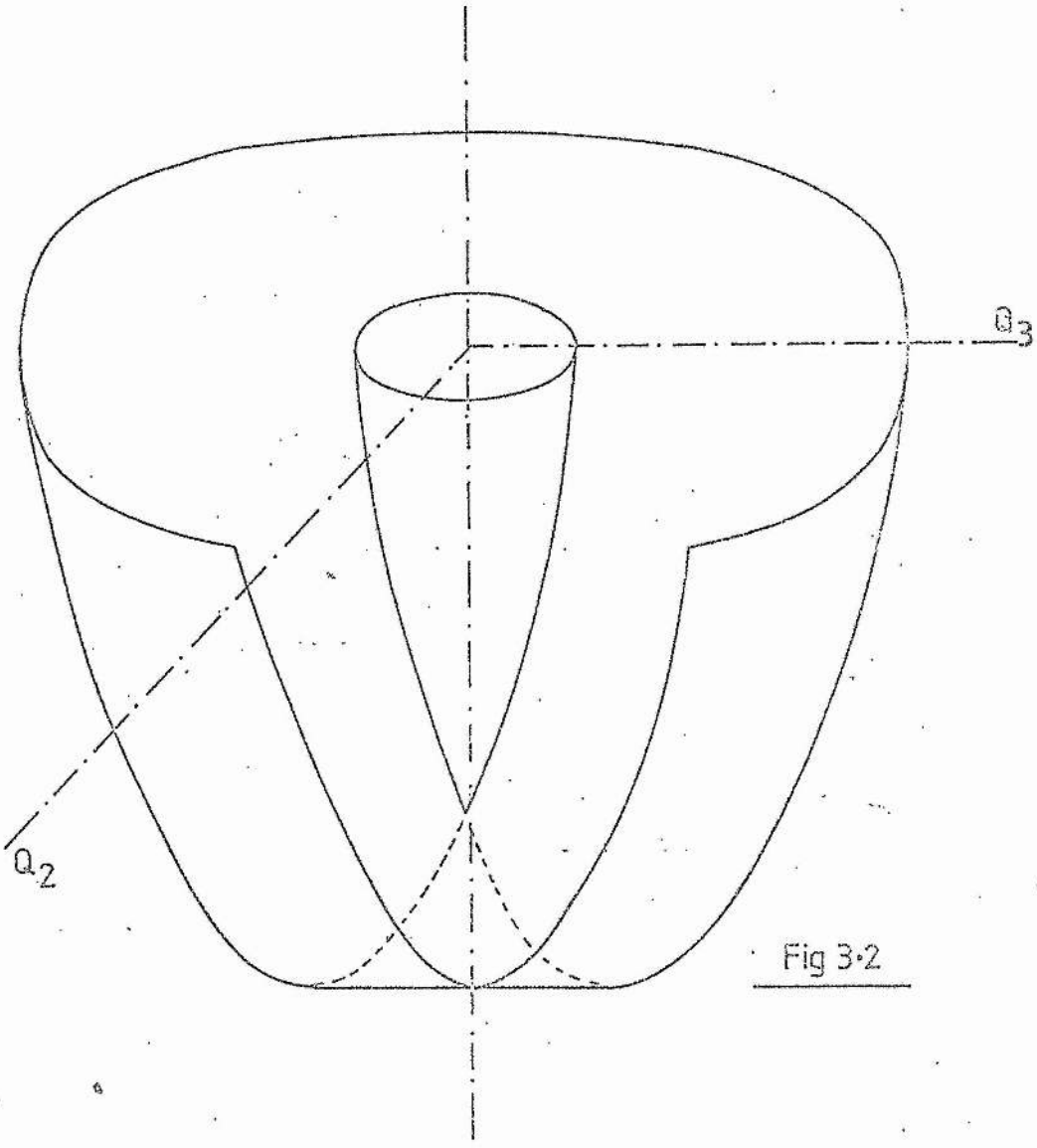

Fig 3·2

Potential surface for an E-state with E-mode coupling (coordinates are defined in [35])

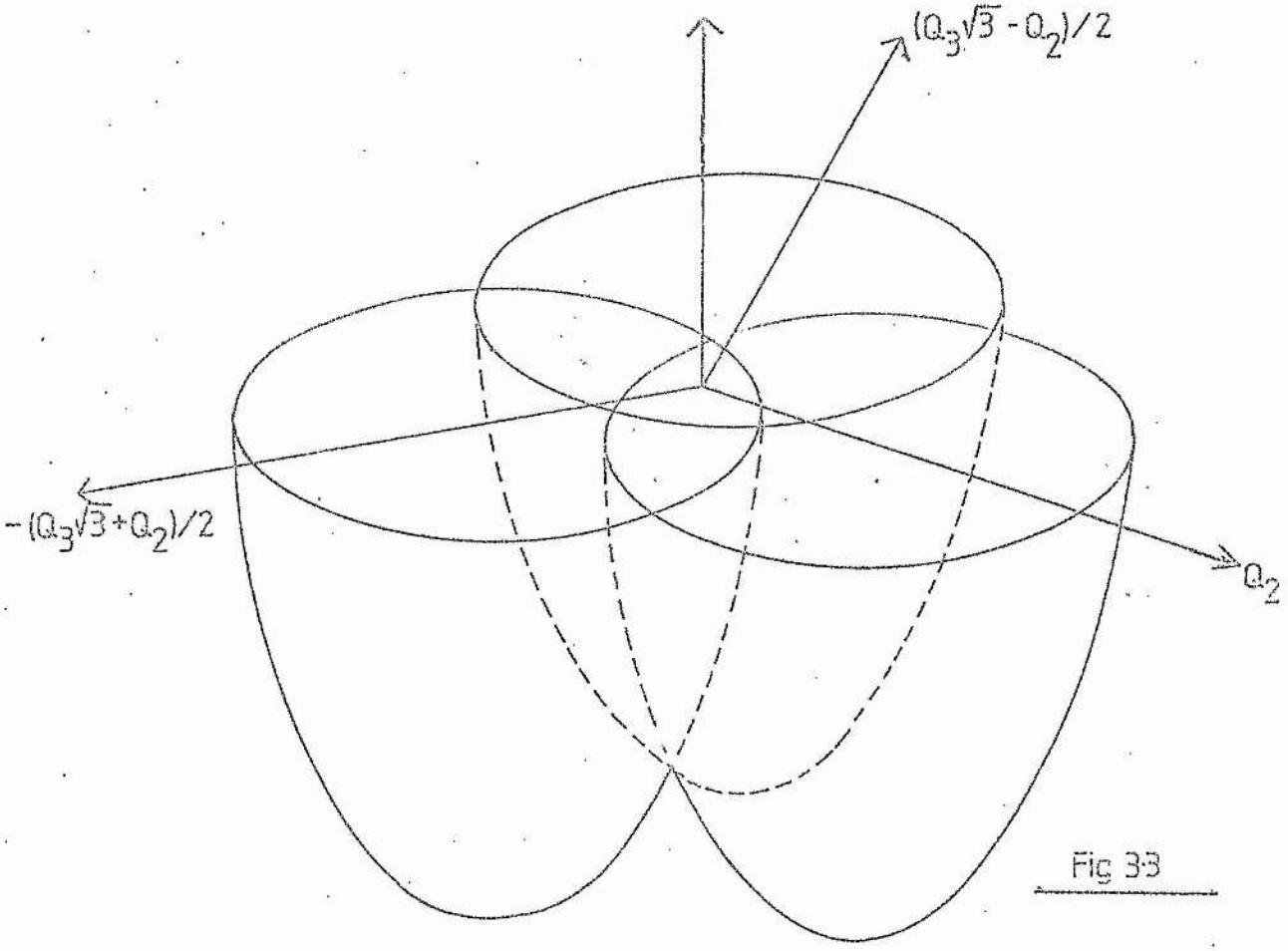

Fig 3-3

Potential surface for a T-state with E-mode coupling
(coordinates are defined in [35])

CHAPTER 4

Zero-Phonon Lines

4.1 Introduction

The quantum-mechanical treatment of broad-band vibronic spectra was developed by a number of authors[15,16,39,40] whose calculations gave reasonable agreement with known experimental data. These early authors do not explicitly discuss zero-phonon lines, whose significance was first realised by Kane[41] who showed that for weak electron-lattice coupling the zero-phonon line would be the dominant feature of the spectrum.

More recently, the importance of zero-phonon lines has been fully appreciated and they have been the subject of a number of reviews[42,43]. These reviews, and a high proportion of the early theoretical work are strictly valid only within the Born-Oppenheimer approximation. Thus for degenerate or nearly degenerate electronic levels, these treatments can only be used with care. In 4.2 the nature and origin of zero-phonon lines will be considered for singlet-singlet transitions, and in 4.3 the complications involved in handling degenerate or nearly degenerate states will be discussed.

4.2 Singlet-Singlet Transitions

Following Kiel[44], the ground and excited state Hamiltonians can be written

$$H_g = \sum_i (T_i + \tfrac{1}{2} M_i \omega_{ig}^2 Q_i^2) \qquad (4.1)$$

$$H_x = E_{xg} + \sum_i (T_i + A_i Q_i + \tfrac{1}{2} M_i \omega_{ix}^2 Q_i^2) + \sum_{i \neq j} A_{ij} Q_i Q_j \qquad (4.2)$$

where Q_i, M_i, ω_i are the normal coordinate, mass and frequency of the

i-th normal mode, T_i is the vibrational kinetic energy operator, and E_{xg} is the difference in energy between the two electronic states as defined in eq (3.10). To obtain eq (4.2) the excited state potential energy has been expanded in the ground state normal coordinates, terminating at quadratic terms.

For purposes of comparison and discussed eqs (4.1) and (4.2) can be written as Hamiltonians expressed in terms of phonon creation and annihilation operators as [18]

$$H'_g = \sum_i \hbar\omega_i \ (a_i^+ a_i + \tfrac{1}{2}) \qquad (4.3)$$

$$H'_x = E_{xg} + H_g + \sum_i (v_i a_i + v_i^* a_i^+) + \tfrac{1}{2} \sum_{i,j} v_{ij} (a_i + a_i^+)(a_j + a_j^+) \qquad (4.4)$$

where a_i^+ (a_i) is the phonon creation (annihilation) operator for phonons of mode i, having frequency ω_i; v_i and v_{ij} are the linear and quadratic coupling coefficients respectively.

Approximations based on these two approaches although often given the same name are not in fact equivalent. For instance, setting $A_{ij} = 0$ in (4.2) and $v_{ij} = 0$ in (4.4) is often referred to as making the 'linear' approximation for both approaches. However these are not identical, because with $v_{ij} = 0$ in eq (4.4), the method based on eqs (4.3) and (4.4) yield identical frequencies within the ground and excited states, whereas with $A_{ij} = 0$ in eq (4.2), the method based on eqs (4.1) and (4.2) can yield different frequencies in the ground and excited states. In order to obtain the same degree of approximation from eq (4.4) as is given by the so-called linear approximation ($A_{ij} = 0$) of eq (4.2), it is necessary for eq (4.4) to include some quadratic coupling terms. If the diagonal quadratic terms of eq (4.4) are non-zero, with the off-diagonal ones set equal to zero, then eq(4.4)

yields the same level of approximation as eq (4.2) with $A_{ij} = 0$. Only with non-zero v_{ii} can eq (4.4) yield vibrational frequencies which are not identical with those of the ground state.

The linear approximation ($v_{ij} = 0$) of eq (4.4) can be obtained from eq (4.2) by setting $A_{ij} = 0$ and $\omega_{ix} = \omega_{ig}$. Making the further assumption of coupling to only one vibrational mode (i.e. all the A_i of eq (4.2) are zero except one) it can be shown[42,44] that the normalised transition probability, for an electric dipole transition from the m-th vibrational level of the ground state to the n-th vibrational level of the excited state, is given by

$$T_{(xn)(gm)} = e^{-s}\left[\frac{m!}{n!}\right] s^{n-m} \left[L_m^{n-m}(s)\right]^2 . \qquad (4.5)$$

The quantity s is related to the single non-zero coupling coefficient A by $s = A^2/2$. The $L_\alpha^\beta(z)$ are Laguerre polynomials.

At zero temperature, only the m = 0 vibrational state is occupied and the total line shape function is[44]

$$I_{xg}(E) = \sum_{p=0}^{\infty} e^{-s} \frac{s^p}{p!} \delta(p\hbar\omega + E_{xg} - s\hbar\omega - E) \qquad (4.6)$$

where $p = n-m$. Thus the line-shape function is a series of evenly spaced δ-functions with varying weights. The maximum weight occurs when $p \simeq s$[45] from which it can be seen that s in eqs (4.5) and (4.6) may be identified with the Huang-Rhys factor defined in 3.4.

The zero-phonon line strength is given by the p=0 term of the summation in eq (4.6)

$$\text{i.e. } I_{xg}^{zp}(E) = e^{-s} \delta(E_{xg} - s\hbar\omega - E) \qquad (4.7)$$

For non-zero temperatures, terms with $m \neq 0$ contribute to eq (4.5) and the lineshape is determined by taking a thermal average over the possible initial states, yielding for the zero-phonon line strength

$$I_{xg}^{zp}(E) = \exp(-s \coth \frac{\hbar\omega}{2kT}) I_o(s \operatorname{csch} \frac{\hbar\omega}{2kT}) \delta (E_{gx} - s\hbar\omega - E) \quad (4.8)$$

where $I_o(z)$ is a Bessel function of the first kind.

Eqs (4.7) and (4.8) show that, in the linear coupling approximation, the zero-phonon line is a δ-function whose width (trivially) and position are temperature independent.

At this point it is valuable to consider the precise definition of a zero-phonon line. Eq (4.7) gives the zero-phonon line strength in the case where both m and n = 0, this is sometimes known as the purely electronic line. However eq (4.8) gives the zero-phonon line strength for the case m = n, with no requirement for m to be zero. Thus, for this reason, eq (4.8) gives a zero-phonon line strength where contributions come from an infinite number of possible transitions, which in this model are degenerate. Since the zero-phonon line consists of a large number of transitions, all with the same energy it is sometimes referred to as a quasiline. Only if these transitions, making up the quasiline, have slightly different energies can the zero phonon line have a finite width.

To obtain the temperature dependence of the width and position of the zero-phonon line, it is necessary to include quadratic terms of the electron-lattice interaction in the calculation. This calculation has been performed by a number of authors[18,46] with a very clear presentation being given in the review by Maradudin[47]. These authors obtain, for the zero-phonon line shape function

$$I_{xg}^{zp}(\omega) = e^{-s}[\Pi_i I_o(c_i)] \frac{2\Gamma_o}{(\omega-\omega_o)^2+\Gamma_o^2} \quad (4.9)$$

which is a Lorentzian curve. In eq (4.9) $I_o(c_i)$ is a zeroth-order modified Bessel function whose argument c_i is given as

$$c_i = s_i \operatorname{csch} \frac{\hbar\omega_i}{2kT}$$

with s_i an individual mode Huang-Rhys factor $\equiv \dfrac{v_i^2}{(\hbar\omega_i)^2}$

(the total Huang-Rhys factor is a thermally weighted average of these), and ω_o is the frequency of the zero-phonon line, given by

$$\hbar\omega_o = E_{gx} - \sum_i \frac{v_i^2}{\hbar\omega_i} + \tfrac{1}{2} \sum_i v_{ii}[\,2n(\omega_i) + 1]\,. \qquad (4.10)$$

Γ_o is the half-width of the zero-phonon line, given by

$$\hbar\Gamma_o = \pi \sum_{i,j} v_{ij}^2\, n(\omega_i)[\,n(\omega_i) + 1]\ \delta(\hbar\omega_i - \hbar\omega_j) \qquad (4.11)$$

where $n(\omega_i)$ is the occupation number of the i-th mode given by the Bose-Einstein distribution.

From (4.10) and (4.11) it is readily seen that if the quadratic coupling coefficients v_{ij} are set to zero, then the width and position of the zero-phonon line are given by eq (4.8).

4.3 Multiplet-Multiplet Transitions

For the purposes of this section, a multiplet is considered to be a set of degenerate or nearly degenerate levels whose energy separation is less than the maximum phonon energy so that the states of a multiplet may be coupled via the electron lattice interaction. It is also assumed that there is no electron-lattice coupling between different multiplets. Because of the coupling between states of the same multiplet, the separation of nuclear and electronic motions through the Born-Oppenheimer approximation is not valid.

In some particular cases (for instance [48]) the problem of transitions between multiplets has been approached by expressing potential surfaces of the form of Figs (3.2) and (3.3) in terms of normal coordinates and essentially using eqs (4.1) and (4.2).

However, the fact that these potential surfaces must be known and be reasonably simple, together with the approximations introduced, such as neglecting the nuclear kinetic energy and ignoring transitions to high-lying vibrational states, make this approach of doubtful value except in special cases of a static Jahn-Teller effect.

A more general treatment of the problem was first proposed by McCumber[49] who found that the presence of a static or dynamic Jahn-Teller effect would not be reflected in a splitting of the zero-phonon line of a transition between truly degenerate multiplets, but that splittings would occur for transitions between nearly degenerate multiplets. The absence of a splitting of the zero phonon line in transitions between multiplets which experience only a Jahn-Teller effect might have been expected, since although the electronic degeneracy is removed, it is replaced by a vibronic degeneracy as explained in 3.5. Thus there is no qualitative difference between a singlet-singlet transition spectrum, and that for a transition between degenerate multiplets. The only distinction which can be drawn is that in the multiplet-multiplet case, the observed spectra are a superposition of bands with the same maximum and width. The maximum number of such bands is equal to the number of irreducible representations in the direct product $\Gamma_1 \times \Gamma_2$ where Γ_1 and Γ_2 are the irreducible representations labelling the two multiplets.

Perlin[50] has obtained similar results for the case of transitions from a singlet to a multiplet, and has also proposed that the temperature dependency of the zero-phonon line-width is given by

$$\hbar\Gamma_o = \pi \sum_i \sum_{x \neq y} \omega_i^2 |M_{xy}|^2 \, n(\omega_i) \delta(\hbar\omega_i - h\Delta_{xy}) \qquad (4.12)$$

for the zero-phonon line corresponding to the transition from the ground state singlet to the state $|y\rangle$ of the multiplet. M_{xy} is the matrix element describing the (phonon) coupling between the state $|y\rangle$ and the other states $|x\rangle$ of the multiplet: $\hbar\Delta_{xy}$ is the energy spacing between the states $|x\rangle$ and $|y\rangle$.

Perlin's results have been further generalised to include multiple - multiplet transitions without affecting his main conclusions[51].

It should be stressed however that all of these calculations[49,50,51] include only linear electron lattice coupling, and that for instance splitting of zero-phonon lines may occur through inclusion of higher order coupling terms. (It was noted in 3.5 that quadratic electron-lattice coupling could remove the vibronic degeneracy caused by the Jahn-Teller effect within a multiplet.) Higher order coupling might also be expected to produce further temperature dependencies of the zero-phonon line through terms analogous to eq (4.11).

4.4 Broadening Mechanisms

Although the temperature-dependent broadening of zero-phonon lines, and the mechanisms by which it occurs is implicit in the discussion of 4.2 and 4.3, this section will consider intuitively appealing models of these mechanisms, and obtain the temperature dependencies of zero-phonon linewidths more explicitly. The first mechanism to be considered will be that embodied in eq (4.11) for transitions between singlets, because an analogous process will be shown to occur for transitions between multiplets.

From eq (4.11) it is obvious that the broadening mechanism arises from the quadratic coupling terms of eq (4.4). That is, the broadening arises from terms which include products of phonon annihilation and creation operators. To be specific, the broadening may be pictured

as the creation (annihilation) and subsequent annihilation (creation) of a phonon, the intermediate state of the system being a 'virtual' one. Such a process effectively decreases the lifetime of the state, and, by the Heisenberg Uncertainty Principle, causes an increase in the energy uncertainty, i.e. a broadening. This is essentially the same mechanism that has been proposed[52] for the broadening of magnetic resonance lines. The relationship between the broadening of zero-phonon lines and magnetic resonance lines has been discussed in detail by Maradudin[47] and McCumber[53]. The temperature dependence of this mechanism has been obtained in more explicit form as[54]

$$\Gamma_o(T) \propto \left(\frac{T}{T_D}\right)^7 \int_0^{T_D/T} \frac{x^6 e^x}{(e^x-1)^2}\, dx \qquad (4.13)$$

where T_D is the Debye temperature and $x = \hbar\omega/kT$. This expression was obtained under the assumptions of a Debye phonon spectrum of acoustic modes, neglecting the effects of optical modes, and that the quadratic coupling constants (the v_{ij} of eq (4.11) are independent of temperature. These are the same assumptions up to a point, since the v_{ij} can be shown[47] to be temperature independent if interaction with acoustic modes only is considered. Often eq (4.13) is taken to be valid only for acoustic modes, but Maradudin[47] has shown that an expression of the form of eq (4.13) should be a reasonable approximation even if interaction with optical modes is considered.

At low temperatures $T << T_D$, eq (4.13) gives that $\Gamma_o(T)$ varies as T^7, whereas at high temperatures it varies as T^2. (The integral in eq (4.13) has been tabulated by Ziman[55].)

The broadening mechanism obtained in 4.3 for the zero-phonon line of a singlet-multiplet transition has a very simple intuitive explanation -

namely that a given state $|x\rangle$ of the multiplet may relax (be excited) into another state of the multiplet by the creation (annihilation) of a phonon. Hence the obvious condition for this to occur is that the energy separation of the state $|x\rangle$ from the other states of the multiplet be less than the maximum phonon energy : this was the original definition of a multiplet in 4.3. Similar processes involving the creation (annihilation) of two or more phonons have been investigated by Kiel[56] who found

(i) the transition probability for the process decreases as the number of phonons involved increases

(ii) the higher-order (i.e. more than one-phonon) processes are essentially temperature independent.

The presence of such one-phonon (direct) processes contributes a temperature-dependent width to zero-phonon lines which may be expressed as[54,57,58,59]

$$\Gamma_o(T) = \pi \sum_{x<y} \beta_{yx} [n(\omega_{yx}) + 1] + \pi \sum_{x>y} \beta_{yx}\, n(\omega_{yx}) \qquad (4.14)$$

where (i) $n(\omega_{yx})$ is the number of phonons with frequencies corresponding to the energy differences $\varepsilon_x - \varepsilon_y$ between the states $|x\rangle$ and the state $|y\rangle$ within the multiplet,

(ii) β_{yx} contains the density of phonon states of energy $\hbar\omega_{yx}$.

Eq (4.14) gives the broadening of the zero phonon line for the transition from some ground state (not vibrationally coupled to the multiplet) to the state $|y\rangle$ of the multiplet caused by the linear coupling of the state $|y\rangle$ to other states $|x\rangle$ in the multiplet. The first summation is over those states $|x\rangle$ for which $\varepsilon_x < \varepsilon_y$ and so a phonon is created. The second summation is over those states $|x\rangle$ for which $\varepsilon_x > \varepsilon_y$ and so a phonon is annihilated.

For very low temperatures $n(\omega_{yx}) \to 0$ and so eq (4.14) is dominated by the factor 1 in the first summation and thus reduces to

$$\Gamma_0(T) = \pi \sum_{x<y} \beta_{yx} \qquad (4.15)$$

Thus the process involving the annihilation of a phonon vanishes - there are so few phonons available at such low temperatures that the probability of absorbing one is vanishingly small. Since β_{yx} is a measure of the density of states, not their occupation, it is temperature independent, and so the direct process gives no temperature dependence for sufficiently low temperatures.

When quadratic electron-lattice coupling is considered for transitions between multiplets, where the multiplets are not vibrationally coupled to each other, it might intuitively be expected that an identical process to the one giving the broadening of the zero phonon line in singlet-singlet transitions would occur. However it is feasible that an additional broadening mechanism might occur which is identical to the two-phonon (Raman) process except that the intermediate state need not be a virtual one, but could be a real state of the multiplet. Such a process, two-phonon with a real intermediate state, is known as a resonant-Raman or Orbach process. It was first considered as a spin-lattice relaxation mechanism in electron spin resonance[60,61]. This process has rarely been considered in connection with optical spectra (eg mentioned but disregarded in[57]), but its presence is fully appreciated in magnetic resonance studies (see for example[62]).

In order to understand how the resonant-Raman process occurs it is necessary to examine more closely the perturbation technique used in [54] to obtain the normal-Raman process. This calculation is essentially dependent on second-order terms (first order terms give the direct process) of the form[62]

$$\sum_{I,i} \left| \frac{\langle y|V'|I\rangle\langle I|V'|y\rangle}{\hbar\omega_i - \hbar\omega_{yx}} \right|^2 \qquad (4.16)$$

where the $|I\rangle$ represent intermediate states and $\hbar\omega_{yx}$ represents the energy difference between the real state $|y\rangle$ and the real state $|x\rangle$. The state $|x\rangle$, another member of the multiplet containing $|y\rangle$, is a member of the set of intermediate states $|I\rangle$. For singlet-singlet transitions it is assumed that neither of the singlets is vibrationally coupled to another real state - $\hbar\omega_i \ll \hbar\omega_{yx}$ for all i and so the denominator of the expression (4.16) can never be zero. However when the state $|y\rangle$ is a member of a multiplet then it is possible for $\hbar\omega_i = \hbar\omega_{yx}$ where $|x\rangle$ is some other real state of the multiplet, and it is thus possible for the denominator of the expression (4.16) to vanish. The mathematical treatment of such a divergence is to add a complex quantity (actually related to the half-width, and hence lifetime of the intermediate state) to the denominator, complete the calculation, and then set this complex quantity equal to zero. Such a procedure was first used in a different context by Heitler[63]. McCumber [64] has given a divergence-free calculation for this process.

This calculation yields two temperature-dependent contributions to the zero-phonon linewidth. The first as expected, is exactly the same as that for a Raman-broadened transition between singlets, described by eqs (4.11) and (4.13). This arises from the non-resonant terms of the expression (4.16). The second contribution is the resonant-Raman or Orbach process from those terms of (4.17) where the demoninator vanishes. This yields a temperature-dependent width to the zero-phonon line of [62]

$$\Gamma_o = \frac{A}{\exp(\frac{\hbar\omega_{yx}}{kT})-1} \xrightarrow[T \to 0]{} A\exp(-\frac{\hbar\omega_{yx}}{kT}) \qquad (4.17)$$

where a Debye distribution of phonons is assumed, and also that there is only one other real state $|x\rangle$ which is coupled to the state $|y\rangle$. Thus from eqs (4.13) and (4.17), the width of the zero phonon line arising from quadratic coupling terms within a multiplet is

$$\Gamma_o = A\exp(-\frac{\hbar\omega_{yx}}{kT}) + BT^7. \qquad (4.18)$$

It should be stressed that the Orbach process is not of 'higher-order' than the Raman one - they both arise from the same quadratic electron-lattice coupling terms. A fuller discussion of these broadening mechanisms is given in [62] and [65].

4.5 Other Contributions to Zero-Phonon Linewidths

First of all, in principle, the width of the line from any optical transition is limited by the radiative lifetimes of the two states involved. If one of these states is a 'ground' state then, since this has effectively infinite lieftime, the limiting factor in the width of the optical line is the radiative lifetime of the excited state. Because this lifetime is non-infinite, the Heisenberg Uncertainty Principle predicts an uncertainty in the energy of the state and hence a broadening of the optical line. Lifetime broadening is a homogeneous broadening and hence results in a lorentzian lineshape[66]. The broadening mechanisms discussed in 4.4 cause a decrease in the lifetime of a state involved in the transition and thus are all examples of lifetime broadening, leading to a lorentzian lineshape.

A broadening mechanism which has not previously been discussed is due to the anharmonicity of lattice vibrations. To appreciate this process fully it is easiest to consider the consequences of electron-lattice coupling to a single (anharmonic) mode. For an

anharmonic oscillator, the energy eigenvalues are not equally spaced. Thus the transitions which make up the zero-phonon line will have slightly different energies and so a broadening of the line will occur. This problem has been treated in detail by a number of authors[67,68] but unfortunately the experimental consequences are not absolutely clear.

In some cases the anharmonic effects have been considered only as giving a lorentzian contribution to the linewidth which is temperature-independent ([43] and references therein) and in other relatively detailed experimental studies[54,57,69] the contribution has been ignored altogether. The justification for this neglect is tenuous, but to an extent is validated by the experimental results. Rebane[19] has attempted to justify the neglect of anharmonic lattice effects at very low temperature using the argument that only the ground vibrational state of the electronic level contributes to the zero-phonon line (i.e. it is a purely electronic line rather than a quasiline) so that it cannot have contributions from transitions with energies other than that of the purely electronic line.

One broadening mechanism which cannot be ignored in an experimental study of zero-phonon lines is that due to inhomogeneities of the host crystal lattice. Even the most carefully grown specimens will not have exactly the same structure from unit cell to unit cell. Microscopic strains, lattice defects, etc., all serve to make the crystalline field 'seen' by an impurity vary slightly from ion to ion. Intuitively one would expect this variation to be a random distribution, and lead to a corresponding random variation in the zero-phonon line energies at different sites. Thus if the zero-phonon line from each impurity ion is a lorentzian, then the observed zero-phonon line would be a

gaussian envelope of lorentzian lines, so that the observed line would be a gaussian-lorentzian mixture. A comprehensive review of strain broadening has been written by Stoneham[70]. For present purposes it is sufficient to note that the contribution of strain broadening to the total linewidth is independent of temperature to a good approximation, although this cannot be rigorously justified[71]. The major effect of such inhomogeneous broadening (assuming it is temperature independent) is to complicate the interpretation of experimental data, and this point will be more fully discussed in Ch. 6.

CHAPTER 5

Experimental Details and Raw Data Processing

5.1 Crystal Growth

Zinc selenide was synthesised from the elements, whereas ZnS powder of Optran quality was purchased from BDH chemicals. For both materials manganese was incorporated and solid boules subsequently grown by vapour transport. A mixed crystal $ZnSe_xS_{1-x}$:Mn was grown in a similar way starting with a mixture of ZnSe and ZnS powders.

All samples used in the experiments to be described were grown by various other members of the research group, whose contribution in this respect is gratefully acknowledged.

5.2 Composition of the Mixed Crystal $ZnSe_xS_{1-x}$:Mn

The composition of the mixed crystal $ZnSe_xS_{1-x}$:Mn can be measured in a variety of sophisticated ways[72,73], but a much simpler method, commonly used by physical chemists and crystallographers appears to have been overlooked, namely that of density determination.

If ρ_c, the density of the mixed crystal, is accurately measured then,

$$\rho_c = x\rho(ZnSe) + (1-x)\rho(ZnS) \qquad (5.1)$$

where[74]

$$\rho(ZnSe) = 5.42 \text{ gm/cc}$$

$$\rho(ZnS) = 4.102 \text{ gm/cc (for cubic structure)} .$$

The density of the mixed crystal was determined by first of all weighing it, to give its mass M_c, then weighing it again, immersed in a liquid of density ρ_L, giving M_c' where

$$M_c' = M_c - \rho_L V \qquad (5.2)$$

where V = the volume of the crystal.

Hence

$$\rho_c = \frac{M_c}{V} = \frac{\rho_L M_c}{M_c - M'_c} \qquad (5.3)$$

This procedure was performed with immersions in water and ethanol, giving the results of Table (5.1). These results, together with eq (5.1), yield a composition for the mixed crystal of (73 ± 2)% ZnSe, (27 ± 2)% ZnS. The ratio of ZnSe to ZnS in the original powder mix was 4:1.

In Fig. (51.) the dependence of the energy gap of the mixed crystal is shown as a function of composition, from [72,73] and from this the energy gap is seen to be (2.95 ± 0.05)eV.

5.3 Absorption Measurements

Highly-polished (one micron finish) samples were mounted on a gold-plated copper cold finger attached to a reservoir of liquid helium. The cold finger was perforated and the cryostat was fitted with Spectrosil(B) windows to allow light to pass through the sample.

The light source used was a 50W tungsten filament bulb. The transmitted light was mechanically chopped at a frequency of 735 Hz before being passed into a Monospek 1000 monochromator with a dispersion of 8Å/mm. Scattered light inside the monochromator was less than 0.1% of incident radiation. By using such an undispersed source as a tungsten filament bulb, the light intensity is constant in time at all wavelengths, and the occupancy of energy levels in the sample reaches a steady state, which does not change with time.

The detector used was a photomultiplier with an S20 photocathode, whose output was amplified by a lock-in device and then displayed on a chart-recorder.

Temperature measurement within the cryostat was by means of a gold-

iron/chromel thermocouple whose output was measured by means of a Thor Cryogenics temperature controller. The reference junction of the thermocouple was maintained at the water triple point, by means of a triple point cell. For the temperature-dependent measurements, the controller was used to supply heat to the cryostat (via a heating coil wound on the cold finger) at a rate proportional to, proportional to the differential of, and proportional to the integral of the difference between the temperature in the cryostat and any (higher) required temperature. Temperature measurement and control within $0.1^{\circ}K$ could be achieved in this way. The lowest attainable temperature in this system was $6^{\circ}K$.

Besides the precise control of temperature, the apparatus had to be capable of high resolution, in order to measure small changes in linewidth, and also have a high signal to noise ratio. To an extent these criteria were mutually exclusive. Since most of the noise in the system was instrument noise, the easiest way to increase the S/N ratio was to increase the signal strength, without causing overloading at any point in the detection system. This could most simply be achieved by using wider entrance and exit slits on the monochromator. However this has the effect of decreasing the optical resolution of the system. The S/N ratio could also be improved by using large time-constants for signal averaging in the phase-sensitive detector. This also decreases the optical resolution, but such decreases can be offset by using very slow scanspeeds on the spectrometer. With the aim of the experiment being to measure small changes in linewidth, a minimum resolution requirement had to be set, which determines the spectrometer slit widths, and improvements in S/N ratio were achieved by using long time constants and slow spectrometer scanning speeds.

The overall system resolution was determined by measuring the widths of the lines in the Hg doublet 3131.55-3131.83Å in second order. The intrinsic width of these lines was assumed to be zero, so that any measured width could be attributed to the apparatus used to measure it. This method gives an over-estimate of the system-induced linewidth. The measured linewidth is a function of both the monochromator slit width and the time-constant for signal-averaging in the detection equipment, this latter being taken in conjunction with the scanning rate of the monochromator. With the monochromator slit width at the instrumental minimum of 0.005 mm, the measured linewidths were 0.15Å, i.e. the resolution of the system was 0.15Å or better. With the slowest possible scanning rate of 0.5Å/min, this resolution could be achieved with time constants of up to 5 secs. in the signal recovery equipment. This resolution (0.15Å) together with the maximum allowable time constant (5 sec) was used in all absorption measurements. Under these conditions the total signal to noise ratio was 45 dB. This figure is rather misleading however, since the zero-phonon line represents a perturbation on the total signal so that the zero-phonon line signal to noise ratio was only 26dB.

In experiments on the $^6A_1 \rightarrow {}^4E$ zero-phonon lines, the "background" signal varied rapidly over the extent of the lines. To combat this a ramp voltage generator was constructed and connected between the lock-in amplifier and the chart recorder. This device generated a voltage which changed linearly with time in the opposite sense to the change in the background signal. This ramp voltage was generated using a long time constant (600. sec), very stable, integrating amplifier. Electromechanical methods, such as motor driven potentiometers, were found to generate too much noise.

The measured signal in such an absorption apparatus, containing no sample, is

$$I_s(\lambda) = R(\lambda)I_o(\lambda) \qquad (5.4)$$

where $I_o(\lambda)$ = source intensity

$R(\lambda)$ is a slowly varying function of wavelength, measuring the effect of lenses, filters, spectrometer dispersion and detector response.

With a sample in the system, the measured signal is

$$I'_s(\lambda) = M(\lambda)I_s e^{-\alpha(\lambda)d} \qquad (5.5)$$

where $\alpha(\lambda)$ = absorption coefficient

$M(\lambda)$ is a slowly varying function of wavelength, measuring reflection and light scattering by the sample.

d = sample thickness .

Since absorption measurements of the zero-phonon lines were made over a wavelength range of approximately 15Å, $R(\lambda)$, $I_o(\lambda)$ and $M(\lambda)$ were assumed consatnt. Thus small changes in the measured signal, characterising zero phonon lines, are given by

$$\begin{aligned}\delta I'_s(\lambda) &= - dR(\lambda)I_o(\lambda)M(\lambda)e^{-\alpha(\lambda)d}\delta\alpha(\lambda) \\ &= - I'_s(\lambda)\delta\alpha(\lambda) \qquad (5.6)\end{aligned}$$

The absorption spectra are shown in subsequent sections as $\delta I'_s(\lambda)$ against λ and thus measure relative numbers of absorbed photons per unit wavelength range.

For the sake of completeness, anticipating the results presented in later chapters, it is noted here that for the $^6A_1 \rightarrow {}^4T_2$ transition $\delta I'_s(\lambda)$ from each chart was measured at intervals of 0.125Å and these data points were computer fitted to the equation

$$\delta I_s'(\lambda) = h_1 \exp\{-\frac{1}{2\sigma_1^2}(\lambda-\lambda_{01})^2\}+h_2 \exp\{-\frac{1}{2\sigma_2^2}(\lambda-\lambda_{02})^2\} \quad (5.7)$$

that is, two gaussian curves. Initial estimates for the peak heights (h_1,h_2) peak positions $(\lambda_{01}, \lambda_{02})$ and half-widths (through σ_1,σ_2) together with the data points, were used as initial values in a fitting program whose output was fitted values h_1', h_2', σ_1', σ_2', λ_{01}', λ_{02}'. The half-widths of the gaussian curves are simply related to σ_1 and σ_2 by

$$\text{half-width at half height} = \delta = (2\ell n2)^{\frac{1}{2}}\sigma \quad (5.8)$$

The justification for fitting the experimental lineshapes to gaussian curves is not simple and will be discussed in Ch. 6.

5.4 Lifetime Measurements

Unpolished (in order to minimise specular reflection) samples were placed in a vacuum cryostat in which the temperature could be varied from 100°K upwards, the upper limit depending only on the size of the heating coil used in the cryostat. Temperature measurement in this system was by means of a copper-constantan thermocouple. The light source used was a 50W tungsten-halogen bulb whose output was mechanically chopped before being passed through an Oriel interference filter (λ_{max} = 5200Å, half-width = 50Å) corresponding to the internal manganese transition $^6A_1 \rightarrow {}^4T_1$. The emitted light was passed through another interference filter (λ_{max} = 5800Å, half-width = 50Å) centred approximately on the peak of the Mn emission band. This emission was detected by a photomultiplier with an S20 photocathode whose output fed a linear gating amplifier which together with a scan delay generator formed a boxcar detector. The output from the boxcar was displayed on a chart recorder.

The major difficulty of this experiment is with the mechanical chopping of the incident beam. If the excited state involved in the transition has a long lifetime, then the incident light beam must be chopped slowly, so that

(i) the incident beam is switched off for a time which is long compared with the lifetime of the transition so that the system is allowed to relax completely.

(ii) the incident beam must be switched on for a time which is long compared with the transition rate so that excited state population can reach a steady state level.

Fulfilling the above two conditions however results in three further difficulties.

(iii) Since (i) and (ii) mean that the switching rate of the light beam is slow, and the signal to noise enhancement provided by the boxcar detector is essentially a function of the number of events over which it averages, the boxcar has to have a very long time constant supplied.

(iv) Since (iii) requires a very long time constant to be used in the detection system, the output rise time of the boxcar cannot respond to sudden changes of the measured signal - such as the point where the incident beam is switched from "on" to "off".

(v) With a low chopping speed, stability in the chopping device becomes a problem. This can be overcome by using a quartz-locked synchronous motor to drive the chopping blade. However since the chopping blade is moving slowly it takes a finite time to traverse the incident beam. The effect of this is

essentially to make the rise time of the boxcar output an unimportant parameter - the rise time of the detection system is dominated by the time taken to switch the incident beam from "on" to "off".

The effect of these factors on experimental data is mainly that, if the time during which the incident beam is being switched off is t_1 (starting at $t = 0$, beam fully off at $t = t_1$), then

(a) the apparent decay of the luminescence between $t = 0$ and $t = t_1$ is a function of the apparatus

(b) the point $t = 0$ is difficult to obtain because of the effect of the system rise time.

Again, in order to explain the method used to analyse the raw data of these lifetime experiments, it is necessary to anticipate the results presented in Ch.7. With a decay which is exponential in time, the intensity at any time may be written,

$$I(t) = I(t = 0)e^{-t/\tau} \qquad (5.9)$$

where τ is the lifetime of the excited state. The most obvious way to evaluate τ is to use

$$\ell n\left(\frac{I(t)}{I(t=0)}\right) = -t/\tau \qquad (5.10)$$

but in practice this is inconvenient for two reasons. As mentioned above, the point $t = 0$ is difficult to determine accurately from the raw data, and also to obtain $I(t=0)$, $I(t=\infty)$ must be known. In principle $I(t=\infty)$ is zero but for accuracy, this would have to be checked for every chart, which would be very time consuming. For these reasons it is both more convenient and more accurate to use a difference method[75] to analyse the data. Eq(5.9) may equivalently be written

$$I^*(t) = I^*_o(1 - e^{-t/\tau}) \qquad (5.11)$$

where $I^*(t) = I(t=0) - I(t)$

$I^*_o = I(t=0) - I(t=\infty)$.

Thus

$$I^*(t+T_m) = I^*_o(1 - e^{-(t+T_m)/\tau}) \qquad (5.12)$$

where T_m is some known time interval. Then from eqs (5.11) and (5.12)

$$I^*(t) = I^*(t+T_m)e^{T_m/\tau} + I^*_o(1-e^{T_m/\tau}) \qquad (5.13)$$

All factors in the second term on the RHS of eq (5.13) are constants for a given chart, and thus a graph of $I^*(t)$ against $I^*(t+T_m)$ yields a gradient $e^{T_m/\tau}$ where T_m is a known quantity and τ is the required lifetime.

5.5 Thermal Quenching Measurements

The apparatus used was essentially the same as that for the lifetime measurements, except that the light source was a monochromator and the exciting light was not chopped. Also the photomultiplier measuring the emitted light was connected directly to a digital voltmeter. This experimental arrangement is such that, if $I(\lambda)d\lambda$ is the intensity of emitted radiation in the wavelength range $d\lambda$ and the exit filter bandpass characteristic is given by $J(\lambda)$, then the measured intensity is given by

$$I_m = \int_0^\infty J(\lambda)I(\lambda)d\lambda \qquad (5.14)$$

In the presentation of data I_m is shown as a function of temperature.

Table 5.1

Liquid	ρ_L (gm/cc)	M'_c (gm)	V (cc)	ρ_c (gm/cc)
water	0.997 ± 0.001	1.610 ± 0.001	0.397 ± 0.002	5.05 ± 0.02
ethanol	0.789 ± 0.001	1.694 ± 0.001	0.395 ± 0.002	5.08 ± 0.02

M_c, the mass of the crystal was 2.006 ± 0.001 gm.

Note. The alloy composition measured in this way is consistent with that obtained from measurements of the absorption edge. The concentration of manganese in all samples is determined by crystal preparation conditions and is less than 1%.

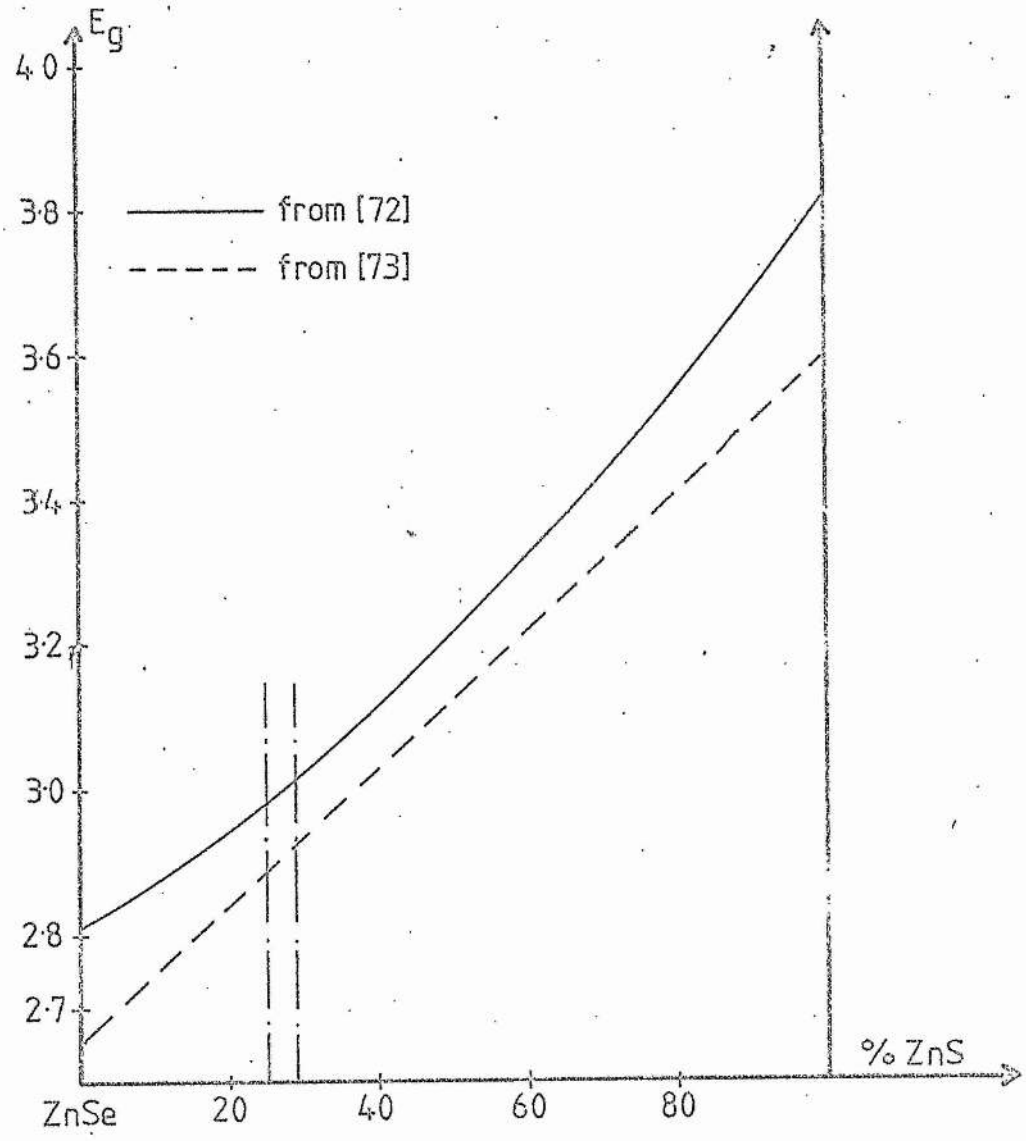

Fig 5·1

Variation of energy gap width E_g with mixed crystal composition

CHAPTER 6

Zero-Phonon Line Measurements

6.1 Introduction

Manganese, as the free atom, has the electronic configuration $(A)3d^5 4s^2$, where (A) represents the electron configuration of argon. As an impurity in ZnSe it substitutes for the zinc cation[76]. A simple model, proposed by Ludwig and Woodbury[76,77] is that enough electrons are removed from the impurity to satisfy the bonding requirements - in this case two electrons. This leaves the manganese substitutional impurity with the configuration $(A)d^5$ which has been confirmed by electron spin resonance measurements[78,79]. In cubic ZnSe crystals the environment of the Mn ion is tetrahedral in form. The ground state of the free Mn ion with configuration $(A)d^5$ is ^6S which in a cubic field means that the orbitals transform as bases of the totally symmetric representation A_1, and the state is labelled $^6A_1$. Since the ground state angular momentum is zero, there is no spin-orbit splitting and since this state is orbitally non-degenerate, there is no Jahn-Teller splitting. The first excited state of the free ion is ^4G, which, under the influence of a cubic field splits into four states, conventionally labelled $^4T_1$, $^4T_2$, $^4A_1$ and ^4E. The identification of these states of Mn in ZnSe was performed by Langer and Richter[80] after a study of both absorption and emission spectra. The lowest energy transition $^6A_1 \rightarrow {}^4T_1$ appeared to have no observable zero-phonon lines in absorption, but the $^6A_1 \rightarrow {}^4T_2$ transition showed a zero-phonon line doublet at 5100-5102.6Å (19598-19608 cm^{-1}). The same authors also note that the $^6A_1 \rightarrow {}^4A_1$, ^4E zero phonon line occurs at 4737.1 Å (21110 cm^{-1}).

Theoretically the energy levels of a d^5 ion in cubic symmetry can be obtained from the work of Orgel[81] or Sugano and Tanabe[82]. These treatments show that if the impurity ion orbitals are considered to be d-orbitals then the $^4A_1$ and ^4E levels are degenerate.

In this chapter the $^6A_1 \rightarrow {}^4T_2$ zero phonon line is investigated in detail, with a briefer study of the $^6A_1 \rightarrow {}^4E$ line. Throughout the following discussion, the notational convention[83,84], where Mulliken's notation is used for irreducible representations when the spin-orbit interaction is ignored and Bethe's notation is used when the spin-orbit interaction is included, will be adopted.

6.2 Experimental Results, $^6A_1 \rightarrow {}^4T_2$ Transition

As has already been noted, the observed zero-phonon line shape (see for example Fig (6.1)) is expected to be a combination of lorentzian and gaussian distributions, commonly known as a Voigt profile. For such a lineshape, the intensity distribution can be written[66]

$$I(a,v) = \int_{-\infty}^{\infty} \frac{e^{-y^2}}{a^2 + (v-y)^2}\, dy \qquad (6.1)$$

where $v = (\nu-\nu_o)/\frac{1}{2}\Delta\nu'_G$ is the distance measured from the line centre in units of $\frac{1}{2}\Delta\nu'_G$.

$\Delta\nu'_G = (2\ell n2)^{-\frac{1}{2}}\Delta\nu_G$ where $\Delta\nu_G$ is the half width of the contributing gaussian component

$a = \dfrac{\Delta\nu_L}{\Delta\nu_G}$ where $\Delta\nu_L$ is the half-width of the contributing lorentzian line.

The analytic solution of (6.1) is not possible, and even a numerical solution has great difficulties[85]. However it has also been demonstrated[86,87] that the gaussian and lorentzian contributions can be calculated to a good approximation by

$$(\Delta\nu_{obs})^2 = (\Delta\nu_G)^2 + (\Delta\nu_L)^2 \qquad (6.2)$$

The degree of accuracy of this approximation is treated by Posener[85] who has shown

(i) eq (6.2) is exact (trivially) if $\Delta\nu_L = 0$

(ii) the maximum error caused by using eq(6.2) is when $\Delta\nu_G$ is equal to $\Delta\nu_L$, and this condition gives an error of ~10% in $\Delta\nu_{obs}$.

Making the assumption that the strain-induced width is temperature independent, this gaussian contribution can be obtained as the T=0 width of the observed spectral line so that eq (6.2) becomes

$$\{\Delta\nu_L(T)\}^2 = \{\Delta\nu_{obs}(T)\}^2 - A \qquad (6.3)$$

where $$A = (\Delta\nu_G)^2 \neq f(T)$$

In fact, for a single Voigt profile, if the values of $\Delta\nu_G$ and $\Delta\nu_{obs}$ are known, $\Delta\nu_L$ may be obtained directly from the numerical tables compiled by Posener[85]. In the present case however, the zero-phonon line is a doublet and this must be separated into two distinct components first. There are three possibilities

(i) fit the data to two overlapping Voigt profiles. This is the exact solution, but involves computer fitting with eight parameters the complicated expression in eq (6.1)

(ii) fit the data to two overlapping lorentzian curves. Since any broadening of the zero-phonon lines will be a broadening of the lorentzian component of the lineshape, this is intuitively appealing. However at low temperatures, the lineshape will be predominantly gaussian and so for these temperatures this is a bad approximation

(iii) fit the data to two overlapping gaussian curves. Because of the dominance of the gaussian contribution at low temperatures this would give the best agreement with data points.

Thus at low temperatures the lineshape is predominantly gaussian and so can accurately be represented by a pure gaussian. In fact all lineshapes at all temperatures were fitted to gaussians and thus this fit becomes progressively worse as temperature increases. This is still not a simple calculation as to fit two overlapping gaussian curves requires six parameters, and in fact with the experimental curves which have a 'background' variation as well, nine parameters were fitted - three to account for the background which was approximated by a quadratic.

Typical spectra for T = 7, 13 and 15°K are shown in Figs (6.1), (6.2) and (6.3) respectively where the solid curves represent the gaussian lineshapes to which the data points were fitted. Fig (6.4) gives the dependence of the half-width at half-maximum on temperature. From this figure, the strain-induced widths were taken to be 0.465Å (1.78 cm^{-1}) for the line at lower energy, and 0.7175Å (2.75 cm^{-1}) for the line at higher energy. The solid curves in Fig. (6.4) correspond to the equation

$$\Delta\nu_{obs} = \{(\Delta\nu_G)^2 + [A\exp(-\frac{E}{kT})]^2\}^{\frac{1}{2}} \qquad (6.5)$$

with the appropriate values of $\Delta\nu_G$ as given above and with E = 2.5 meV for the line at lower energy and E = 2.2 meV for the line at higher energy. The separation of the two lines was found to be 3.0 ± 0.1Å (11.5 cm^{-1}) at all measured temperatures, and no perceptible shift of the lines with temperature was observed, although the fact that

the spectrometer used could only reproduce absolute wavelength measurements to within $\pm$ 0.5Å (caused by take-up slack in the gearing mechanism) may have masked any such absolute displacement.

6.3 Discussion, $^6A_1 \rightarrow {}^4T_2$ transition

The main features of the experimental results requiring explanation are

(i) the fact that only two lines are observed where more might have been expected

(ii) the separation of the two lines which are observed

(iii) the temperature dependence of the two lines

(Throughout the following discussion, the splitting of the $^6A_1$ ground state measured by electron paramagnetic resonance[78,79,88] as 10^{-3} cm^{-1} will be ignored).

Previous authors (whose work will be subsequently discussed) have observed a doublet zero phonon line for this transition in both ZnS:Mn and ZnSe:Mn. The value for the separation of the two components has been more accurately obtained in the present work. The temperature dependence of the lines in ZnSe:Mn has not previously been reported and, as will be shown, this feature allows a more accurate determination of splittings within the $^4T_2$ manifold to be made.

The occurrence and separation of the two zero-phonon lines arising from the $^6A_1 \rightarrow {}^4T_2$ transition has been treated generally by Koidl[89] who attempted to explain the splittings of both the $^4T_1$ and $^4T_2$ states of manganese for a variety of systems in which it is tetrahedrally coordinated. Taking into account only first order spin-orbit coupling, both the $^4T_1$ and $^4T_2$ levels split into four components, conventionally labelled Γ_6, Γ_7 (both Kramer's doublets) and two Γ_8 levels, $\Gamma_8(3/2)$ and

$\Gamma_8(5/2)$. For the $^4T_2$ state the Γ_6 Kramer's doublet and the $\Gamma_8(5/2)$ levels are degenerate, whereas, for the $^4T_1$ state the Γ_7 Kramer's doublet and the $\Gamma_8(3/2)$ levels are degenerate, so that in either case three levels would be observed. The inclusion of second-order spin-orbit coupling effects removes the degeneracy of the Γ_6 and $\Gamma_8(5/2)$ levels in the $^4T_2$ state and the Γ_7 and $\Gamma_8(3/2)$ levels in the $^4T_1$ state. The overall splittings predicted in this way are $\sim$70 cm^{-1} for the $^4T_1$ state and $\sim$120 cm^{-1} for the $^4T_2$ state (see figs (6.5) and (6.6)). This contrasts with the observed splittings of the $^4T_1$ state in ZnSe:Mn of 20 cm^{-1}(80) and 10cm^{-1}(80) or 11.5 cm^{-1} (this work) for the $^4T_2$ state. To explain the discrepancy, Koidl then considers the effect of a Jahn-Teller interaction with either E or T_2 modes. As explained in 3.6 quenching of the spin-orbit interaction may then take place through the action of the Ham effect. This calculation was performed under the usual assumptions (see 3.5) of coupling with a single mode of either T_2 or E symmetry, with a single effective frequency. The results of these calculations are shown in Fig. (6.5) (reproduced from Koidl(89)) for the $^4T_1$ state and Fig. (6.6) (evaluated from parameters given by Koidl(89)) for the $^4T_2$ state. These results were obtained by assuming a Jahn-Teller coupling to an E vibrational mode. For a strong Jahn-Teller effect, the four distinct energy levels merge into two, whose splitting is consistent with observed splitting for all (ie. ZnS:Mn, CdS:Mn, GaP:Mn) materials studied except ZnSe:Mn.

There is a flaw in the analysis however in that Koidl appears to have treated the spin-orbit interaction as a perturbation on the energy levels determined by the Jahn-Teller effect, regardless of the strength of the Jahn-Teller interaction. If this is weak then it should be treated as a perturbation on the spin-orbit interaction and

not vice versa. Fortunately other authors have treated the problem of the $^4T_1$ state in ZnS:Mn[90] and ZnSe:Mn[91] and have agreed as to the general description of the two zero-phonon lines arising from a strong Jahn-Teller coupling to E modes - i.e. the region where Koidl's calculation is valid.

The discrepancy between the theoretical values obtained by Koidl and those obtained experimentally for ZnSe:Mn was attributed by him to the effect of covalency[92,93]. This effect arises through the admixture of ligand (i.e. Se) orbitals, which are p-functions, into the central ion d-functions. There will be symmetry limitations on the possible admixtures, caused by the requirement that the total wavefunctions still transform as bases of the irreducible representations (in the cases under discussion either T_1 or T_2). In this way the effect of the ligands on the first-order spin-orbit coupling may be written[92]

$$\mathcal{H}_{so} = \sum_{\mu,i} \xi^{\mu} \underline{\ell}_i(\mu).\underline{s}_i \qquad (6.6)$$

where the summation over μ is over the central ion plus the four ligands, ξ^{μ} is the one-electron spin-orbit constant of the μ-th ion, and $\underline{\ell}_i(\mu)$ the orbital angular momentum of the i-th electron of the μ-th ion, centred at the origin of the μ-th ion. From eq (6.6) it is readily seen that the first order spin-orbit interaction depends on the spin-orbit constant of the ligands, which as a crude approximation is dependent on the mass of the ligands, and so the effect should be greater for selenium ligands than for sulphur ones.

As given in eq (6.6), the effect of the ligands is a first-order one in the spin-orbit coupling, and according to Koidl[89], the first order spin-orbit coupling is fully quenched by the strong Jahn-Teller

effect. However the effect of covalency in determining the residual splitting of the states in the $^4T_1$ or $^4T_2$ manifold would then appear in second order spin-orbit interactions, although this calculation has not been performed.

Using the same model as Koidl[89], Parrot et al[91] claim reasonable agreement between theory and experiment for the splitting of the $^4T_1$ state of ZnSe:Mn, without considering the effect of covalency. This is due to a more accurate experimental determination of this splitting (obtained as 11.5 cm^{-1}[91]) than the value 20 cm^{-1}[80] used by Koidl[89] for comparison with his theoretical value of $\sim$7.5 cm^{-1}. A comparison of theoretical and experimental values for the splittings of the $^4T_1$ and $^4T_2$ states is given in table (6.1) for both ZnSe:Mn and ZnS:Mn.

Study of table (6.1) reveals that Koidl's[89] model of strong Jahn-Teller coupling with an E vibrational mode gives approximately correct values of the splittings for the $^4T_1$ and $^4T_2$ states in ZnS:Mn and also for the $^4T_1$ state in ZnSe:Mn.

The model proposed by Koidl cannot however explain the splitting of the $^4T_2$ manifold in ZnSe:Mn, although including the effects of covalency to second order in the spin-orbit interaction would be an interesting calculation. As noted by Fournier et al,[90] the $^4T_1$ state appears to be more strongly coupled to the lattice than the $^4T_2$ state (see 4.1 and ref. (41)) and so might be expected to experience a stronger Jahn-Teller effect. This fact, together with the results of uniaxial stress measurements has led to a different model being proposed for the $^4T_2$ states in both ZnS:Mn and ZnSe:Mn[97.98], namely one in which the spin-orbit interaction and Jahn-Teller interaction are of approximately equal magnitude, so that neither can be

treated as a perturbation on the other. (This approximation cannot be obtained from Figs. (6.5) and (6.6) since the calculations leading to these diagrams are valid only for a strong Jahn-Teller effect.) Due to the difficulty in diagonalising the Hamiltonian with respect to the spin-orbit and Jahn-Teller effects simultaneously, only spin-orbit interactions within the $^4T_2$ manifold were considered, with no allowance for covalent effects except that the spin-orbit coupling strength was treated as a parameter. The Jahn-Teller coupling strength was also treated as a parameter. The experimental observations[97] for ZnSe:Mn were best fitted by taking the spin-orbit coupling parameter as 750 cm^{-1} (against $\sim$ 400 cm^{-1} [4] for the free Mn ion) and a Jahn-Teller coupling strength of 1.2 (measured in units of $\hbar\omega$, the coupling mode frequency taken as 75 cm^{-1} [92,99], this being the lowest energy peak in the phonon density of states). Fig. (6.7) shows the splittings of the $^4T_2$ state in ZnSe:Mn, determined from the data presented in[97] as a function of Jahn-Teller coupling strength, for a spin-orbit constant of 750 cm^{-1}. The occurrence of only two lines was also explained in this work[97] on the basis of the relative dipole strengths of transitions from the $^6A_1$ level to various states within the $^4T_2$ manifold. These are shown in Fig. (6.8) as a function of Jahn-Teller coupling strength for a spin-orbit parameter of 750 cm^{-1}, from which it can be seen that only two levels, $\Gamma_8(5/2)$ and Γ_6 have an appreciable dipole strength. The $\Gamma_8(3/2)$ line is weak, and the strength of the Γ_7 line is identically zero.

The splitting of the $^6A_1 \rightarrow {}^4T_2$ zero phonon line in ZnSe:Mn as measured here, is however 11.5 cm^{-1} (3Å, 1.42 meV), which would require (from Fig. (6.7)) a Jahn-Teller coupling strength of 1.6. Calculating

the relative peak heights from Fig. (6.8). one obtains 1.71 for a Jahn-Teller coupling strength of 1.2, and 1.73 for a Jahn-Teller coupling strength of 1.6, a difference which is hardly significant, bearing in mind that the absolute peak heights were determined in [97] by an arbitrarily chosen admixture parameter.

The major objection to the splitting values shown in Fig. (6.7) is in trying to fit the activation energies obtained from the Orbach broadening mechanism, given by eq. (6.5). These are 2.5 meV (20 cm^{-1}) for the $\Gamma_8(5/2)$ line and 2.2 meV (18 cm^{-1}) for the Γ_6 line, and should, according to the Orbach model, correspond to energy differences between real states. Such energy differences cannot be fitted on the splittings diagram of Fig. (6.7) .

However, re-evaluating the model presented in [97] for a spin-orbit coupling parameter of 675 cm^{-1}, the splitting of the $^4T_2$ manifold is then given by Fig. (6.9), where these energies can be fitted. Considerations of this diagram in conjunction with the activation energies of the $\Gamma_8(5/2)$ line (20 cm^{-1}) and the Γ_6 line (18 cm^{-1}) shows that the $\Gamma_8(5/2)$ line could be broadened by interaction with the Γ_7 level, and the Γ_6 line could be broadened by interaction with the $\Gamma_8(3/2)$ level. Since the $\Gamma_8(5/2)$-Γ_6 splitting decreases, for a given value of Jahn-Teller coupling strength, for decreasing values of the spin-orbit parameter, a Jahn-Teller coupling strength of 2.1 (in units of $\hbar\omega$=75 cm^{-1}) must be adopted to fit the zero-phonon line spacing. The peak heights are shown in Fig. (6.10) for a spin-orbit parameter of 675 cm^{-1}, and the ratio of these for a Jahn-Teller coupling strength of 2.1 is 1.68, compared with 1.71 for a spin-orbit parameter of 750 cm^{-1} and Jahn-Teller strength of 1.2 which was used in [97] to fit the experimental data.

The existence of an Orbach broadening mechanism for zero-phonon lines seems to have been very rarely considered, even in relatively detailed studies[43] (and references therein),[54, 100, 101, 102]. There appears to be only one report[103] of an exponential temperature dependence of zero phonon linewidth, although the information presented in this paper is rather sketchy. The system for which the effect was observed was for the $^2A_2 \rightarrow {}^3T_1$ transition of nickel in cadmium suphide. The orbital triplet state is split by a Jahn-Teller effect. The activation energy for the broadening mechanism was obtained as 22 cm^{-1}.

At first sight it is surprising that broadening of zero phonon lines can be dominated by interaction with such low energy phonons, given that in ZnSe, the characteristic TA lattice phonon has energy 49 cm^{-1} [83] with the dominant local tetragonal mode phonon having energy 69 cm^{-1} [92] or 75 cm^{-1} [99]. The TA lattice phonon is the lowest frequency peak in the phonon density of states which has local tetragonal symmetry at the impurity site, and might be expected to dominate the average local tetragonal mode. However it should be remembered that the density of states for acoustic phonons is non-zero except, trivially, at zero energy so that phonons with energies 18 cm^{-1} and 20 cm^{-1} can and do exist. It still remains however, to account for the dominance of a second-order broadening mechanism utilising only a fraction of the phonon spectrum, over both a first order process utilising the same fraction of the phonon spectrum (i.e. only those phonons whose energy corresponds to the separation of actual states) and a second order process in which the whole of the phonon spectrum may play a part.

In the general argument presented by Orbach[60], it was shown that Orbach processes could dominate Raman ones, and be the major second order

contribution to spin-lattice relaxation, and his argument equally well applies to the broadening of zero phonon lines. That is, although the Orbach process utilises only a fraction of the phonon spectrum, the fact that the contribution is a resonant one, more than makes up for the scarcity of the phonons required for the mechanism (see eq. 4.16). The argument for the domination of the direct process by the Orbach one is however not so readily obtained.

To be specific, consider the broadening of the $\Gamma_8(5/2)$ level shown in Fig.(6.9). In order for this level to be broadened by a direct process, one of the following transition sequences must occur

(i) $\Gamma_8(5/2) + \hbar\omega \rightarrow \Gamma_6 \rightarrow {}^6A_1$

(ii) $\Gamma_8(5/2) + \hbar\omega \rightarrow \Gamma_7 \rightarrow {}^6A_1$

(iii) $\Gamma_8(5/2) + \hbar\omega \rightarrow \Gamma_8(3/2) \rightarrow {}^6A_1$

Given the relative dipole strengths (see Fig. (6.10)) for transitions from the states of the ${}^4T_2$ manifold to the ${}^6A_1$ ground state, the relaxation mechanisms $\Gamma_8(3/2) \rightarrow {}^6A_1$ and $\Gamma_7 \rightarrow {}^6A_1$ are unlikely and a transition from these states might more probably be either to the $\Gamma_8(5/2)$ or Γ_6 levels. Such a sequence would however represent an Orbach process. Nevertheless, these transitions from the $\Gamma_8(5/2)$ level might be expected to be more probable than one which has the Γ_6-level as its final state, since this latter is a lower energy transition and so fewer phonons are available for it to be made. (Such an argument, based on the scarcity of required phonons would also explain why the intermediate state of the Orbach broadening of the Γ_6 level is the $\Gamma_8(3/2)$ one and not the Γ_7 one). Essentially similar arguments, based on the relative dipole strengths of transitions from the various levels to within the ${}^4T_2$ manifold to the ${}^6A_1$ ground state may be used to explain

the dominance of an Orbach braodening mechanism being operative for the Γ_6 level.

Whilst the above yields a plausible argument for the existence of an Orbach broadening mechanism, definitive proof could only be obtained through detailed knowledge of phonon occupation numbers, including those for any local modes which might occur, as well as transition probabilities within the manifold. Neither of these could be readily obtained from either calculation or experiment. It is perhaps significant that the activation energies for broadening are approximately the same for the two levels, since this could correspond to the energy of some local low-frequency mode. The possible existence of such modes has been discussed by Boyn[104] whose arguments were used[103] to justify the existence of such low energy phonons (in this case 22 cm^{-1}) causing the broadening of $^3A_2 \rightarrow {}^3T_1$ transition of nickel in cadmium sulphide.

6.4 Conclusions, $^6A_1 \rightarrow {}^4T_2$ Transition

The width of the zero-phonon lines of the $^6A_1 \rightarrow {}^4T_2$ transition of manganese in ZnSe:Mn has been measured as a function of temperature, and the functional dependence has been shown to be characteristic of an Orbach broadening mechanism. There are relatively few measurements of zero phonon linewidth as a function of temperature over this temperature range with such high resolution, and the rapid broadening has previously been regarded as puzzling. Using the information from this broadening, namely that the activation energies correspond to separations between real states, it has been possible to propose a more accurate determination of the energy levels within the $^4T_2$ manifold. Previous interpretation[97] was based only upon

(i) the existence of two lines

and (ii) their separation.

It should however be noted that the model proposed in [97] and adopted here is one in which a number of approximations has been made. No account was taken of second order spin-orbit coupling outwith the $^4T_2$ manifold, and in addition covalency was only taken into account by assuming an isotropic spin-orbit coupling model, with the spin-orbit constant being treated as a parameter. The true energy level scheme could only be obtained theoretically by using two spin-orbit coupling constants (one for the central Mn ion and one for the Se ligands) and all second order spin-orbit effects arising from the interaction of the $^4T_2$ manifold with other multiplets of the central Mn ion, in conjunction with a Jahn-Teller effect.

It should also be remarked that some of the techniques developed to explain broadening of zero phonon lines[18,105] both ignore the possibility of Orbach processes and can lead to a surfeit of adjustable parameters[101] so that data can be fitted by a variety of broadening mechanisms.

6.5 Experimental Results, $^6A_1 \rightarrow {}^4A_1$, ^4E Transition

The zero-phonon line for this transition was observed at 4737 Å (21,110.5 cm^{-1}) in agreement with the work of Langer and Richter[80]. This line was very weak, and the signal to noise ratio which could be achieved was poor. For this reason a number of recordings were made and then a hand average of five of these was performed. The superposition was determined by the position of the centre of the line rather than absolute wavelength, because slack in the spectrometer gearing mechanism made absolute values of wavelength differ by $\pm$ 0.5 Å, which would have defeated the purpose of the hand-averaging process. A typical spectrum used in this process is shown in Fig. (6.11) and the hand-averaged spectrum is shown in Fig. (6.12).

Langer and Richter[80] saw only a single line; with better resolution (2 cm^{-1}) Blanchard et al[106] saw a single asymmetric line; with the resolution used here (0.25Å, 1 cm^{-1}) this line has been resolved into a triplet, with approximately equal spacing of its components = 0.5Å (2.23 cm^{-1}).

6.6 Discussion, $^6A_1 \rightarrow {}^4A_1$, ^4E Transition

This transition has been reported for the case of manganese in zinc sulphide[107,108] where a triplet zero-phonon line was observed. For the case of ZnSe:Mn the triplet had not been resolved in previouc work[106].

The existence of a triplet zero-phonon line for the case of ZnS:Mn has been interpreted[107] in terms of a model originally proposed by Koide and Pryce[109]. Within this model, the degeneracy of the ^4E and $^4A_1$ levels is removed by the effects of covalency. Covalency is taken into account by considering the impurity orbitals as being composed partly of a ligand orbital admixture, the effect of which is to introduce extra terms, dependent on the degree of admixture (sometimes known as the covalency parameter) into the energy matrices of Tanabe and Sugano[82]. This both shifts and removes the degeneracy of the ^4E and $^4A_1$ levels. This theory was then adapted to the case of tetrahedral symmetry[107] where the separation of the ^4E and $^4A_1$ levels is even more sensitive to slight covalent admixtures than in the octahedral case considered by Koide and Pryce[109]. The dipole strength of the $^6A_1 \rightarrow {}^4A_1$ transition has been found to be vanishingly small[108], a corollary of the feature that first order spin-orbit coupling couples the $^6A_1$ level only with the $^4T_1$ level[110], coupling between the $^6A_1$ level and the ^4E level is via a second order spin-orbit interaction

(as is coupling between $^6A_1$ and $^4T_2$ [97]) and coupling between the $^6A_1$ level and the $^4A_1$ level is via a third order perturbation.

Thus the three observed components of the zero-phonon line for the $^6A_1 \rightarrow {}^4A_1$, ^4E transition of manganese in ZnS:Mn have been attributed to the $^6A_1 \rightarrow {}^4E$ transition, where the ^4E state is split by spin-orbit effects. Within the ^4E state the orbital angular momentum is quenched so that the first order spin-orbit interaction is identically zero [2,109]. The splitting of the ^4E state is attributed [107,108] to second order spin-orbit interactions and spin-spin interactions. The dominant contribution to the second order spin-orbit interaction has been shown to arise from the coupling of the ^4E states to the high lying doublets in the energy level scheme of Mn [108], rather than from the closer quartet levels [107].

Essentially the same argument should apply to ZnSe:Mn; i.e. the degeneracy of the ^4E and $^4A_1$ levels should be lifted by covalency - intuitively one would expect the separation of the two levels to be even greater in ZnSe than in ZnS, because the greater spatial extent of the ligand (Se) wavefunctions in ZnSe would allow a greater admixture of these into the impurity ion wavefunctions. This, however, would be almost impossible to check because of the low dipole strength of the $^6A_1 \rightarrow {}^4A_1$ transition, which makes the precise value of the covalency parameter (degree of admixture) indeterminable.

The pressure dependence of the zero-phonon line in ZnSe:Mn, measured in [106], should however be the same as for ZnS:Mn which was reported in [108]. This however has been found not to be so. The second order spin-orbit and spin-spin interactions split the ^4E level into three levels, labelled Γ_6, Γ_7, Γ_8. The effect of a uniaxial stress [108] is

to cause mixing of these states, in such a way that the separation of the states becomes pressure dependent and can be expressed parametrically in the form[108]

$$E(\Gamma_6) = + \frac{3}{2}(X^2 + |Z|^2P^2)^{\frac{1}{2}}$$
$$E(\Gamma_8) = \pm \tfrac{1}{2}|Z|P \qquad (6.6)$$
$$E(\Gamma_7) = - \frac{3}{2}(X^2 + |Z|^2P^2)^{\frac{1}{2}}$$

where X is the zero-pressure splitting (determined by the second-order spin-orbit and spin-spin interactions), and Z is a parameter which determines the combined effect of changes in the spin-orbit interaction with the deformation of the crystal. (In eq (6.6) the unsplit, i.e. zero-pressure Γ_8 level is taken as reference.) For ZnSe:Mn however the splittings under pressure have been characterised by the parametric equations[106]

$$E(\Gamma_6) = + \frac{3}{2}|Z|P$$
$$E(\Gamma_8) = \pm \tfrac{1}{2}|Z|P \qquad (6.7)$$
$$E(\Gamma_7) = - \frac{3}{2}|Z|P$$

In principle the form eq (6.6) should also apply to ZnSe:Mn. In [106] the parameter X had to be taken to be zero because the triplet could not be resolved. Here the triplet has been resolved. Here, the triplet has been resolved and from the splittings shown in Fig. (6.12), $\frac{3}{2}X = 2.23\ cm^{-1}$.

With the zero pressure splittings of the ^4E level obtained here, the data presented in [106] can be reinterpreted using eq (6.6). With $\frac{3}{2}X = 2.23\ cm^{-1}$, the data from [106] yields $|Z| = 74 \times 10^{-10}\ cm^{-1}/dyn\ cm^{-2}$ (the value obtained in that work, for X = 0, was $|Z| = 76 \times 10^{-10}\ cm^{-1}/dyn\ cm^{-2}$). Replotting the data points in [106], and using the parameter values determined here for X and $|Z|$ in eq (6.6) yields Fig. (6.13). As can be seen

from this diagram, the pressure dependent data of [106] are not inconsistent with the zero pressure splitting obtained here, so that the model proposed in [108] to explain the pressure dependence of the $^6A_1 \rightarrow {}^4E$ zero-phonon line in ZnS:Mn, also applies to the same transition in ZnSe:Mn, a feature which might have been expected, given the similarity between the two materials.

The absolute magnitude of the splitting of the zero-phonon line components is difficult to explain quantitatively. Essentially it is determined by the second order spin-orbit and spin-spin interactions. The spin-orbit calculation includes a single spin-orbit coupling constant and the spacings of the ^4E levels from all others. As shown in [107] covalency not only lifts the degeneracy of the ^4E and $^4A_1$ levels but shifts both of them in energy. Covalent effects should cause a shift of all other multiplets, the amount of the shift depending on the degree of admixture of the ligand orbitals with the orbitals of a given multiplet, which would not necessarily be the same for multiplets corresponding to different irreducible representations. Such an effect would lead to great complications in accurately determining the Racah parameters from experiment and hence the spacing of the multiplets becomes uncertain, so that their contribution to the second-order spin-orbit interaction is also uncertain.

6.7 Conclusions, $^6A_1 \rightarrow {}^4E$, $^4A_1$ Transition

It has been qualitatively shown that the $^6A_1 \rightarrow {}^4E$, $^4A_1$ transition of Mn in ZnSe:Mn can be explained by exactly the same model as used to describe the same transition in ZnS:Mn. This has been possible because in this work the splitting of the ^4E level has been observed for the first time.

The effect of covalency is to lift the degeneracy of the ^4E and $^4A_1$ states, the ^4E state lying lower in energy than the $^4A_1$ state. Second order spin-orbit and spin-spin interactions split the ^4E level into Γ_6, Γ_7 and Γ_8 states whose separation has been measured here as 0.5Å (2.23 cm^{-1}) allowing the stress-dependent data presented in [106] to be interpreted in terms of the model proposed in [108] for ZnS:Mn.

The zero-pressure splitting of the $^6A_1 \rightarrow {}^4E$ zero-phonon line in ZnSe:Mn measured here is less than than obtained for ZnS:Mn by a factor of $\sim \frac{1}{2}$ (2.23 cm^{-1} as against 5.5 cm^{-1} [108] and this difference is not easily accounted for. These splittings are determined theoretically[108] by using the calculated positions of all multiplets in the energy spectrum of the manganese ion, the dominant contribution arising from the high-lying $^2T_1$ and $^2T_2$ levels, of which there are respectively eight and ten[2], and these have not been observed experimentally. Covalent effects may shift the positions of these levels and so the values of the Racah parameters (obtained from those transitions which have been observed, i.e. $^6A_1 \rightarrow {}^4T_1$, $^6A_1 \rightarrow {}^4T_2$ and $^6A_1 \rightarrow {}^4E$) which are used to calculate the positions of these high-lying levels may yield a misleading energy spectrum.

Strictly, also, when calculating the second order spin-orbit splitting of the ^4E state through interaction with the other multiplets, an isotropic spin-orbit model may not be applicable and the effect of the ligands must be calculated explicitly.

Table (6.1)

Splitting of $^4T_1$ and $^4T_2$ zero phonon lines in ZnSe:Mn and ZnS:Mn

	Splitting (cm^{-1}).	
	Theory	Experiment
ZnS:Mn	$^4T_1$:- 9.8[89], 9.5[90], 7.7[91]	9.6[94,95], 10[90,91]
	$^4T_2$:- 5.4[89], 3.3[97]	3[96,97]
ZnSe:Mn	$^4T_1$:- 7.5[89], 7.4[91]	11.5[91], 20[80]
	$^4T_2$:- 5.4[89], 10[97]	10[98,80,97], 11.5[this work]

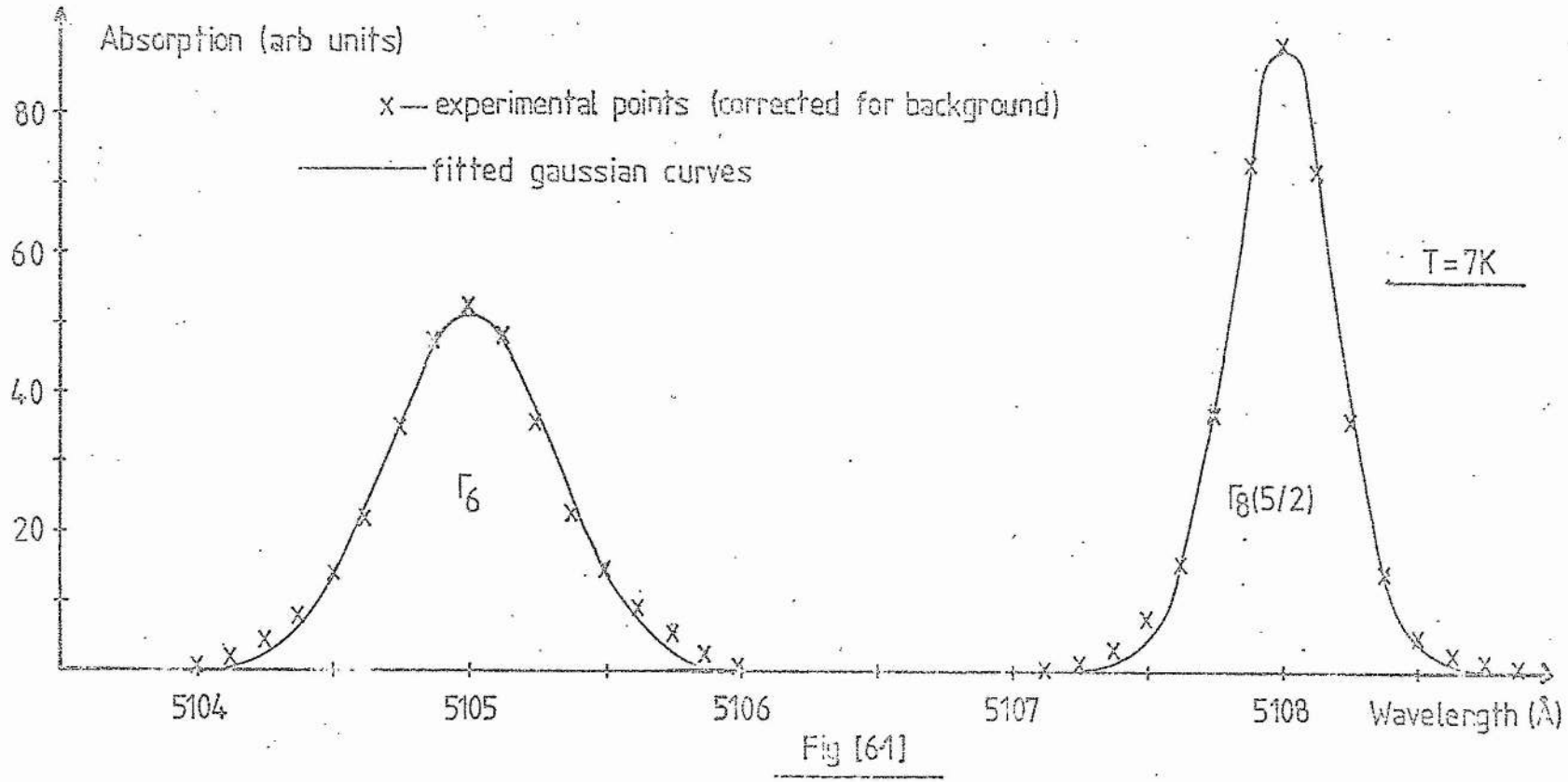

Fig [6-1]

Absorption spectrum of the $^6A_1 \rightarrow {}^4T_2$ zero phonon line in ZnSe:Mn

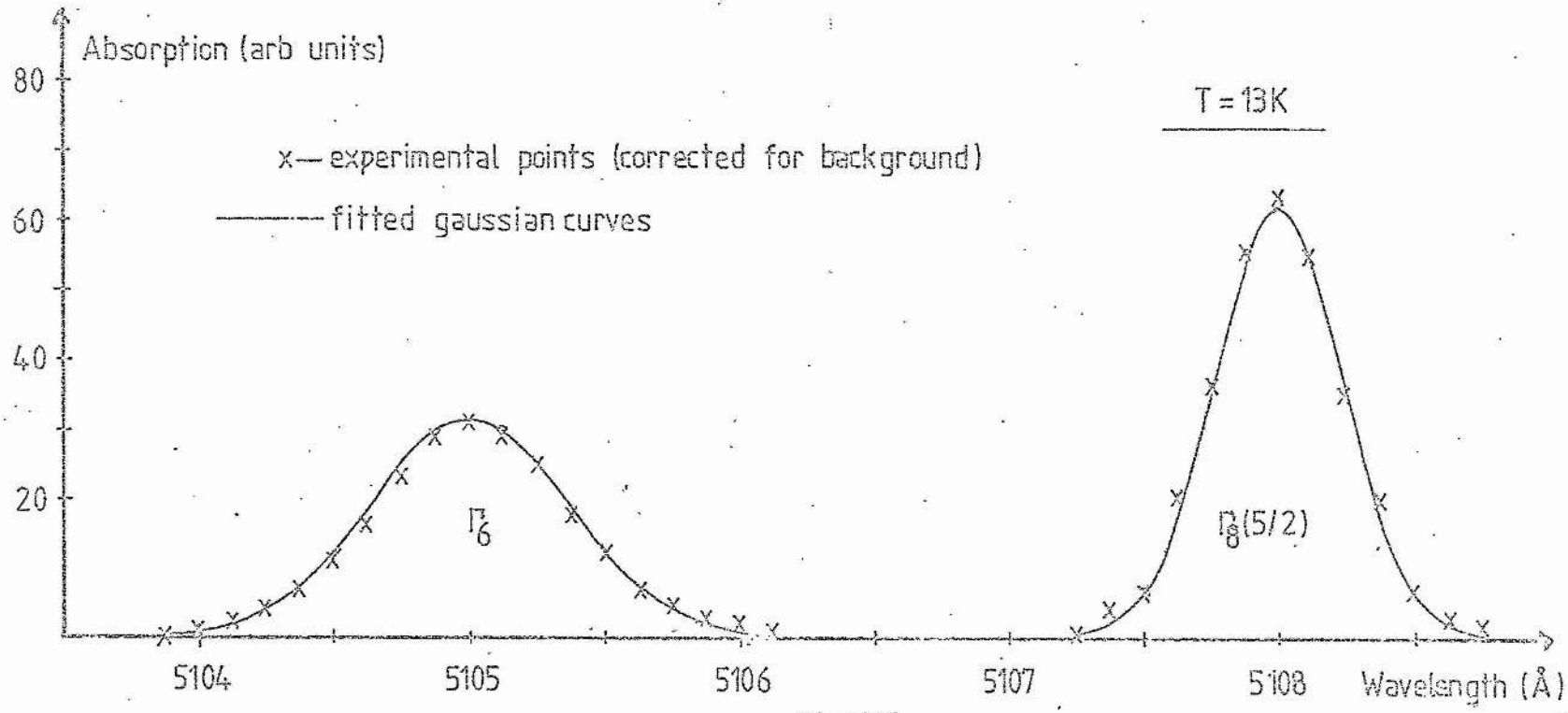

Fig [6·2]

Absorption spectrum of the $^6A_1 \rightarrow {}^4T_2$ zero phonon line in ZnSe:Mn

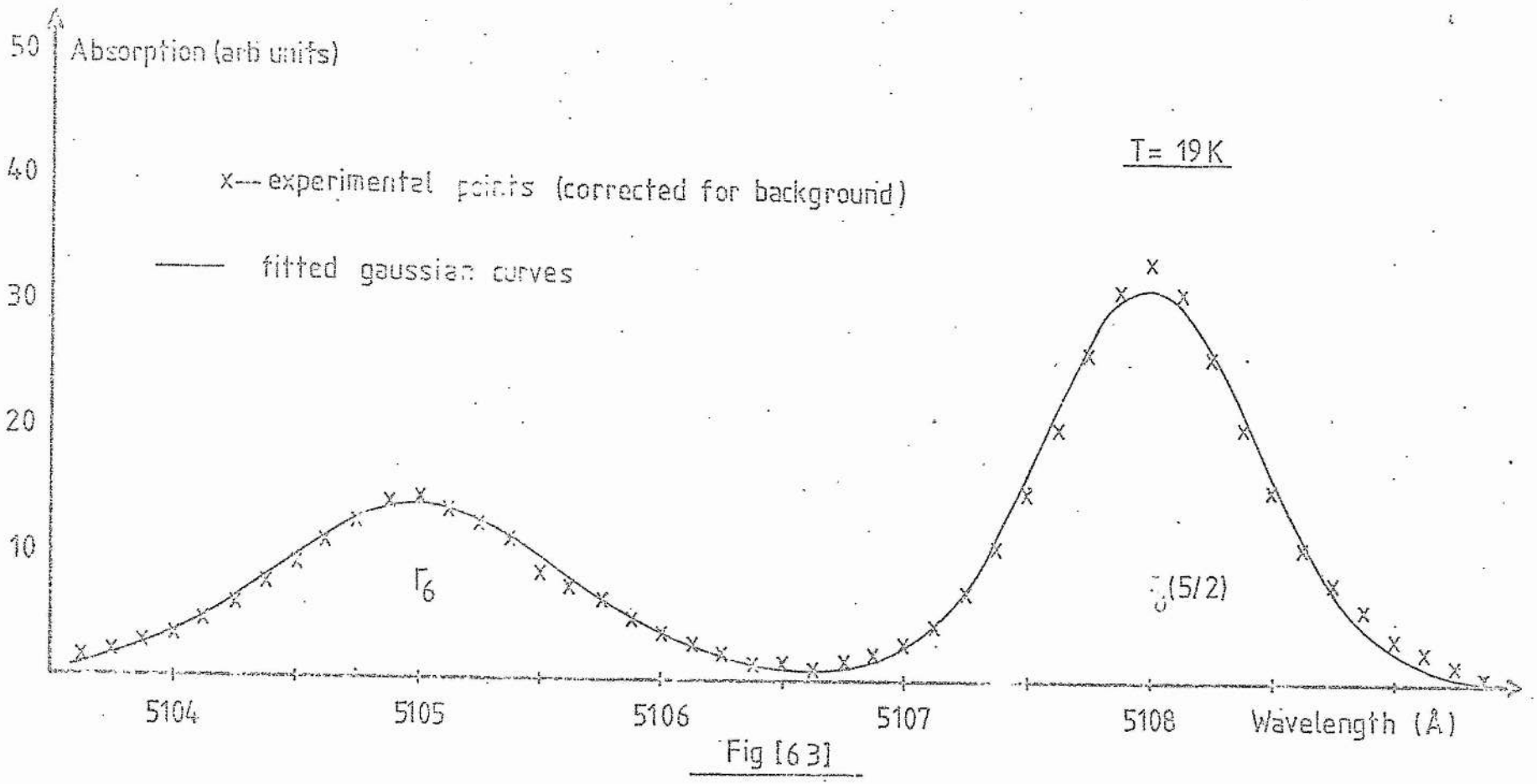

Fig [6 3]

Absorption spectrum of the $^6A_1 \rightarrow {}^4T_2$ zero phonon line in ZnSe:Mn

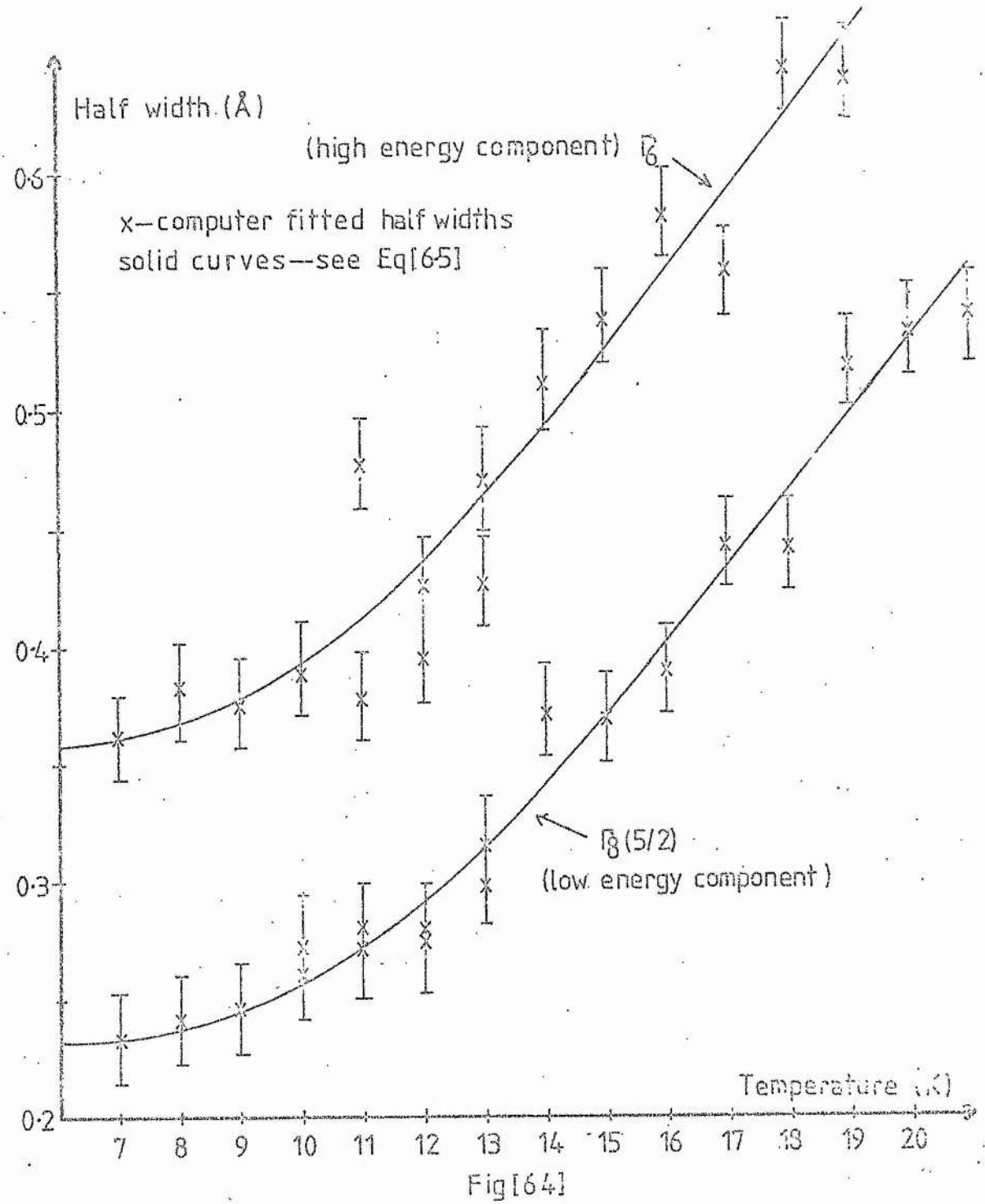

Fig [6 4]

Half-widths of the components of the $^6A_1 \rightarrow {}^4T_2$ zero phonon line in ZnSe:Mn as a function of temperature

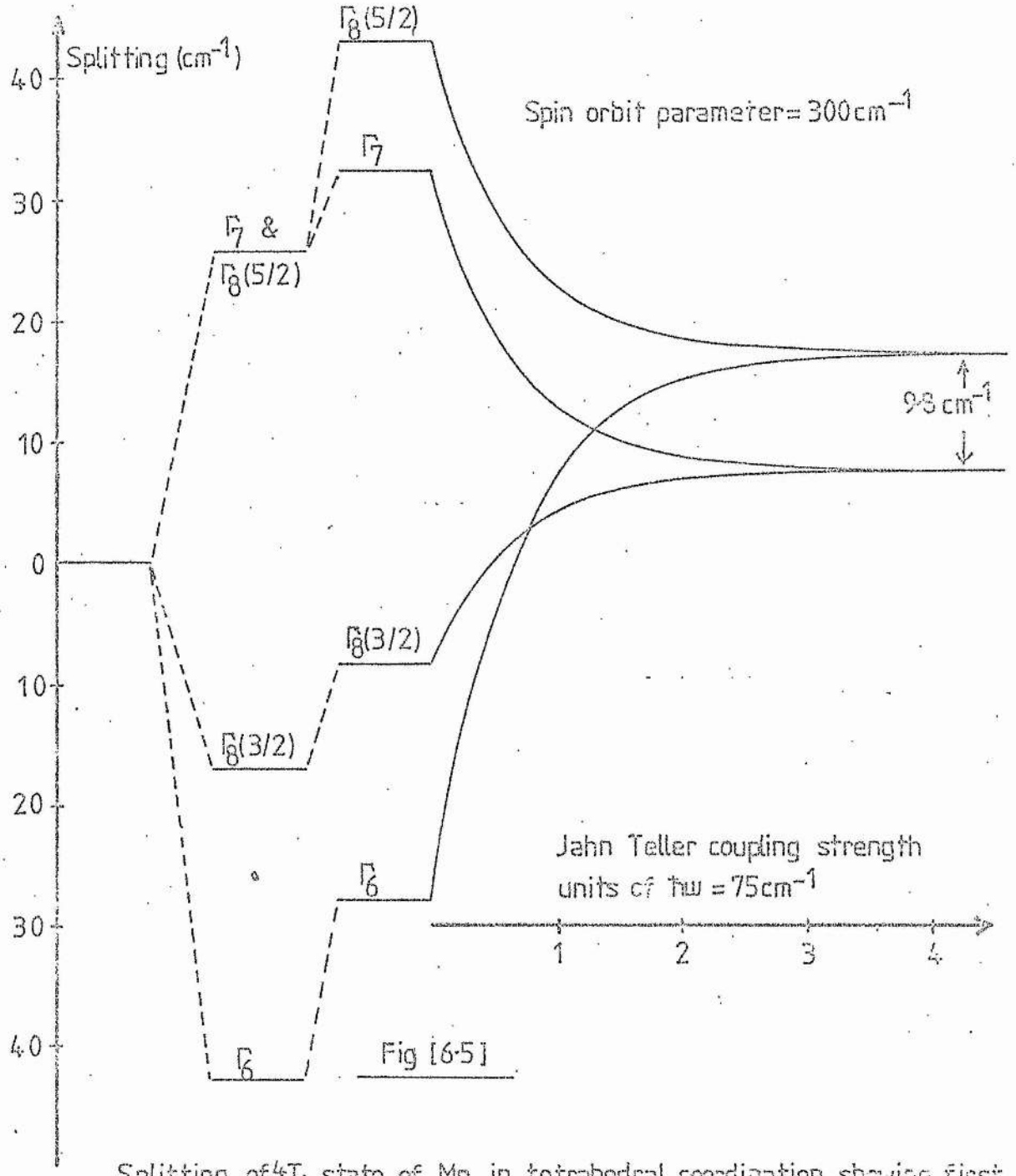

Fig [6·5]

Splitting of $^4T_1$ state of Mn in tetrahedral coordination showing first order and second order spin orbit effects and increasing Jahn Teller interaction

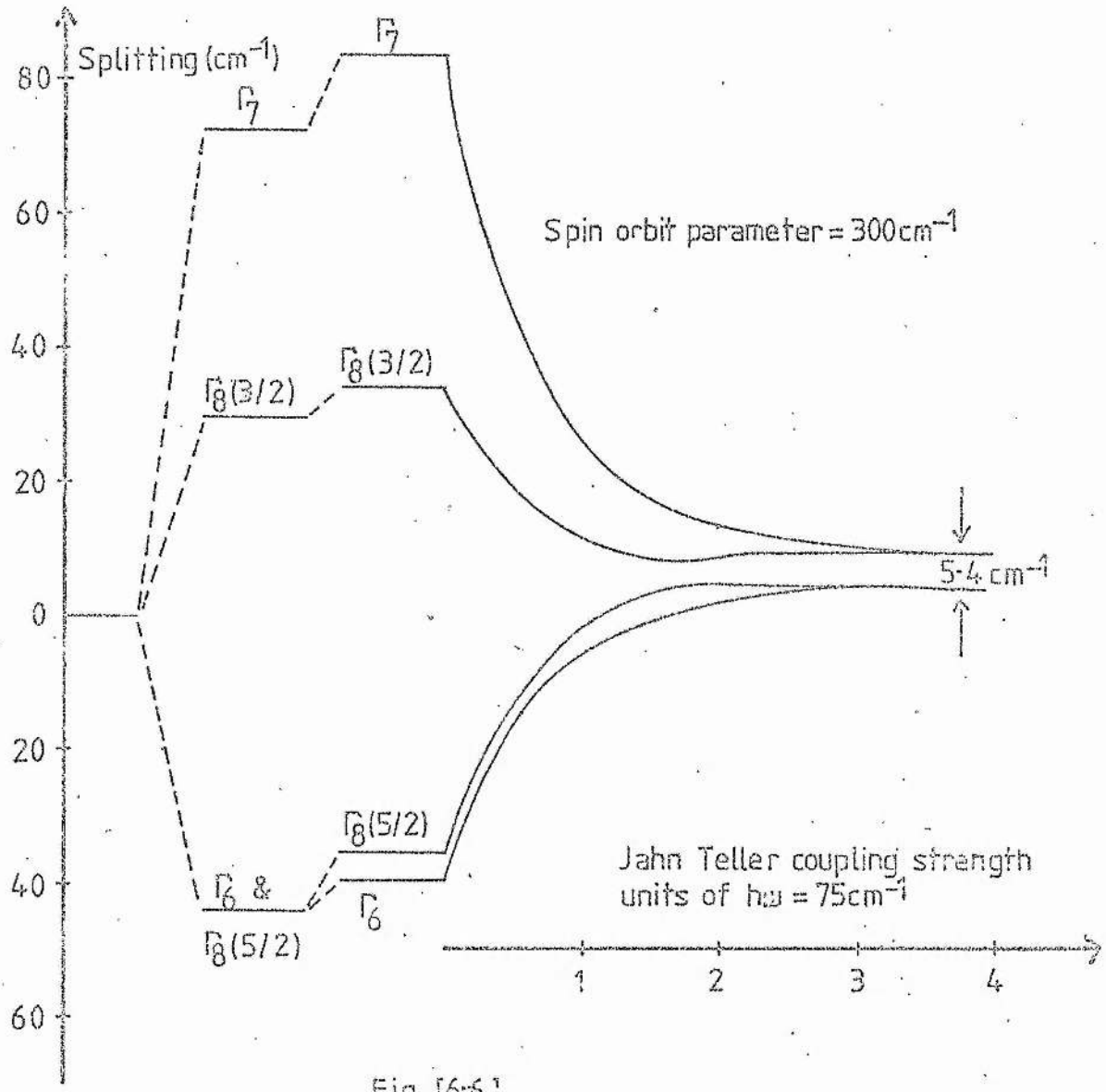

Fig 16·6

Splitting of $^4T_2$ state of Mn in tetrahedral coordination showing first order and second order spin orbit effects and increasing Jahn Teller interaction

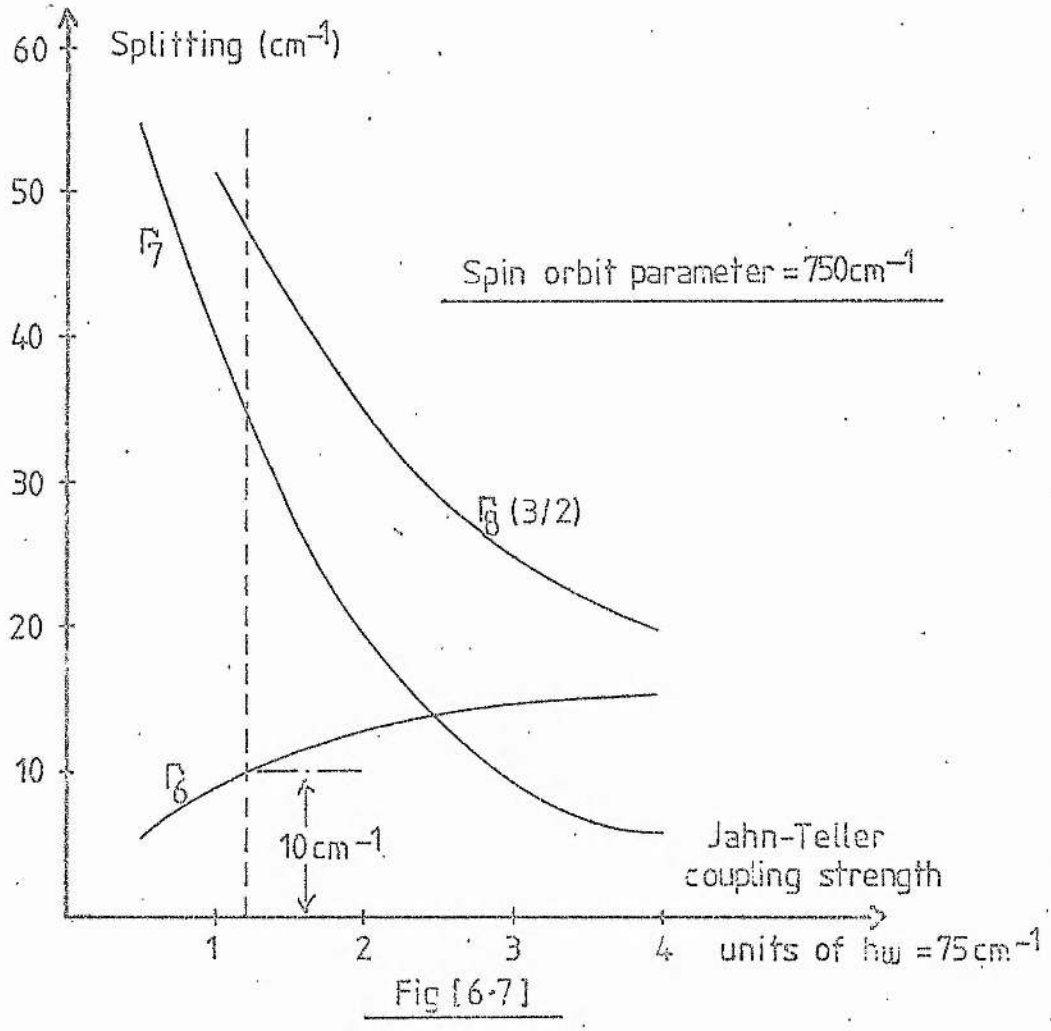

Fig [6-7]

Splitting of levels in $^4T_2$ manifold relative to Γ_8(5/2) level as a function of Jahn Teller coupling strength

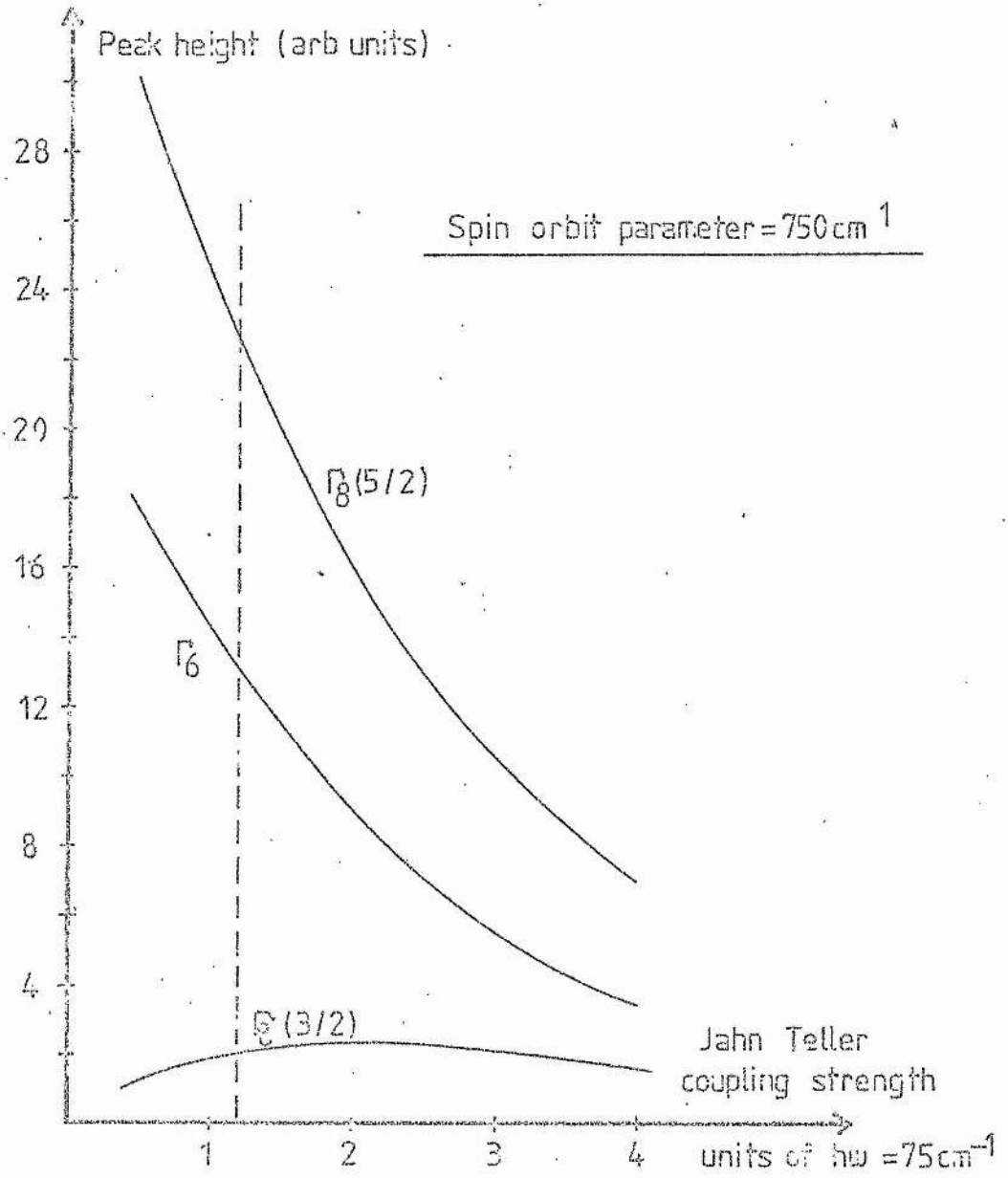

Fig [6-8]

Relative strengths of transitions from $^6A_1$ to levels within the $^4T_2$ manifold as a function of Jahn Teller coupling strength ($^6A_1$ Γ_7 transition strength = 0)

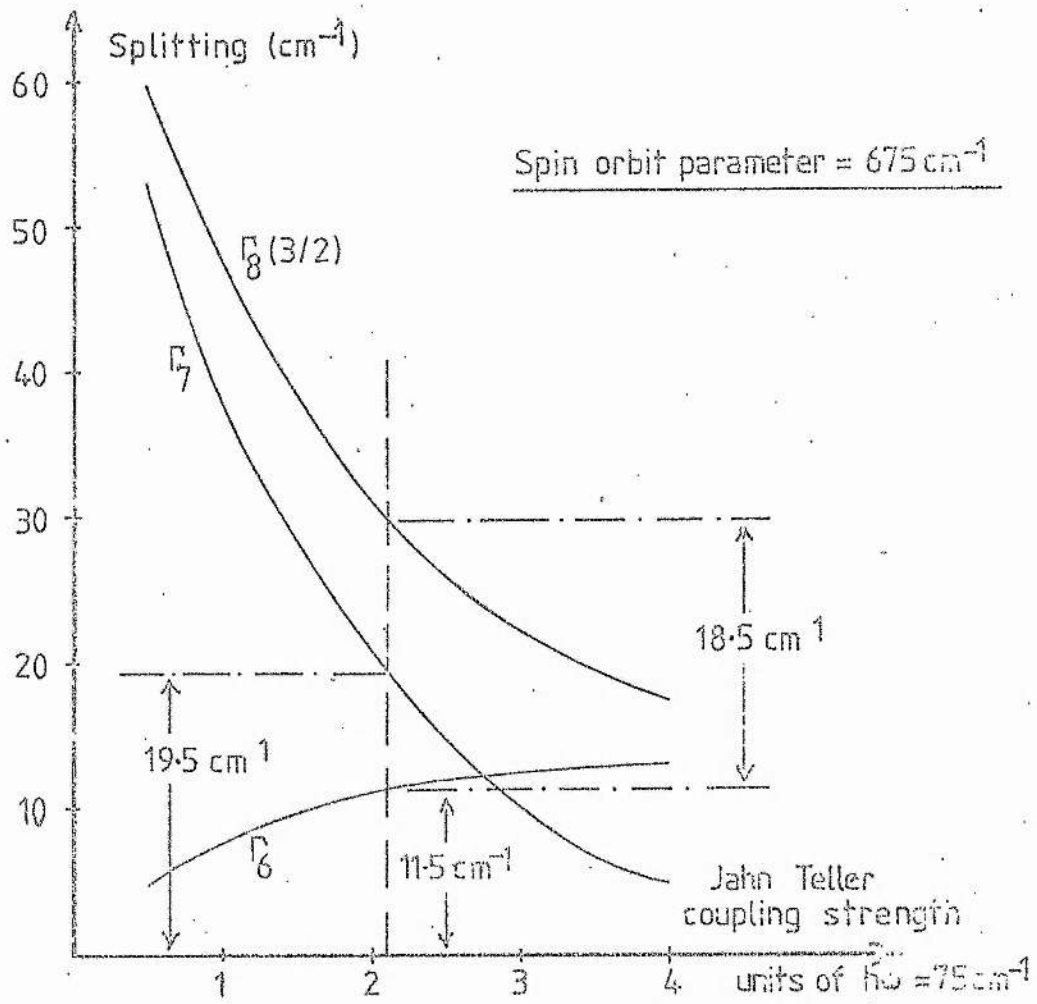

Fig [6·9]

Splitting of levels in $^4T_2$ manifold relative to Γ_8 (5/2) level as a function of Jahn-Teller coupling strength

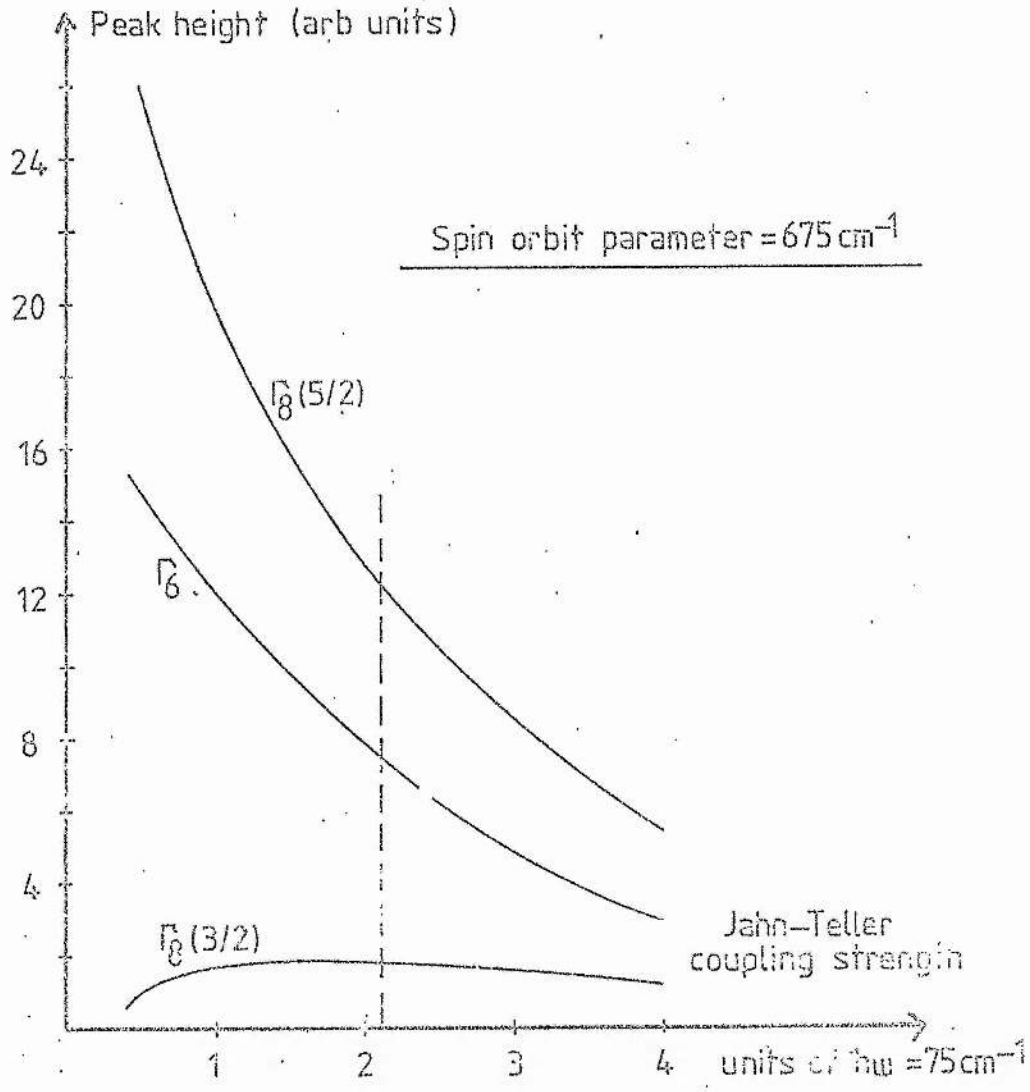

Fig [6·10]

Relative strengths of transitions from $^6A_1$ to levels within the $^4T_2$ manifold as a function of Jahn Teller coupling strength ($^6A_1 \rightarrow \Gamma_7$ transition strength = 0).

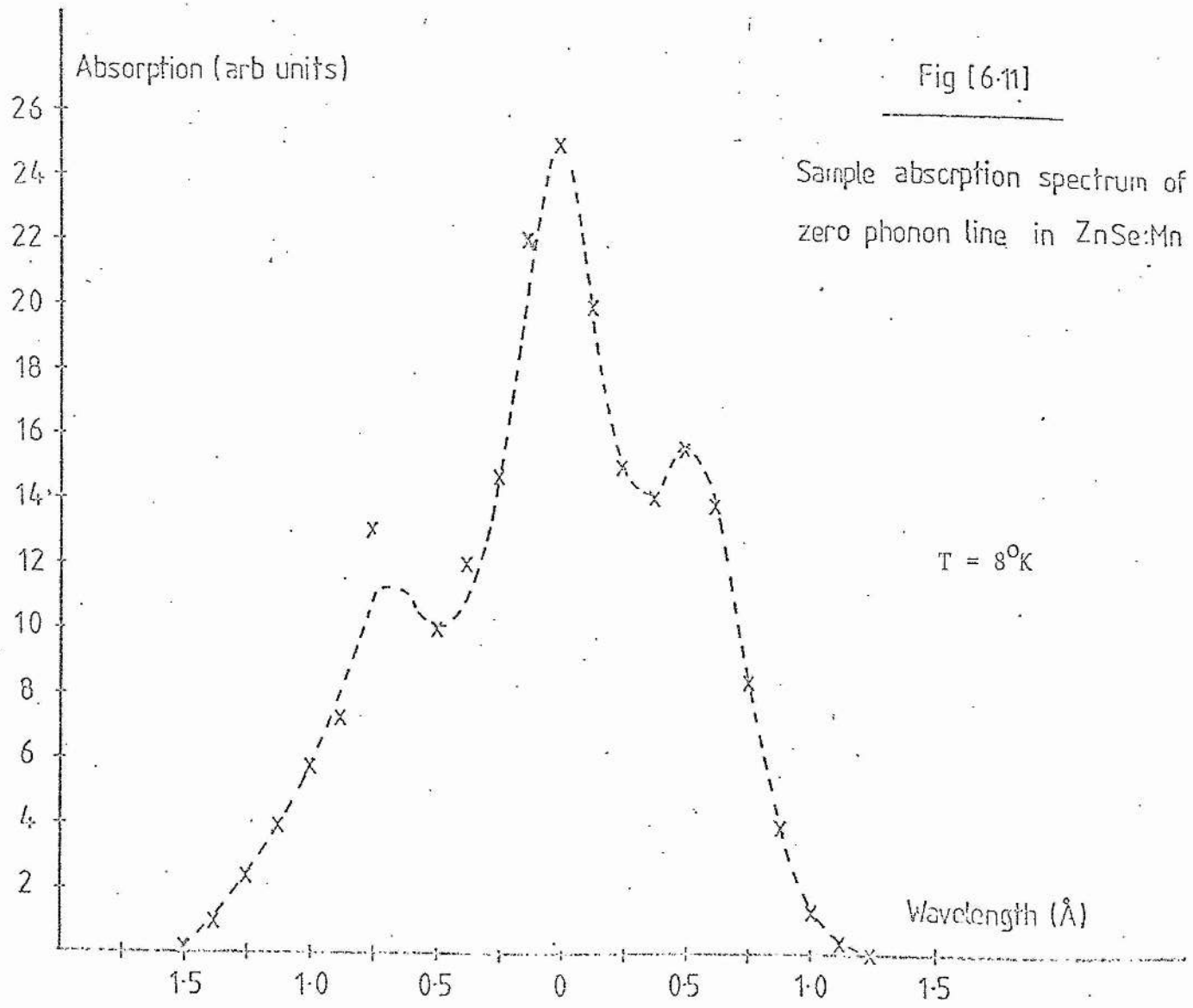

Fig [6·11]

Sample absorption spectrum of the $^6A_1 \rightarrow {}^4E$ zero phonon line in ZnSe:Mn

$T = 8^oK$

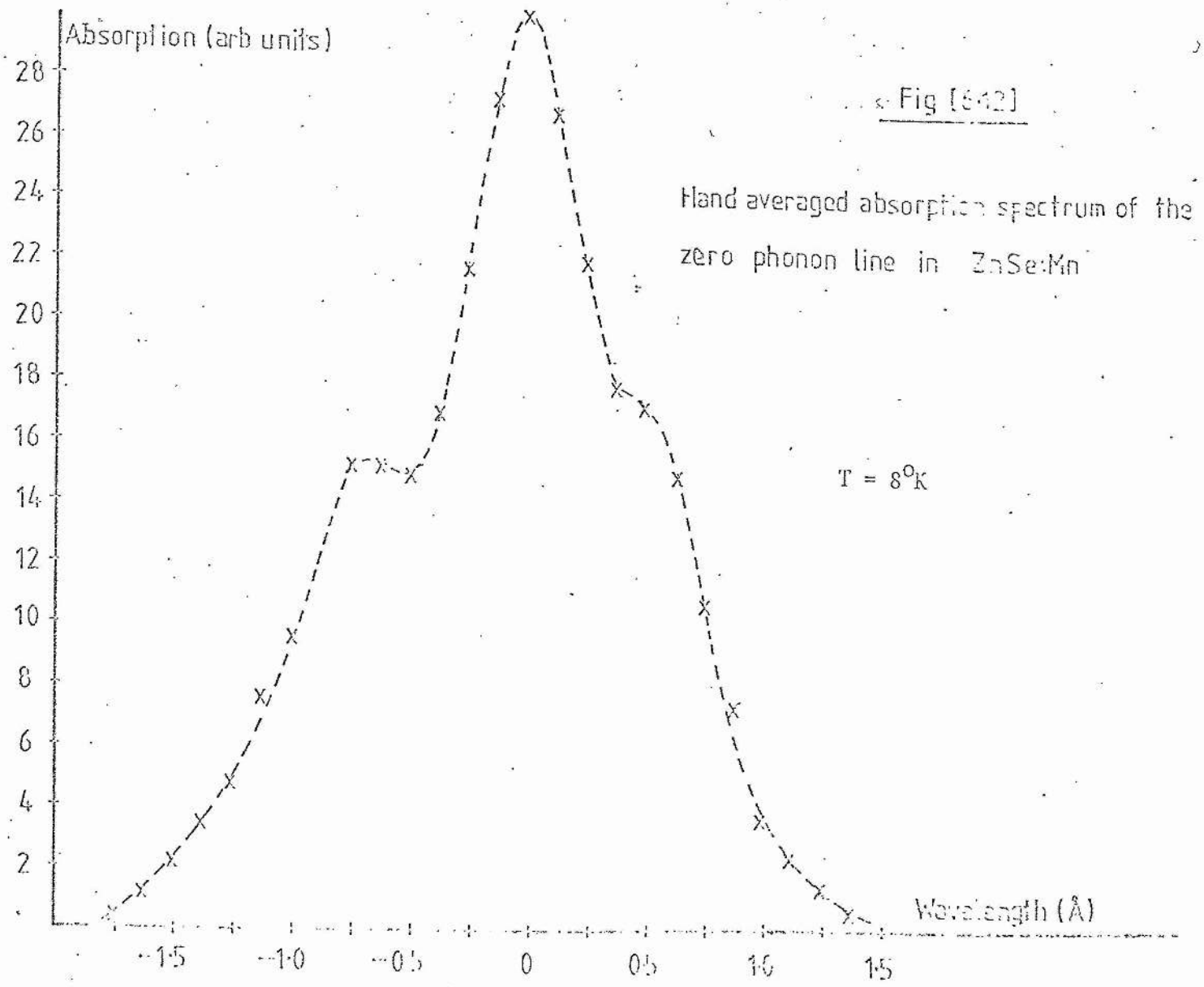

Fig [5·12]

Hand averaged absorption spectrum of the $^6A_1 \rightarrow {}^4E$ zero phonon line in ZnSe:Mn

$T = 8^oK$

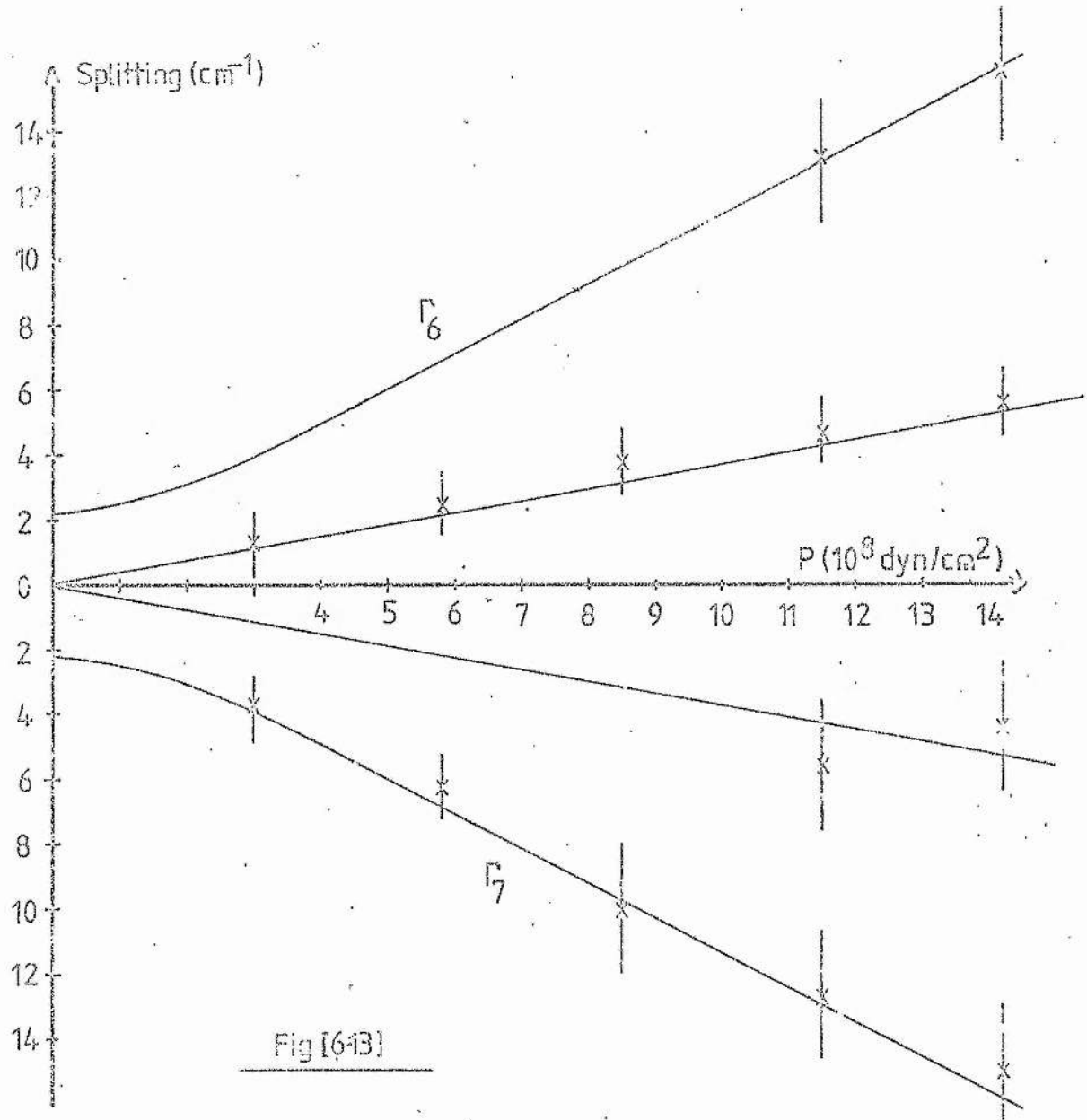

Fig [6-13]

Splitting of the ^4E level of Mn in ZnSe:Mn as . . . of applied pressure, P//[1$\bar{1}$0]

CHAPTER 7

Thermal Quenching and Lifetime Measurements

7.1 Introduction

The investigation of thermal quenching of impurity-activated luminescence provides information on the relationship between the impurity energy levels and those of the host crystal, since the activation energy for quenching helps to delimit the possible non-radiative transition mechanisms. Previous work on ZnS:Mn has been described by Vlasenko[111] and Garlick and Wilkins[112] giving 0.36eV as the activation energy for quenching. Experiments on ZnSe:Mn have been performed by Jones and Woods[113] who obtained a quenching activation energy of 0.3eV. Both Vlasenko and Jones and Woods attribute the quenching to a multiphonon transition within the manganese impurity levels. However there is some doubt as to whether these measurements were performed at temperatures sufficiently far into the quenching region for a true activation energy to be obtained.

7.2 Experimental Results

Before proceeding to give the experimental results, it is necessary to consider the effect of an approximation inherent in the method used to obtain them. This approximation is that no correction was made for the fact that both the position and width of the Mn emission band are temperature dependent, so that in the course of the experiments the emission band is changing both position and shape. It will be shown that this correction is small and can, in any case, be introduced in the analysis of the data.

It has been shown[113] that λ_{OT}, the position of the Mn emission band maximum, varies linearly with temperature and that δ_T the half-width of the band, varies as the square root of temperature (at high temperatures).

i.e.
$$\Delta\lambda_{OT} \propto T$$
$$\delta_T \propto T^{\frac{1}{2}} \tag{7.1}$$

Approximating the Mn emission band by a gaussian curve

i.e.
$$I(\lambda) = \frac{1}{\sigma_T\sqrt{2\pi}} \exp\{-\frac{(\lambda-\lambda_{OT})^2}{2\sigma_T^2}\} \tag{7.2}$$

where $\sigma_T = (2\ell n2)^{-\frac{1}{2}}\ \delta_T \propto T^{\frac{1}{2}}$ by eq (7.1) and writing the filter bandpass characteristic as another gaussian curve

$$J(\lambda) = J(\lambda_f) \exp\{-\frac{(\lambda-\lambda_f)^2}{2\sigma_f^2}\} \tag{7.3}$$

then eq (5.14) yields for the measured intensity

$$I_m = \frac{J(\lambda_f)}{\sigma_T(2\pi)^{\frac{1}{2}}} \int_o^\infty \exp\{-\frac{(\lambda-\lambda_f)^2}{2\sigma_f^2} - \frac{(\lambda-\lambda_{OT})^2}{2\sigma_T^2}\}d\lambda$$

$$= \frac{J(\lambda_f)}{\sigma_T(2\pi)^{\frac{1}{2}}} \exp\{-\frac{(\lambda_f-\lambda_{OT})^2}{2(\sigma_f^2+\sigma_T^2)}\} \int_o^\infty \exp\{-\frac{(\lambda-\lambda_{fT})^2}{2\sigma_{fT}^2}\}\ d\lambda$$

where
$$\lambda_{fT} = \frac{\lambda_f\sigma_T^2 + \lambda_{OT}\sigma_f^2}{\sigma_T^2 + \sigma_f^2}\ ,\ \sigma_{fT}^2 = \frac{\sigma_f^2\sigma_T^2}{\sigma_T^2 + \sigma_f^2}$$

and thus
$$I_m = \frac{J(\lambda_f)\sigma_f^2\sigma_T}{\sigma_T^2+\sigma_f^2} \exp\{-\frac{(\lambda_f-\lambda_{OT})^2}{2(\sigma_T^2 + \sigma_f^2)}\} \tag{7.4}$$

Thus the percentage change in I_m due solely to the changing position and width of the Mn emission band is Δ where

$$\Delta = \frac{I_m(T_1) - I_m(T_2)}{I_m(T_1)} \tag{7.5}$$

As an illustrative example of the magnitude of this effect, choose $T_1 = 300^oK$ and $T_2 = 330^oK$ (approximately the quenching region as will be seen later) then Figs (7.1) and (7.2) (adapted from [113]) give

$$\lambda_{OT_1} = 5911\text{Å}, \quad \sigma_{T_1}^2 = 236038\text{Å}^2$$

$$\lambda_{OT_2} = 5915\text{Å}, \quad \sigma_{T_2}^2 = 254466\text{Å}^2$$

and using eq (7.4) in eq (7.5) yields $\Delta = 3.5\%$. By far the largest contribution to this correction comes from the preexponential factors of eq (7.4)

$$\text{i.e.} \quad I_m \doteq \frac{J(\lambda_f)\sigma_f^2\sigma_T}{\sigma_T^2 + \sigma_f^2} \tag{7.6}$$

so that the error in the data points can be corrected by multiplying the intensity at each temperature by the factor

$$\frac{\sigma_T^2 + \sigma_f^2}{J(\lambda_f)\sigma_f^2\sigma_T}.$$

From simple arguments[114], the variation of luminescent efficiency η, with temperature is

$$\eta = \frac{\eta_o}{1 + A\exp(-E_A/kT)} \tag{7.7}$$

where A is a constant and E_A is the activation energy for quenching. In the limit of high temperatures, this becomes

$$\eta = \frac{\eta_o}{A}\exp\left(\frac{E_A}{kT}\right) \tag{7.8}$$

Thus by plotting $\ln(\eta)$ against T^{-1}, a straight line of gradient E_A/k should be obtained at high temperatures. Fig. 7.3 shows the results obtained, with Fig. 7.4 showing the quenching region. For comparison, the results obtained by Vlasenko[111] and Jones and Woods[113] are given in Fig. (7.5).

For two samples of ZnSe:Mn, the quenching energies obtained were 0.66 ± 0.05eV (Fig (7.4)a) and 0.61 ± 0.05 eV (Fig (7.4)b). For ZnS:Mn, the quenching energy obtained was 0.60 ± 0.05eV (Fig.(7.4)c) and that for the mixed crystal was 0.3eV (Fig (7.4)c). This value of the quenching energy for the mixed crystal should be treated with reservation, since full quenching may not have been obtained.

Incorporating into the data the correction embodied in eq (7.6) the above activation energies become respectively 0.65 ± 0.05 eV, 0.60 ± 0.05eV and 0.59 ± 0.05 eV. These results, together with the uncorrected values are given in table (7.1).

It is significant that the onset of thermal quenching occurs at different temperatures in two samples of the same material (ZnSe:Mn), because this implies that the preexponential factor A in eq (7.7) varies from sample to sample in the same material. Similarly the quenching behaviour of the sample of ZnSe:Mn used by Jones and Woods (Fig (7.5)a) is different from that of the materials tested here; the ZnS:Mn quenching curves of Fig (7.4)c and Fig (7.5)b also differ.

7.3 Discussion

Models used to describe thermal quenching of luminescence may be subdivided into two broad categories (for a review see Curie[114])

(a) an internal non-radiative relaxation transition of the luminescent centre.

(b) a non-radiative relaxation arising from an interaction involving the impurity and some band effect (such as the production of holes and electrons).

Models of type (a) have been invoked to explain thermal quenching in both ZnS:Mn (by Vlasenko[111]) and ZnSe:Mn (by Jones and Woods[113]). The mechanism proposed by Jones and Woods is that the activation energy is the height above the minimum of excited state curve at which the excited and ground state curves on a single mode configurational coordinate diagram intersect (E_b in Fig (7.6)). A full description of this model has been given by Robertson and Friedman[115] and Struck and Fonger[116].

However, there are a number of objections to the application of this model to the results presented here. Firstly it predicts that all samples of the same material should exhibit the same quenching behaviour. This has been shown not to be the case since quenching occurs at different temperatures in different samples of the same material. Secondly, the activation energy which can be calculated from this model is in disagreement with the value obtained from experiment. Using the well-known relation (see for example[12]) for the variation of the width W(T) of emission spectra with temperature,

$$W(T)^2 = W(T=0)^2 \coth\frac{\hbar\omega}{2kT} \qquad (7.9)$$

(where $\hbar\omega$ is the dominant phonon energy) and assuming that the emission band is gaussian in shape so that the equation (4)

$$W(T=0) = \hbar\omega\, s^{\frac{1}{2}}(8\ell n2)^{\frac{1}{2}} \qquad (7.10)$$

applies, it is possible to obtain both $\hbar\omega$ and s (the Huang-Rhys factor). For ZnSe:Mn, Jones and Woods[113] have obtained $\hbar\omega$ = 0.032eV

and $W(T=0)^2 = 0.02eV^2$, from which, using eq (7.10), the Huang-Rhys factor s is found to be 3.52. Using the results of Langer and Richter[80] for the zero-phonon line energy (E_{zp} = 2.239eV) and the peak emission energy (E_e = 2.136eV), the form of the configuration coordinate diagram, Fig (7.6), may be calculated explicitly, assuming that the curves are parabolic and exhibit the same curvature. A simple geometrical calculation, given as an appendix to this chapter, demonstrates that, in this model, E_b is given by

$$E_b = \frac{(E_e - \frac{1}{2}\hbar\omega)^2}{4s\hbar\omega} - \frac{1}{2}\hbar\omega \qquad (7.11)$$

and thus E_b = 9.96eV for ZnSe:Mn. The results of Vlasenko[111] and Langer and Ibuki[94] for ZnS:Mn indicate that s = 2.69, $\hbar\omega$ = 0.0405eV, E_{zp} = 2.218eV and E_e = 2.129eV so that eq (7.11) yields E_b = 11.1eV for this material.

These calculated values are more than an order of magnitude greater than the experimental ones. Relaxing the parameters of the single mode configurational coordinate diagram cannot remove this discrepancy.

Because of these objections, it is unlikely that the internal multiphonon relaxation process is the one by which thermal quenching occurs in either ZnSe:Mn or ZnS:Mn, and it is necessary to consider other mechanisms. These alternative mechanisms will now be discussed using the type of energy band diagram described in 2.5.

A: The first possibility is one in which ionisation of the manganese impurities takes place, an electron being removed from the Mn excited state to the conduction band by thermal excitation. Such a mechanism has been considered by Radlinski[117] to describe the temperature

dependence of luminescence for the case of ZnSe:Co. Radlinski[117] does not consider how the impurity could then deionise, but this could occur through the capture of an electron from the host valence band. For this process to occur, both transitions (1) and (2) of Fig. (7.7) must be allowed. Then the activation energy for quenching would be determined by which one of these two transitions involves the higher energy. This model is plausible for ZnSe:Mn, since it is consistent with an energy level diagram of the form of Fig (7.8) which has previously[118] been proposed for this material on the basis of photocapacitance measurements. Later work[119] has however cast doubt on such an energy level scheme. In any case, in ZnS:Mn, the bandgap is approximately 3.6eV, and the energy difference between the ground and excited states of the Mn impurity is stillapproximately 2.1eV. This means that the minimum possible quenching energy is 0.75eV (= $\frac{1}{2}$(3.6-2.1)eV) which is not in agreement with the 0.6eV obtained.

B: The second possibility is to propose that the excited state of the Mn impurity if 0.6eV below the edge of the conduction band in both ZnSe:Mn and ZnS:Mn, and that the simultaneous deexcitation and deionisation transition labelled (1) in Fig. (7.9) is both allowed and is non-radiative. As in model A, thermal ionisation can take place from the Mn excited state to the conduction band. Consider the steady-state equations for the Mn impurities

ground state: $\alpha I(N_T - N^* - N^+) = \beta N^* + \varepsilon n N^+$ (7.12a)

excited state: $\alpha I(N_T - N^* - N^+) + \delta n N^+ = \beta N^* + \gamma N^*$ (7.12b)

where

N_T = total number of Mn centres

N^* = number of excited Mn centres

N^+ = number of ionised Mn centres

I = incident light flux

n = number of conduction electrons

α = transition probability from ground to excited state

β = transition probability from excited to ground state

γ = $\gamma_o \exp[-E/kT]$ is the probability of an excited Mn centre ionising

δ = probability of an ionised Mn centre deionising to an excited Mn centre

ϵ = probability of an ionised Mn centre simultaneously deionising and relaxing to the ground state

Eliminating N^+ from eq (7.12) gives

$$N^* = \frac{\alpha I N_T}{\frac{\alpha I \gamma}{(\epsilon+\delta)n} + \frac{\epsilon\gamma}{(\epsilon+\delta)} + \alpha I + \beta} \qquad (7.13)$$

This is sensibly independent of n, unless I/n is a constant (i.e. the photoconductivity is linear in the incident intensity). If I/n is constant eq(7.13) has (through γ) the temperature dependence of eq(7.7). If Mn is the only impurity present then I/n does not vary from sample to sample, but when other centres are present (which can trap electrons[120]) then I/n may vary from sample. This variation from sample to sample occurs in the pre-exponent of eq (7.7) and could correctly account for the observed behaviour. This model implies that the Mn ground state is about 2.7 eV below the conduction band edge in both ZnSe:Mn and ZnS:Mn; i.e. it lies 0.9eV above the valence band edge in ZnS:Mn and close to the valence band edge in ZnSe:Mn. The major objection to this model is that it places the Mn ground state in ZnS:Mn much higher in energy than has previously been proposed. It should be noted

however that the position of the Mn ground state in ZnS:Mn has been a source of controversy for some time: it has been located 6 eV below the top of the valence band[121,122] and up to about 0.3 eV[7,123,124] above the edge of the valence band.

C: The third possibility is to consider the effects of energy levels (caused, for example, by unwanted impurities or lattice defects) which can capture electrons from the valence band, leaving excess holes. There is some evidence for an energy level in ZnSe:Mn about 0.6 eV above the valence band[125], and also in ZnS:Mn[126]. These excess holes may then be captured by an excited manganese centre, forming an excited ion complex, which could then deexcite and deionise non-radiatively. The mechanism by which this relaxation could take place is dependent upon the position of the energy of the excited complex with respect to the host crystal bands, a feature which is undetermined. Such a mechanism would require that the Fermi energy in both materials be low enough to ensure only partially filled levels 0.6eV above the valence band. The Fermi energy has not been adequately measured in these materials, essentially because the low carrier concentration makes any kind of conductivity or resistivity measurements very difficult. Also the Fermi energy is an equilibrium quantity, and when impurity states exist deep in the energy gap, non-equilibrium distributions of holes and electrons in deep levels may exist, with long relaxation times before equilibrium is reached, making equilibrium quantities difficult to measure. The mechanism for non radiative relaxation in this model requires that the Fermi energy be rather lower than those values which have been obtained[127,128].

D: A fourth possibility is that of resonant transfer of excitation

energy between the manganese centres and other defect centres. These defect centres may be able to de-excite non-radiatively, e.g. by the multiphonon relaxation process, or indeed any of A,B,C above, but with the relaxation model being applied to the defect centre energy level system, and not the manganese system. In effect the temperature dependence of the Mn emission band is monitored by the defect centres, and not by the Mn itself. In certain ways this is analogous to the case presented in[120], where it is proposed that the temperature dependence of the Mn luminescence in CdF_2:Mn is governed by the thermal ionisation potential of an unidentified sensitizer.

These latter two mechanisms (C and D) are often known as shunt-path processes. The characterisation and removal of shunt-path mechanisms in the commercially successful III-V luminescent devices has been a major part of the research into improving the performance obtainable with these materials. A review of the current status in this field has been given by Dean[129]. Although this is not directly relevant to either ZnS:Mn or ZnSe:Mn, such research on III-V compounds does demonstrate that even for systems whose preparation and properties have been studied at great length, unwanted impurities and defects can still exist and in some cases remain unidentified.

Of the models discussed, only B and D appear possible. (C is excluded because of the rather low Fermi energy which is required).

7.4 Lifetime Measurements

In order to further quantify the non-radiative relaxation mechanism appropriate to these materials, measurements of the temperature dependence of the lifetime of the excited ($^4T_1$) state of the manganese impurity

in ZnS:Mn, ZnSe:Mn and $ZnSe_xS_{1-x}$:Mn were performed.

Similar measurements have been made, for the ZnS:Mn system by a number of authors[130,131,132,133,135] whose main interest was the dependence of the excited state lifetime on the concentration of the manganese impurity. These authors are generally in agreement that, at low manganese concentrations, the lifetime of the $^4T_1$ state is $\sim$ 1mS. At higher Mn concentrations, the lifetime of the $^4T_1$ state shortens. This has been attributed by Selle[135] to a concentration quenching effect. However there is a general consensus amongst other authors[130,131,133] that this lifetime shortening is due to the appearance of exchange-coupled pairs of manganese ions on neighbouring (cation) sites. The effect of the exchange coupling is to offer an alternative relaxation method and hence a measured decrease in the lifetime of the state involved. Thus for this higher concentration case, there are two distinct contributions to the observed lifetime (one from single ions, and one from exchange-coupled pairs) which can be separately evaluated. In one instance[132] the detection of three separate processes - due to single Mn ions, nearest-neighbour (cation) Mn ion pairs, and next-nearest-neighbour (cation) Mn ion pairs was reported. The concentrations at which the shorter lifetime of an excited state of an ion in a coupled pair has an appreciable effect on the overall observed lifetime is a matter of some debate. In principle, the probability of pairs always exists, but below about 0.5% by weight concentration of manganese their effect appears negligible. In one of the reports cited[130], the contribution from Mn pairs to the overall observed brightness was found to be <30% with Mn concentration below 0.5% by weight. (The probability of impurity atom clustering, in principle, can be found from the tables of Kreitmann

and Barnet[135] - see also [132,136]. In only one of the works mentioned[130] was the effect of temperature on lifetime considered, the authors' conclusion being that trapping effects in the decay process were negligible over the temperature range of $153^{o}K \rightarrow 393^{o}K$ (measurements were made only at these two temperatures).

In this work, the decay times of the luminescence in ZnSe:Mn have been obtained for the first time, and also the temperature dependence of the lifetime of the Mn $^4T_1$ state in ZnS:Mn, ZnSe:Mn and $ZnSe_xS_{1-x}$:Mn has been ascertained.

Examples of the decay curves obtained in the present work are given in Fig. (7.10) for ZnS:Mn, Fig. (7.11) for ZnSe:Mn and Fig. (7.12) for $ZnSe_xS_{1-x}$:Mn. Mangelsdorff plots (see 5.4) of these decay curves are given in Figs. (7.13), (7.14) and (7.15) respectively. The fact that these latter three are linear dependencies implies that the decay curves are exponential in form, i.e. they can be described by the rate equation[134]

$$\dot{n}_x = A - \alpha n_x \qquad (7.12)$$

where

n_x = number of excited emission centres

A = number of photons absorbed by the centres in unit time

α = probability for a transition to the ground state

From eq(7.12) the decay of luminescence follows the exponential relation

$$I(t) = \alpha n_x(t) = I_o e^{-t/\tau}, \quad \tau = 1/\alpha \qquad (7.13)$$

where τ is the decay time, or average lifetime of the excited state.

The effect of temperature on this lifetime is shown for the three systems in Figs (7.15) (for ZnS:Mn), (7.16)(for ZnSe:Mn) and (7.17) (for $ZnSe_xS_{1-x}$:Mn).

An immediately noticeable feature of these curves requiring explanation is that the low temperature lifetime of the Mn excited state ($^4T_1$) in the ZnSe host ($\sim$0.105 mS) is approximately an order of magnitude less than that for the ZnS host ($\sim$1.1mS). Qualitatively this may be explained in the following way. As mentioned in 6.3, (although for a different transition) the $^4T_1 \rightarrow {}^6A_1$ transition is both spin and parity forbidden. The spin restriction is lifted by spin-orbit coupling and the parity restriction by the fact that there is no inversion centre in a tetrahedral system, so that parity is not well-defined. (That the transition is only weakly allowed is obvious from the measured lifetimes, since for an allowed transition, the excited state lifetime would be expected to be of the order of 10^{-9}s). Since the symmetry of the Mn environment is the same in both ZnS and ZnSe, the effect of the parity restriction may be ignored in discussing differences between the two systems. The spin-orbit interaction will however be different in the two materials. This effect is embodied in eq (6.6), where it is seen that because of the admixture of the ligand orbitals (which are p-functions)into the central ion d-functions, the spin-orbit interaction for the Mn centre includes the spin-orbit coupling constants of the ligands. As a crude approximation the spin-orbit coupling constant of the ligands is proportional to the mass of the ligands and so the effect of the ligands should be greater when they are selenium rather than sulphur. Strictly speaking, eq. (6.6) applies only the first-order spin-orbit interaction, which is quenched by the Jahn-Teller effect[89]. However the effect of covalency (i.e. admixture of ligand orbitals into those of the central ion) will still be present in second-order, and the

interaction will be greater in the case where the anions are selenium, and not sulphur.

For this reason, the $^4T_1 \rightarrow {}^6A_1$ transition is less forbidden in the ZnSe:Mn system, implying that the lifetime of the $^4T_1$ state of Mn is less in the ZnSe environment than in the ZnS one. Such an argument, based on the effects of covalency, also requires that the lifetime of the $^4T_1$ state of Mn in any mixed crystal of the type $ZnSe_xS_{1-x}$:Mn should lie between those obtained for the ZnS:Mn and ZnSe:Mn systems.

Comparison of Figs (7.16), (7.17) and (7.18) with Fig. (7.4) demonstrates that the variation in lifetimes with temperature occurs at the same temperatures as those for which quenching of the luminescence occurs. This might intuitively have been expected, and can be explained by a more careful consideration of eq (7.12); in this equation, α, the transition probability for a transition out of the excited state is the sum of radiative and non-radiative contributions, and the measured light intensity is proportional to the fraction of these transitions which is radiative. Thus, more correctly, eq (7.13) should be written

$$I(t) \propto \frac{\alpha_r}{\alpha_r + \alpha_{nr}} e^{-(\alpha_r+\alpha_{nr})t} \qquad (7.14)$$

where

$$\tau = \frac{1}{\alpha_r+\alpha_{nr}} \qquad (7.15)$$

Writing eq (7.7) in a slightly different form

$$\eta = \frac{\alpha_r}{\alpha_r+\alpha_{nr}} \qquad (7.16)$$

Comparison of eqs (7.15) and (7.16) shows that both the luminescent efficiency, and the excited state lifetime are proportional to the reciprocal of the non-radiative transition probability (at high enough temperature for the non-radiative transitions to dominate), and so should exhibit the same temperature dependence, at high temperatures. Thus, if α_r is independent of temperature, then $\tau \propto \eta$.

To facilitate this comparison, Figs (7.16), (7.17) and (7.18) are replotted as Figs (7.19), (7.20) and (7.21) respectively, in the form of $\ell n\ \tau$ vs $1/T$. From these, an activation energy can be measured in the same way as from Fig (7.4), which should be in agreement with the activation energies measured by thermal quenching. Absolute confirmation is, however, impossible because of the large scatter of experimental points, giving large errors in the activation energy obtained. The actual values obtained were, for ZnSe:Mn - 0.45 ± 0.15 eV, for $ZnSe_xS_{1-x}$:Mn - 0.59 ± 0.15 eV and for ZnS:Mn - 0.58 ± 0.15 eV. These are in reasonable agreement with those values obtained from quenching measurements (shown in table (7.1)).

Two other features of the results obtained for ZnS:Mn are worthy of mention. The first is that no conclusive identification of the short-lifetime decay mechanism, due to exchange-coupled Mn ion pairs could be made. This is almost certainly an inherent limitation in the experimental method. In order for short lifetimes effects to be measured, the fall time of the exciting light has to be very rapid ($\sim$ 1/10 of the lifetime which is to be measured); this cannot be achieved using a rotating blade to chop the incident rotation, without having the blade velocity too rapid for the steady state (described by eq (7.12) to be achieved. The second feature requiring explanation is the slow variation of lifetime with temperature between $100^{\circ}K$ and $250^{\circ}K$.

This was not observed by Walentynowicz et al[130], indicating that the process is not characteristic of the ZnS:Mn system, but must be attributed to some defect induced relaxation process, which then saturates. From the data on thermal quenching, Fig (7.4)c, there is no appreciable variation in luminescent efficiency over this range implying that the process is a radiative one, with an emission energy in the region of the manganese emission band.

7.5 Conclusions

Whilst conclusive identification of the non-radiative relaxation mechanism which determines the thermal quenching of luminescence has not been made, the number of possibilities has been reduced. From the standpoint of possible device applications a number of important features arise. (For a review of the use of ZnS:Mn, ZnSe:Mn and other II-VI compounds as devices, see[137] and references therein.)

Firstly, the non-radiative recombination process is not an internal multiphonon one, nor an inherent property of the ZnSe:Mn or ZnS:Mn systems. Thus by identification and removal of unwanted impurities, it should be possible to manufacture devices capable of operation at temperatures higher than previously supposed. Also it appears generally true that the temperature at which quenching of luminescence occurs is higher for ZnS:Mn than ZnSe:Mn. This is illustrated in Fig. (7.22) with results from this work, that of Vlasenko[111] and that of Jones and Woods[113]. The temperature at which quenching occurs, for the purposes of this figure, was chosen to be the temperature at which the luminescent efficiency, or light output, was 75% of its value in the lower temperature region where quenching is insignificant. Even if the non-radiative transition mechanism in ZnSe:Mn cannot be

precisely identified and removed, higher quenching temperatures might be achieved by the use of mixed crystals $ZnSe_xS_{1-x}$:Mn.

In switching applications, where fast rise and fall times of luminescence are required, ZnSe:Mn is the better system by approximately an order of magnitude. This could be of importance in the manufacture of thin-film electroluminescent TV display panels ([138] and references therein), which are currently manufactured using ZnS:Mn. Since it is to be expected that the same exchange coupling of Mn pairs would occur in ZnSe:Mn as in ZnS:Mn for high enough Mn concentrations, the initial decay of luminescence from ZnSe:Mn might be dominated by a process having an even shorter lifetime; if enough of the energy of the emission could be concentrated in the relaxation of these pairs (by making the probability of pair formation much greater than the probability of an uncoupled ion), the switching speed of ZnSe:Mn would be effectively even faster than that obtained here.

Table (7.1)

Material†	Activation Energy(E_A)	Corrected Activation Energy
ZnSe:Mn(a)	0.66 ± 0.05 eV	0.65 ± 0.05 eV
ZnSe:Mn(b)	0.61 ± 0.05 eV	0.60 ± 0.05 eV
ZnS:Mn(c)	0.60 ± 0.05 eV	0.59 ± 0.05 eV
$ZnSe_xS_{1-x}$:Mn(d)	0.3 eV	-

† The letters after each material identify it with the appropriate curve of Fig. (7.4).

APPENDIX 7.1

In Fig. (7.6) let the point A be given by the coordinates (x_o, y_o) and the point B be (x_1, y_1). It is obvious from the figure that

$$y_o = E_b + E_e + S\hbar\omega$$
$$= E_{zp} + \tfrac{1}{2}\hbar\omega + E_b \qquad (A.1)$$

For the lower curve, with the origin at the minimum, and assuming that it is parabolic

$$y = Ax^2 \qquad (A.2)$$

For the upper curve, with origin at the minimum of the lower curve, assuming that it is parabolic with the same curvature as the lower curve

$$y' = A(x - x_1)^2 + E_{zp} \qquad (A.3)$$

At (x_1, y_1), $y_1 = S\hbar\omega$ which with eq (A.2) yields

$$A = \frac{S\hbar\omega}{x_1^2} \qquad (A.4)$$

Substituting eq (A.4) into eqs (A.2) and (A.3) yields

$$y = \frac{S\hbar\omega}{x_1^2} x^2 \qquad (A.5)$$

$$y' = \frac{S\hbar\omega}{x_1^2} (x-x_1)^2 + E_{zp} \qquad (A.6)$$

at the point (x_o, y_o), $y = y'$, thus from eqs (A.5) and (A.6)

$$x_o^2 = \frac{(E_{zp} + S\hbar\omega)^2 x_1^2}{4(S\hbar\omega)^2} \qquad (A.7)$$

Substitute eq (A.7) into eq (A.5) to obtain y_o

$$y_o = \frac{(E_{zp} + S\hbar\omega)^2}{4S\hbar\omega} \qquad (A.8)$$

from eq (A.1) eliminate y_o in eq (A.8) to obtain

$$E_b = \frac{(E_{zp} - S\hbar\omega)^2}{4S\hbar\omega} - \tfrac{1}{2}\hbar\omega \qquad (A.9)$$

or from eq (A.1) since $E_{zp} - S\hbar\omega = E_e - \frac{1}{2}\hbar\omega$, eq (A.9) can be written

$$E_b = \frac{(E_e - \frac{1}{2}\hbar\omega)^2}{4S\hbar\omega} - \tfrac{1}{2}\hbar\omega \ . \qquad (A.10)$$

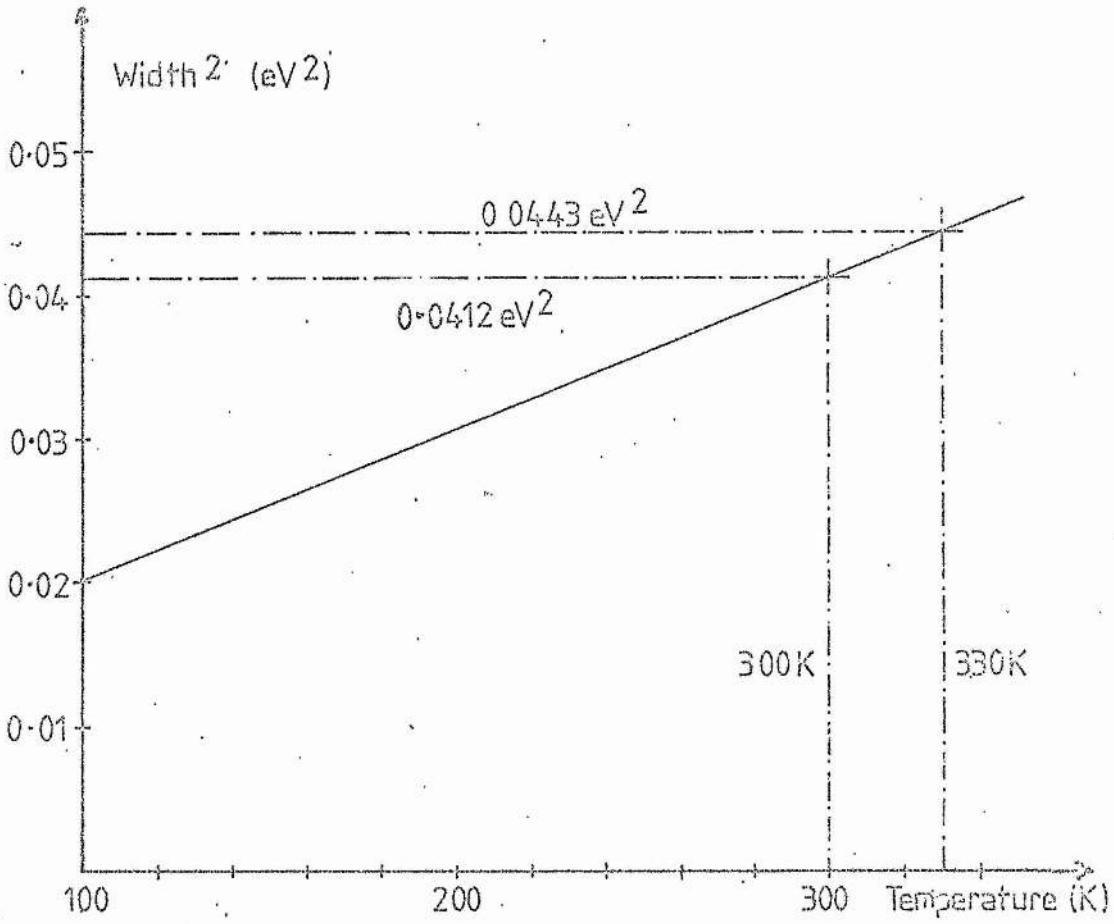

Fig [7-1]

Variation of the width of the $^4T_1 \rightarrow {}^6A_1$ emission band of Mn in ZnSe Mn as a function of temperature (from [113])

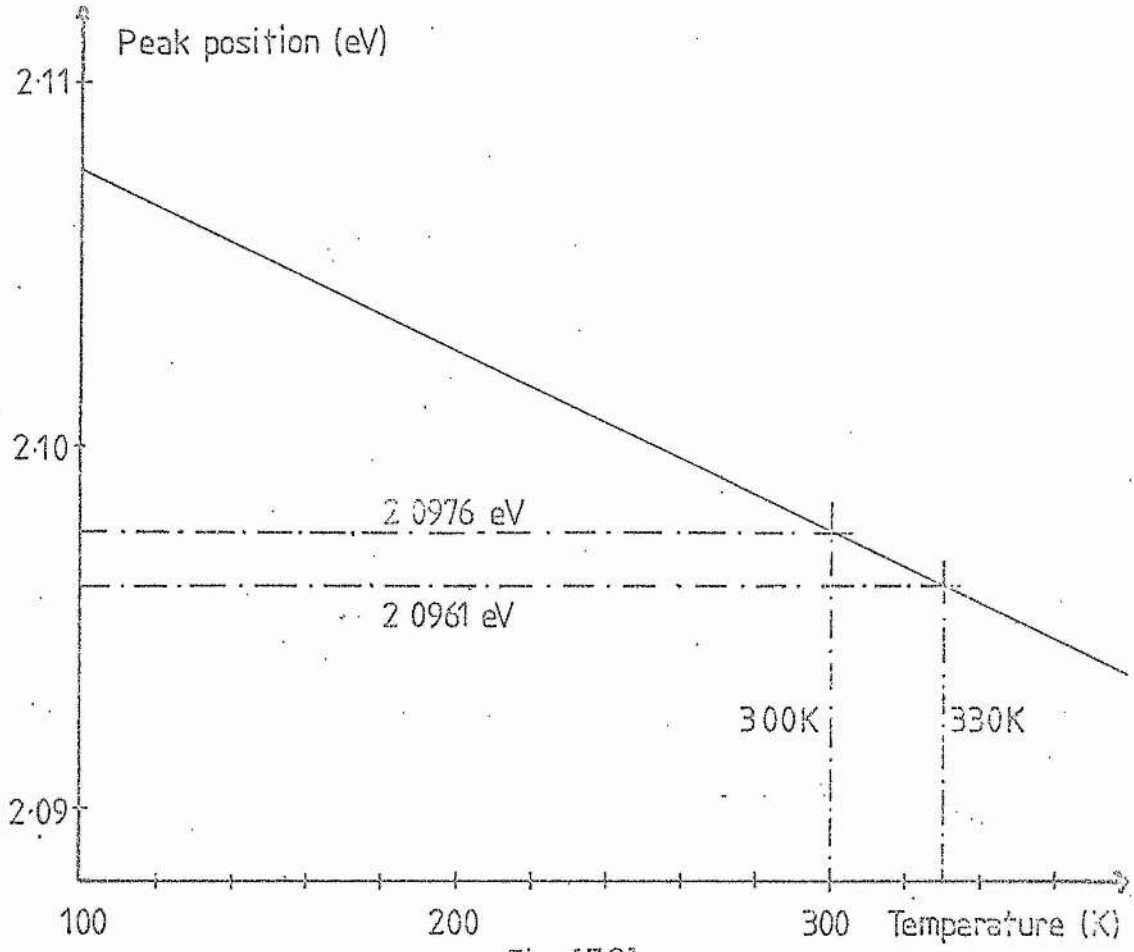

Fig [7-2]

Variation of the peak position of the $^4T_1 \rightarrow {}^6A_1$ emission band of Mn in ZnSe Mn as a function of temperature (from [113])

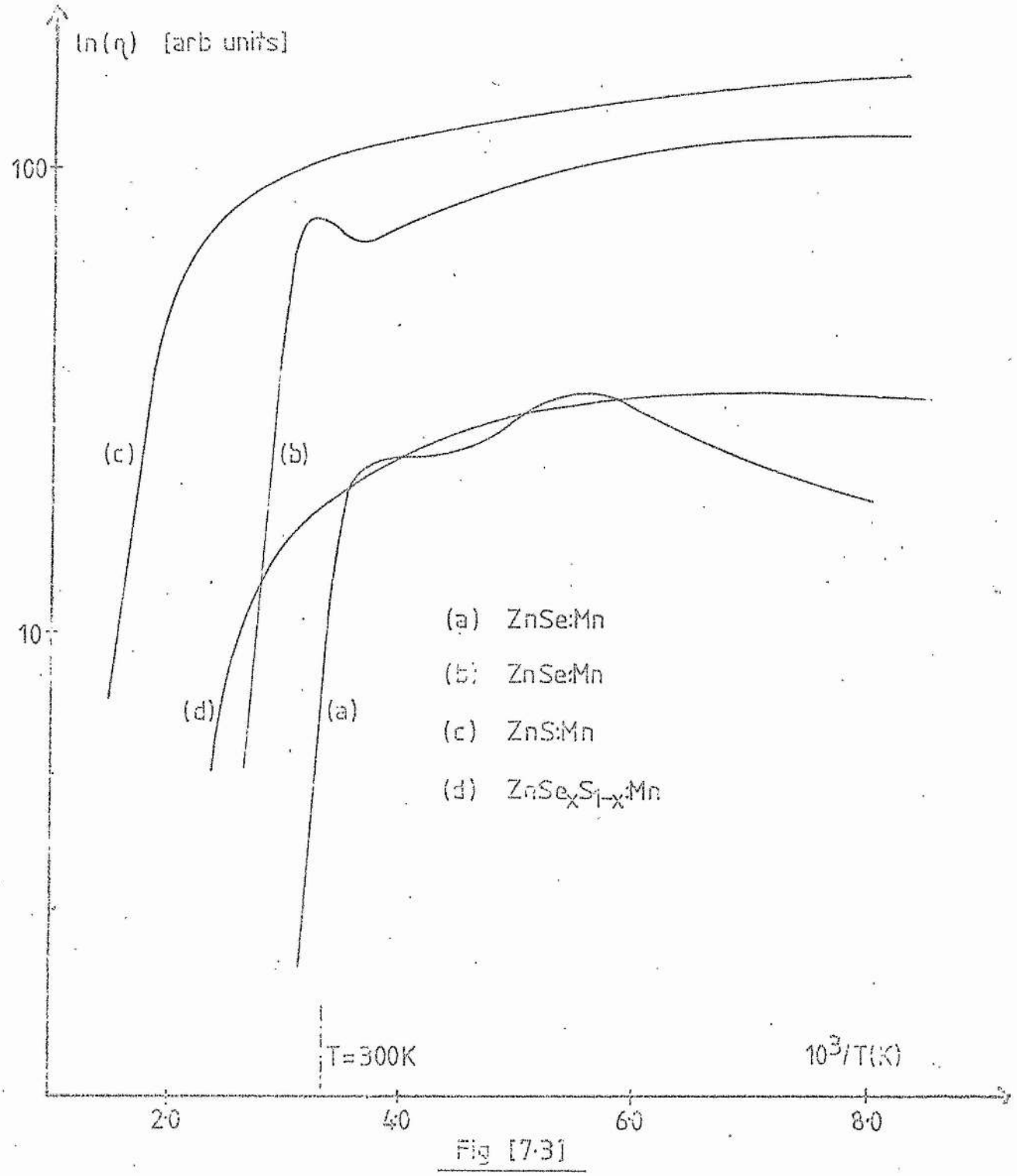

Fig [7·3]

Intensity of the Mn emission band as a function of 1/T

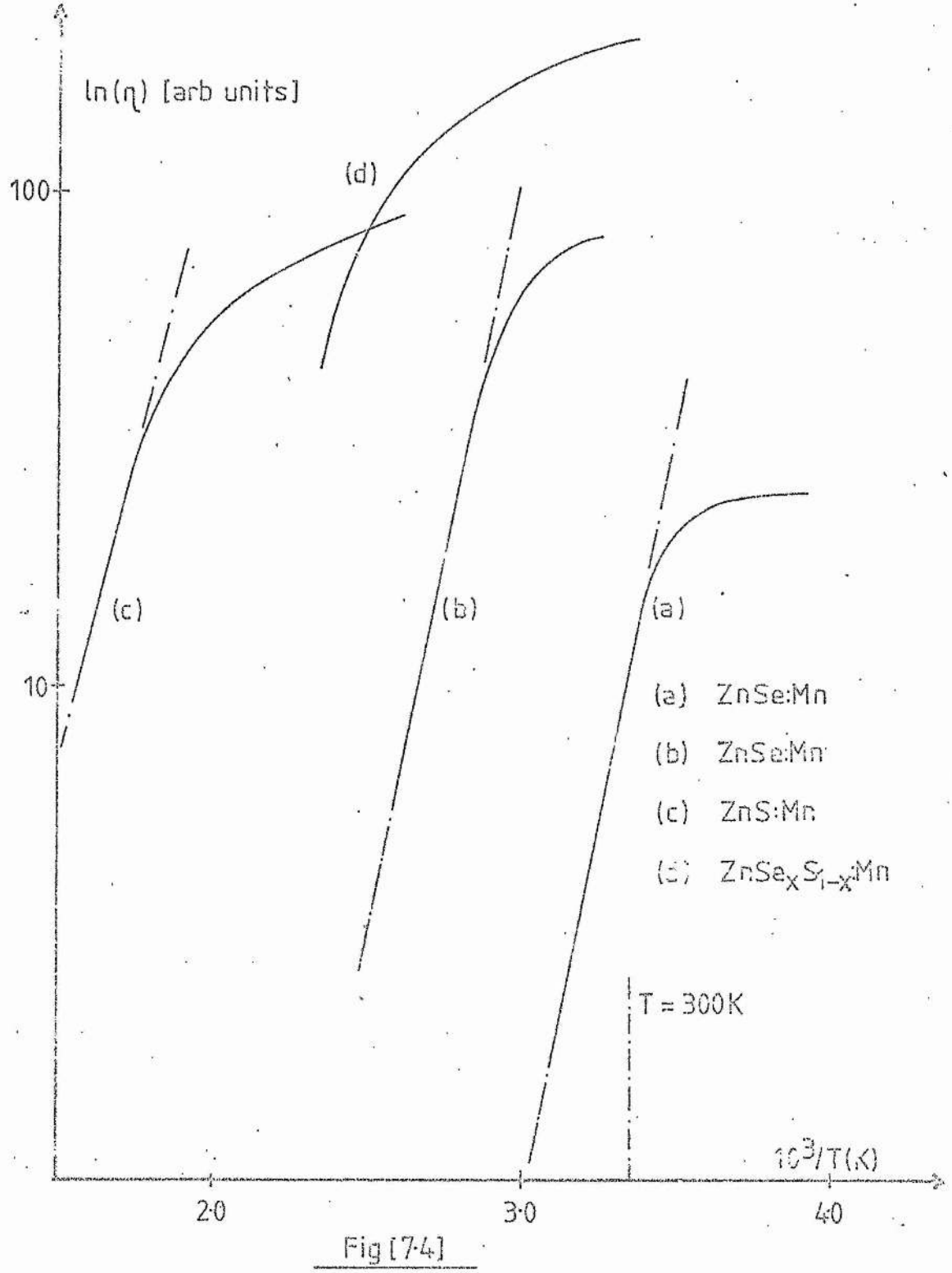

Fig [7·4]

High temperature region of the quenching curves of Fig [7·3]

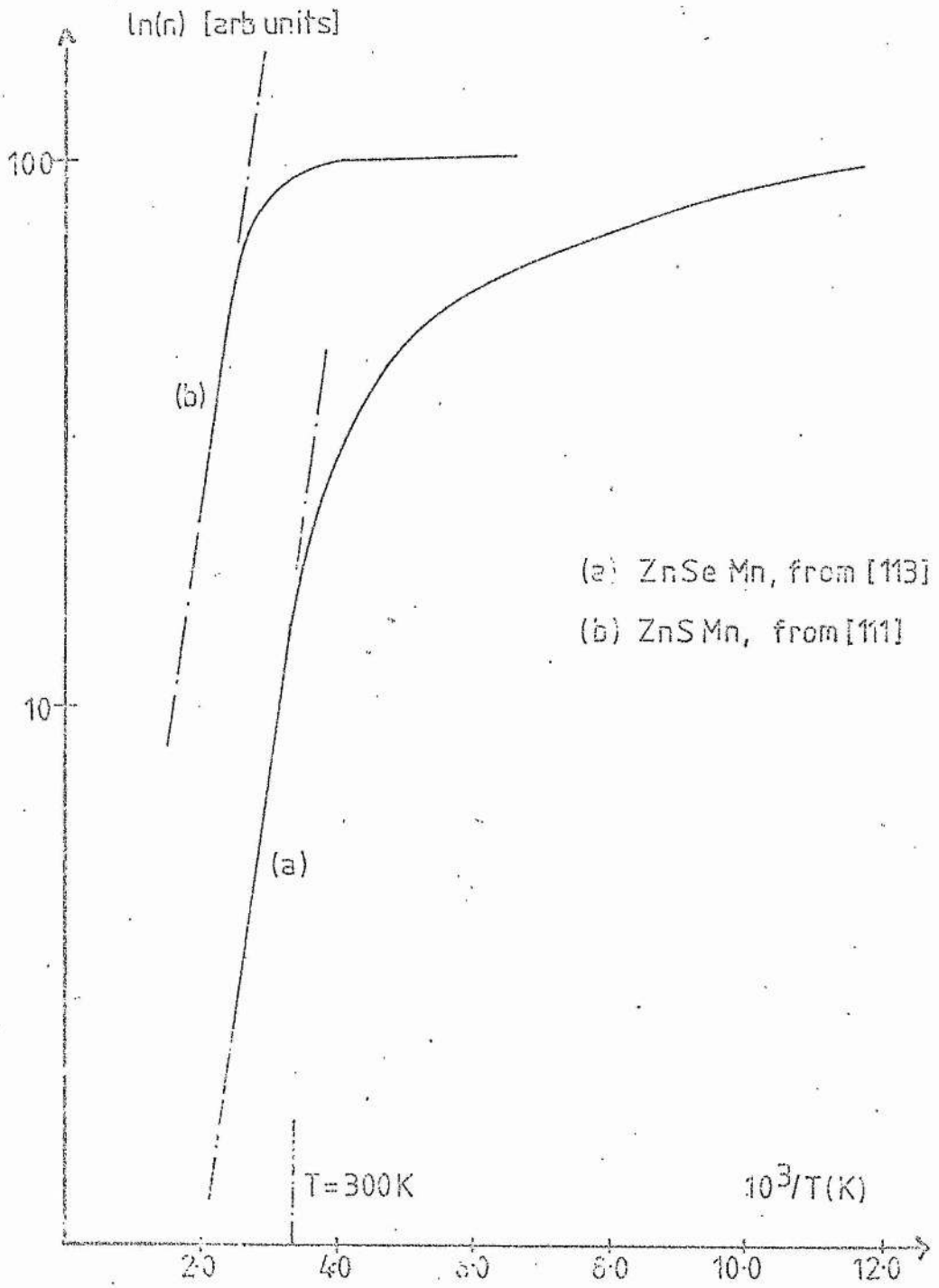

Fig [7·5]

Thermal quenching curves obtained in [111] and [113] for ZnS:Mn and ZnSe:Mn respectively

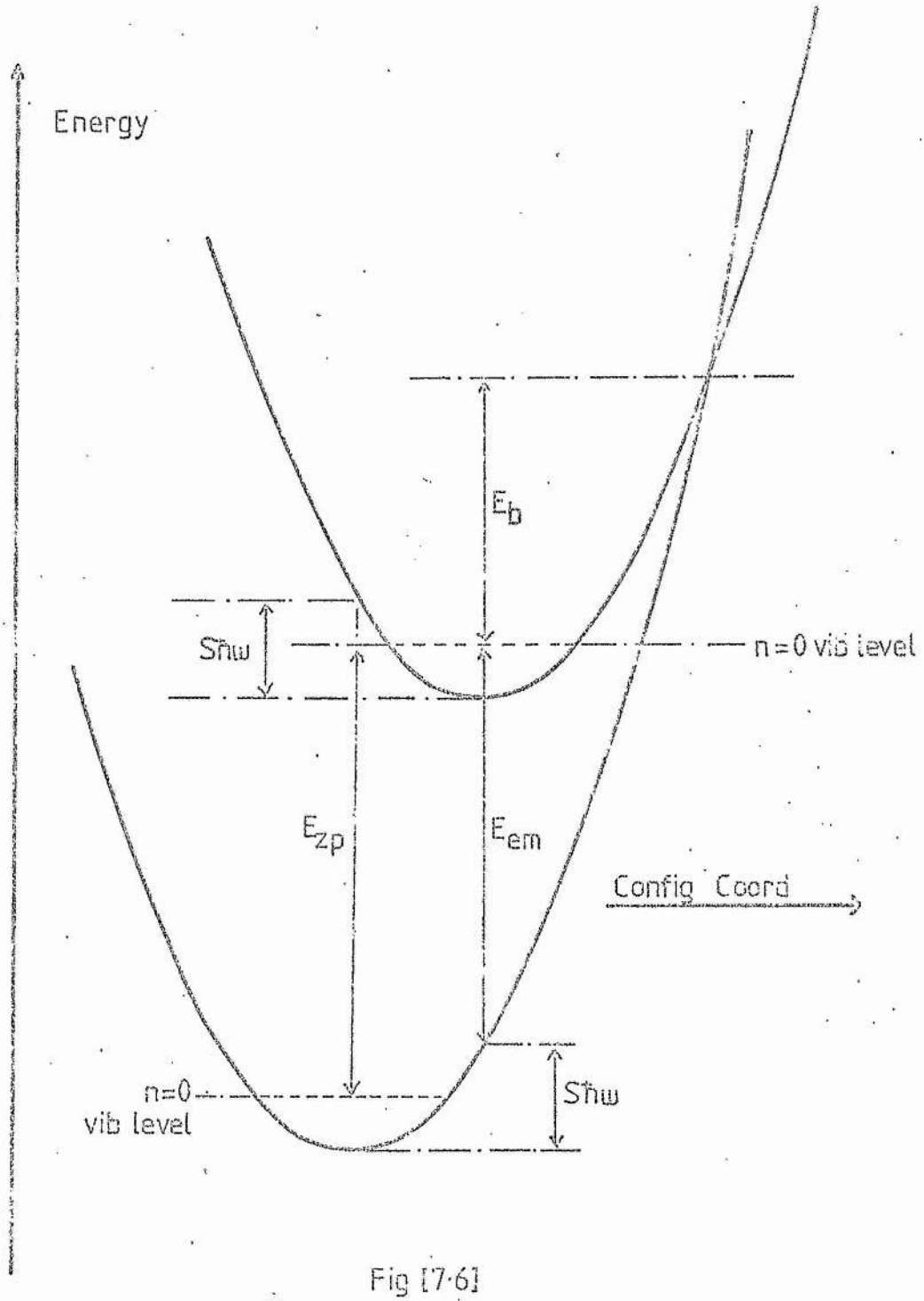

Fig [7·6]

Single mode configurational coordinate diagram

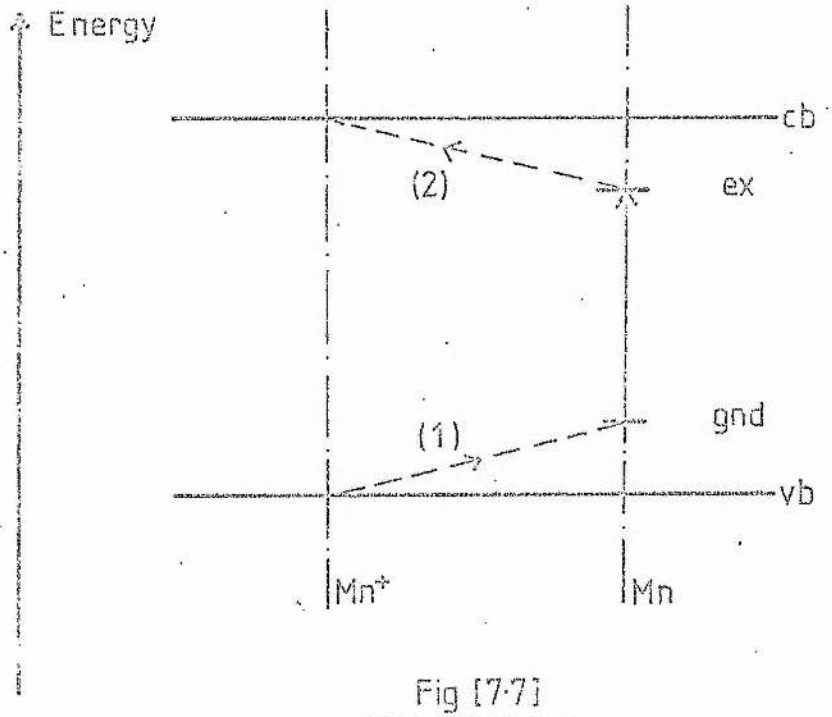

Fig [7·7]

Energy level diagram proposed for model [A]

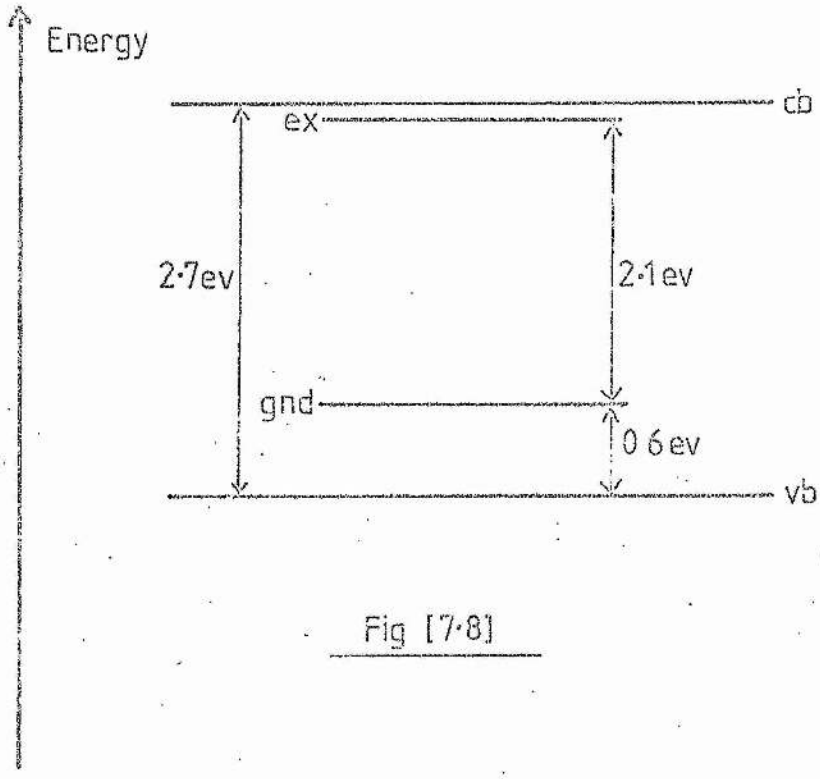

Fig [7·8]

Energy level scheme proposed in [117] for ZnSe:Mn which is consistent with model [A]

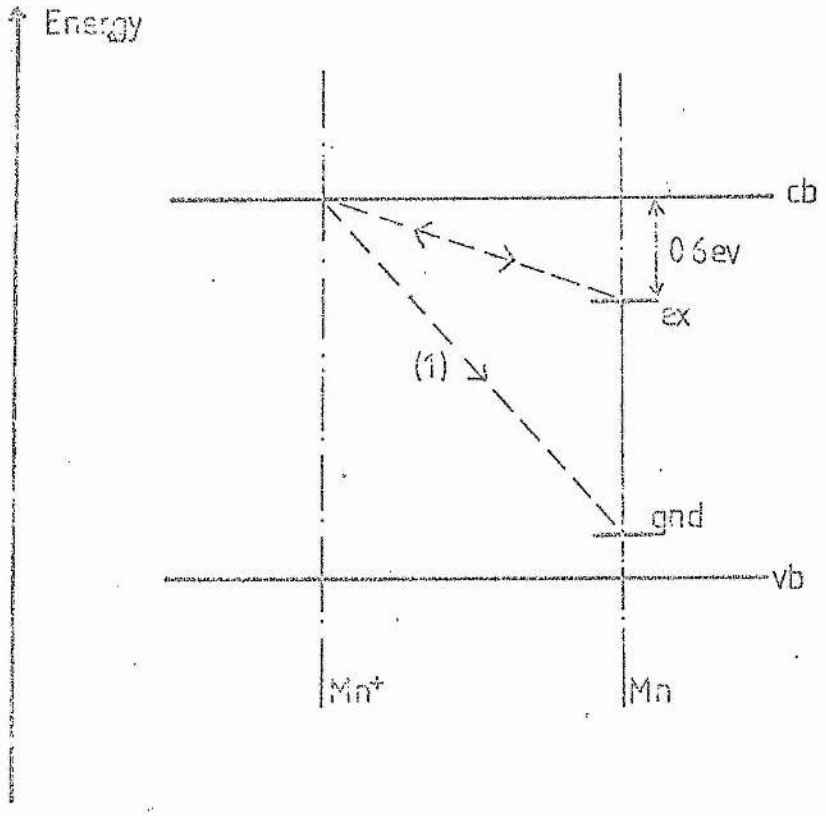

Fig [7·9]

Energy level scheme proposed for model [B] where the transition (1) must be allowed and non-radiative

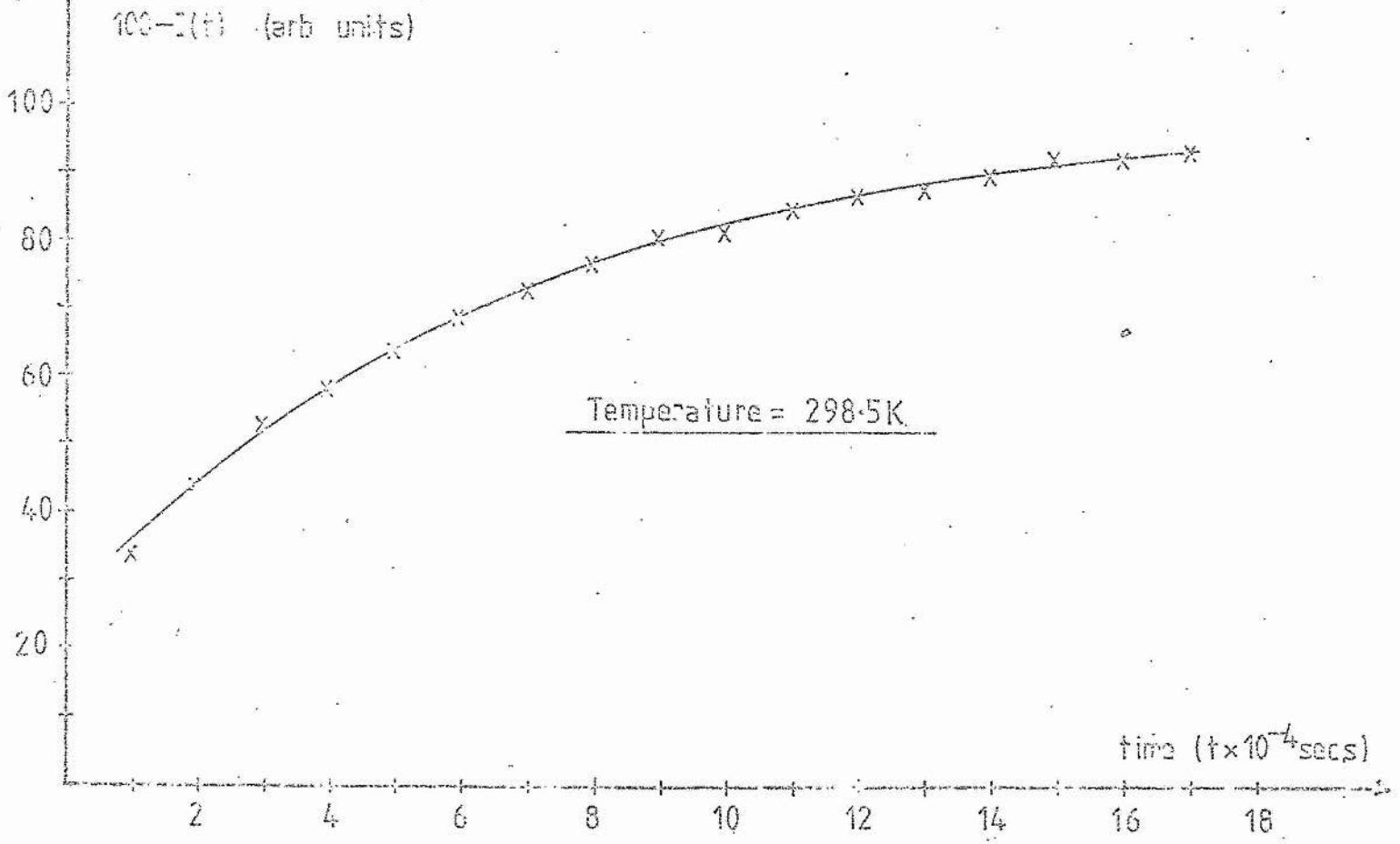

Fig [7·10]

Decay of photoluminescence in ZnS:Mn as a function of time INS true origin on either axis is undetermined — see §5·4

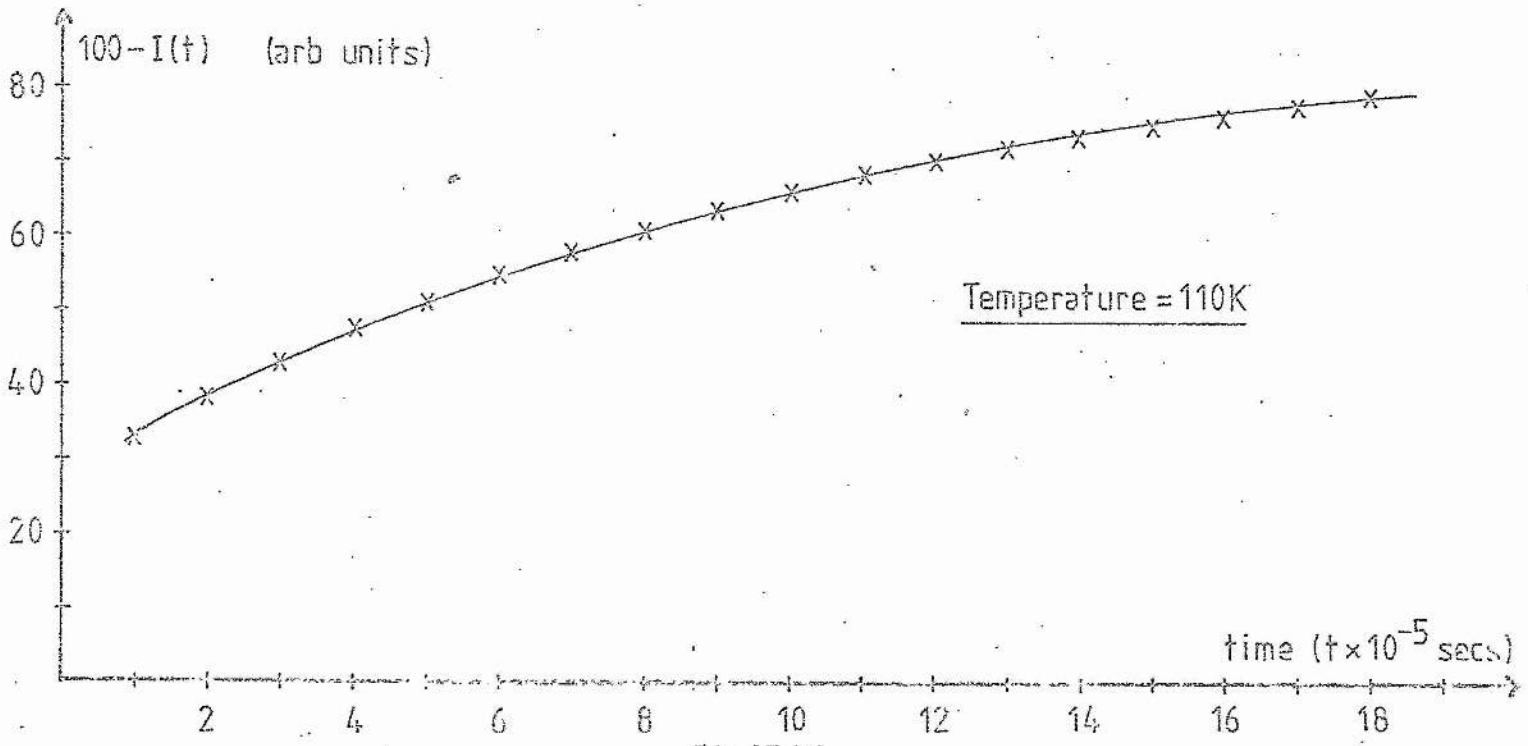

Fig [7·11]

Decay of photoluminescence in ZnSe:Mn as a function of time. [N.B. true origin on either axis is undetermined---see §5·4]

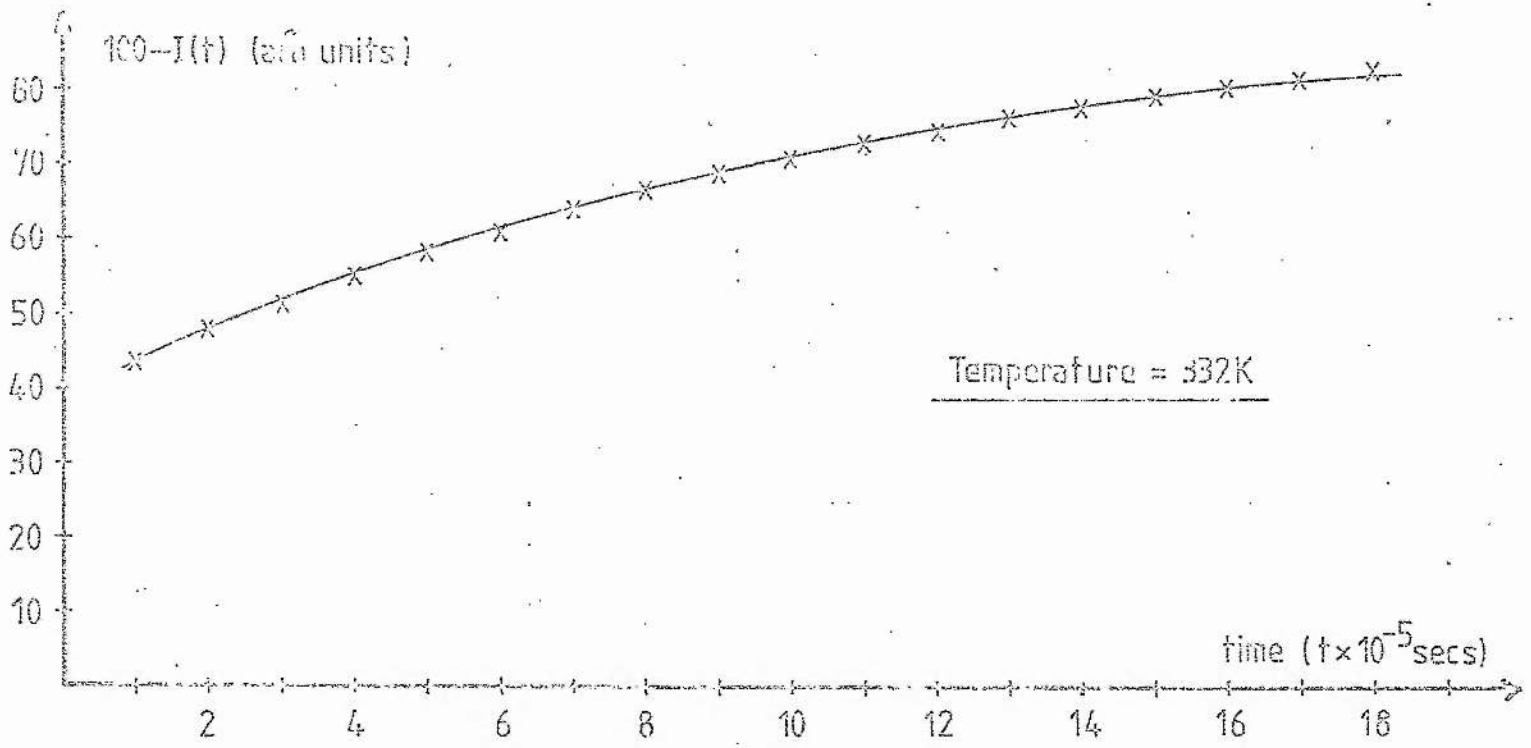

Fig [7·12]

Decay of photoluminescence in $ZnSe_xS_{1-x}$:Mn as a function of time. [N.B. true origin on either axis is undetermined see § 5·4

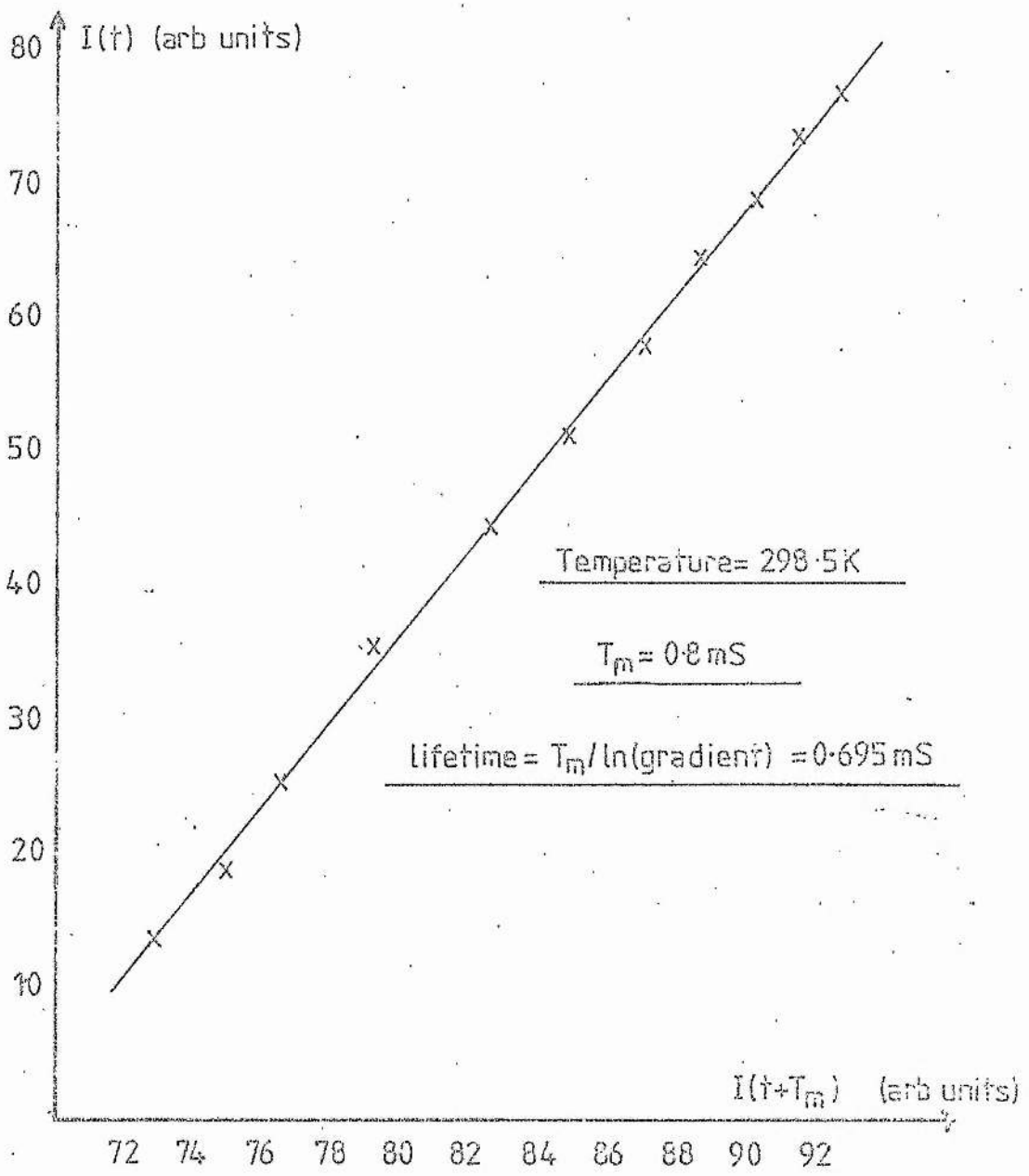

Fig [7·13]

Decay of photoluminescence in ZnS:Mn plotted using the Mangelsdorff difference method described in §5·4

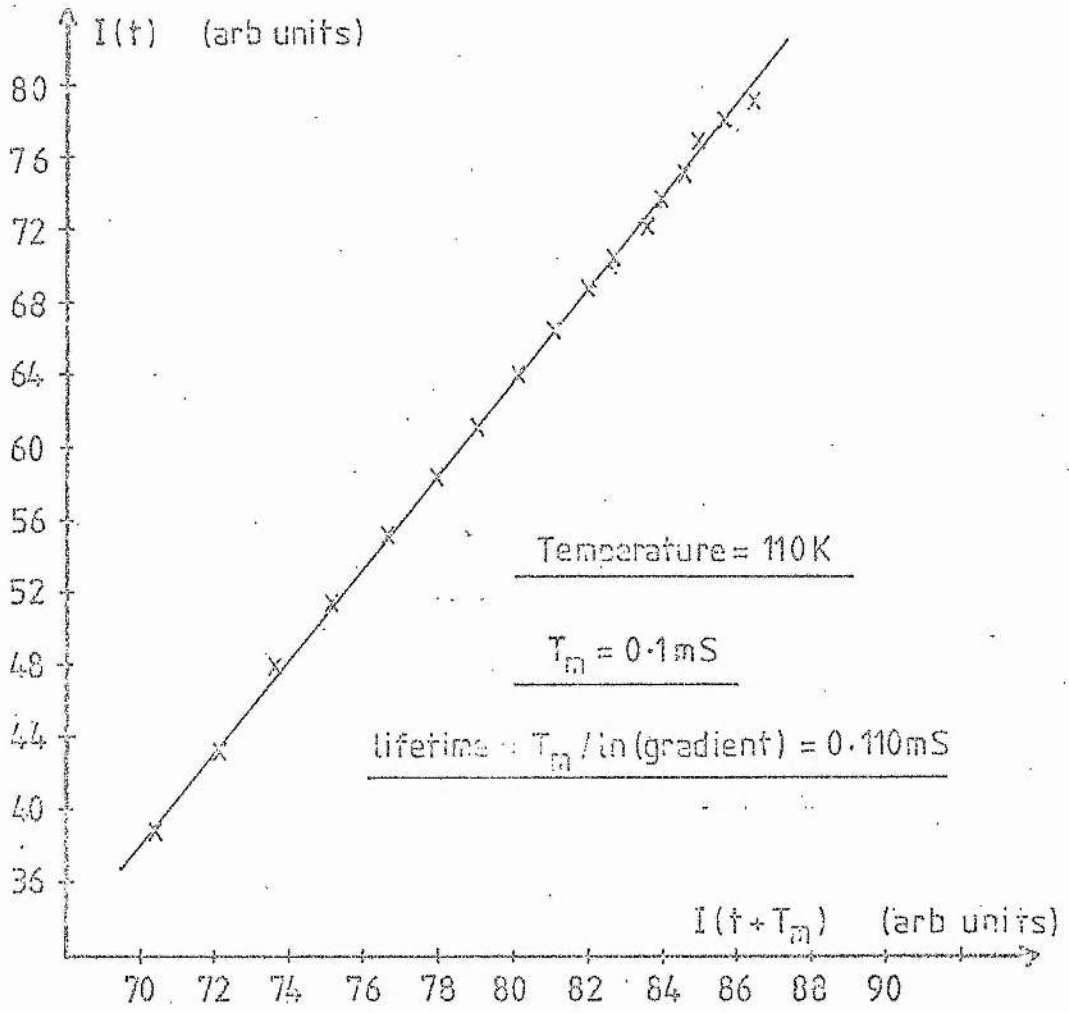

Fig (7·14)

Decay of photoluminescence in ZnSe Mn plotted using the Mangelsdorff difference method described in §5·4

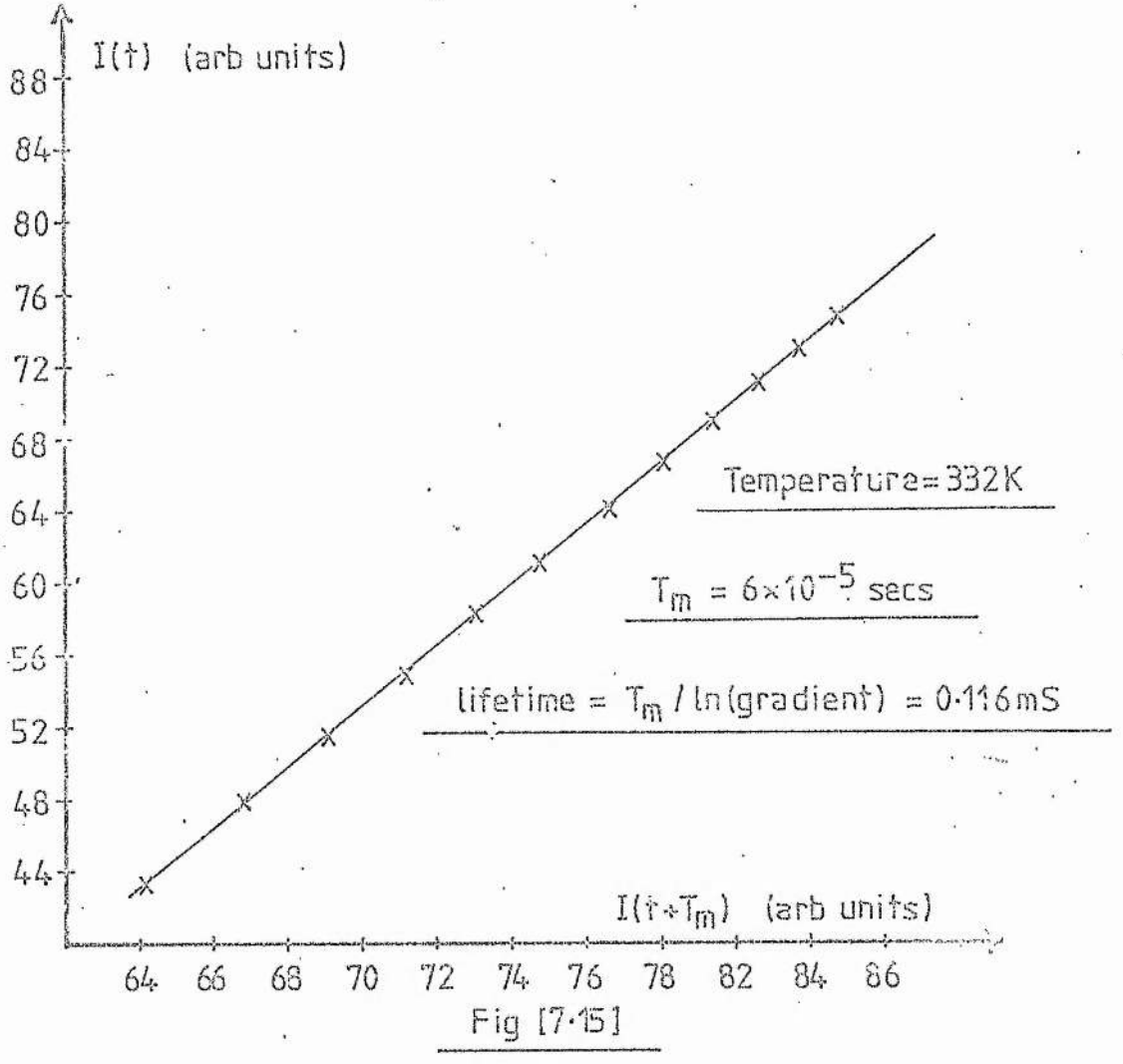

Fig [7·15]

Decay of photoluminescence in $ZnSe_xS_{1-x}Mn$ plotted using the Mangelsdorff difference method described in §5·4

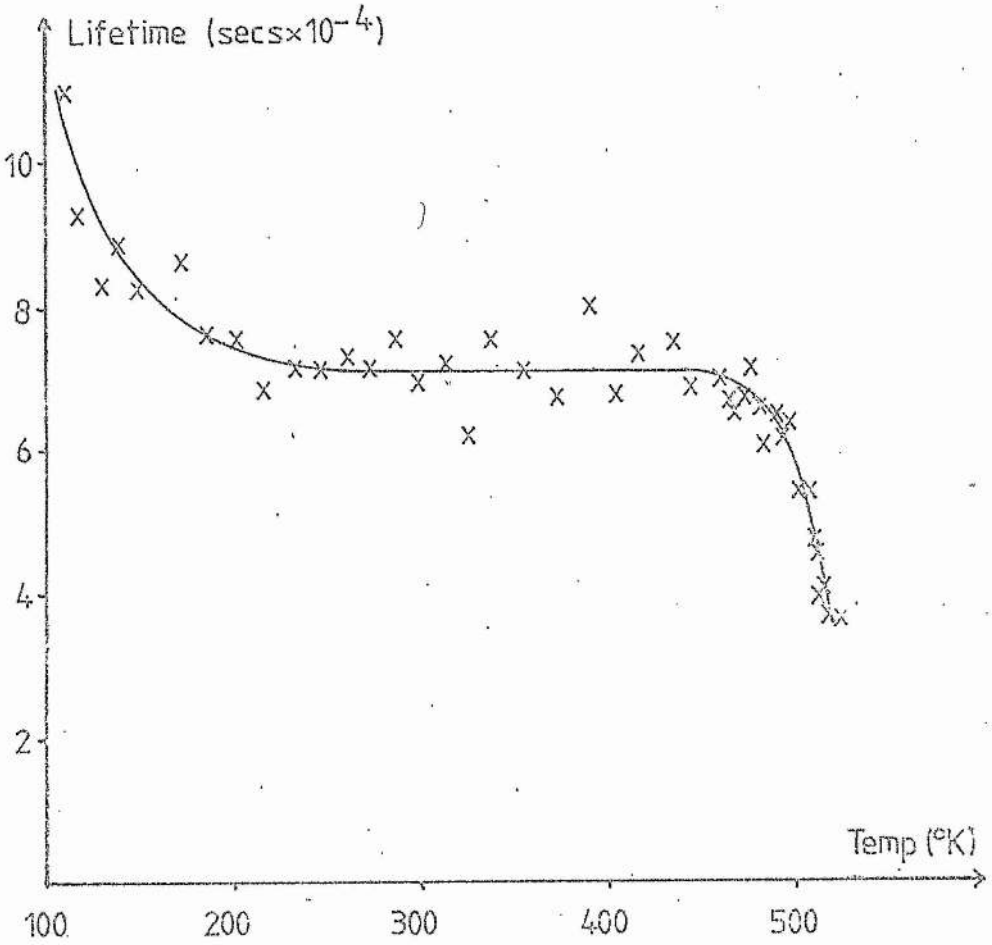

Fig [7-16]

Lifetime of the $^4T_1$ state of Mn in ZnS:Mn as a function of temperature

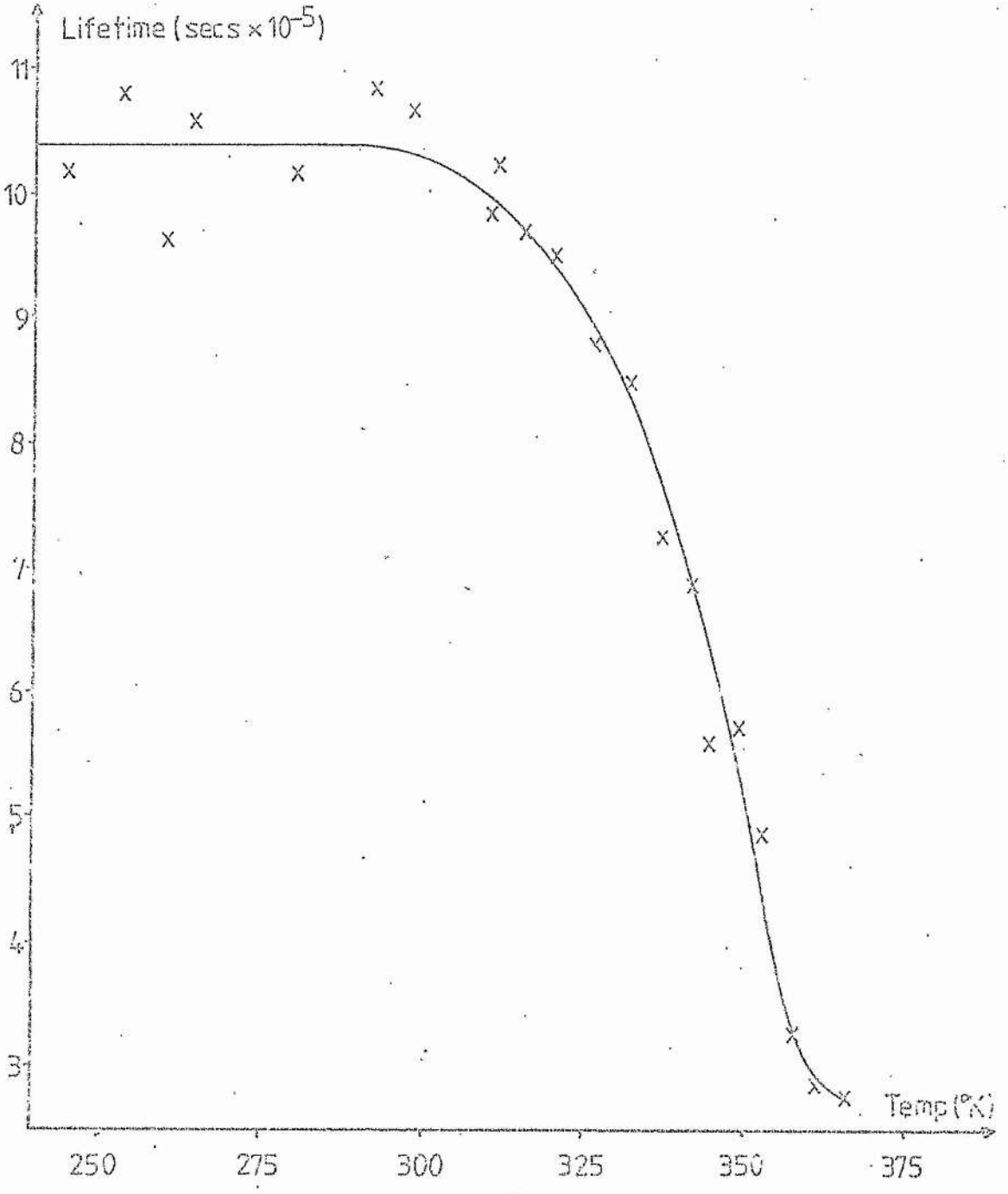

Fig [7·17]

Lifetime of the $^4T_1$ state of Mn in ZnSe:Mn as a function of temperature

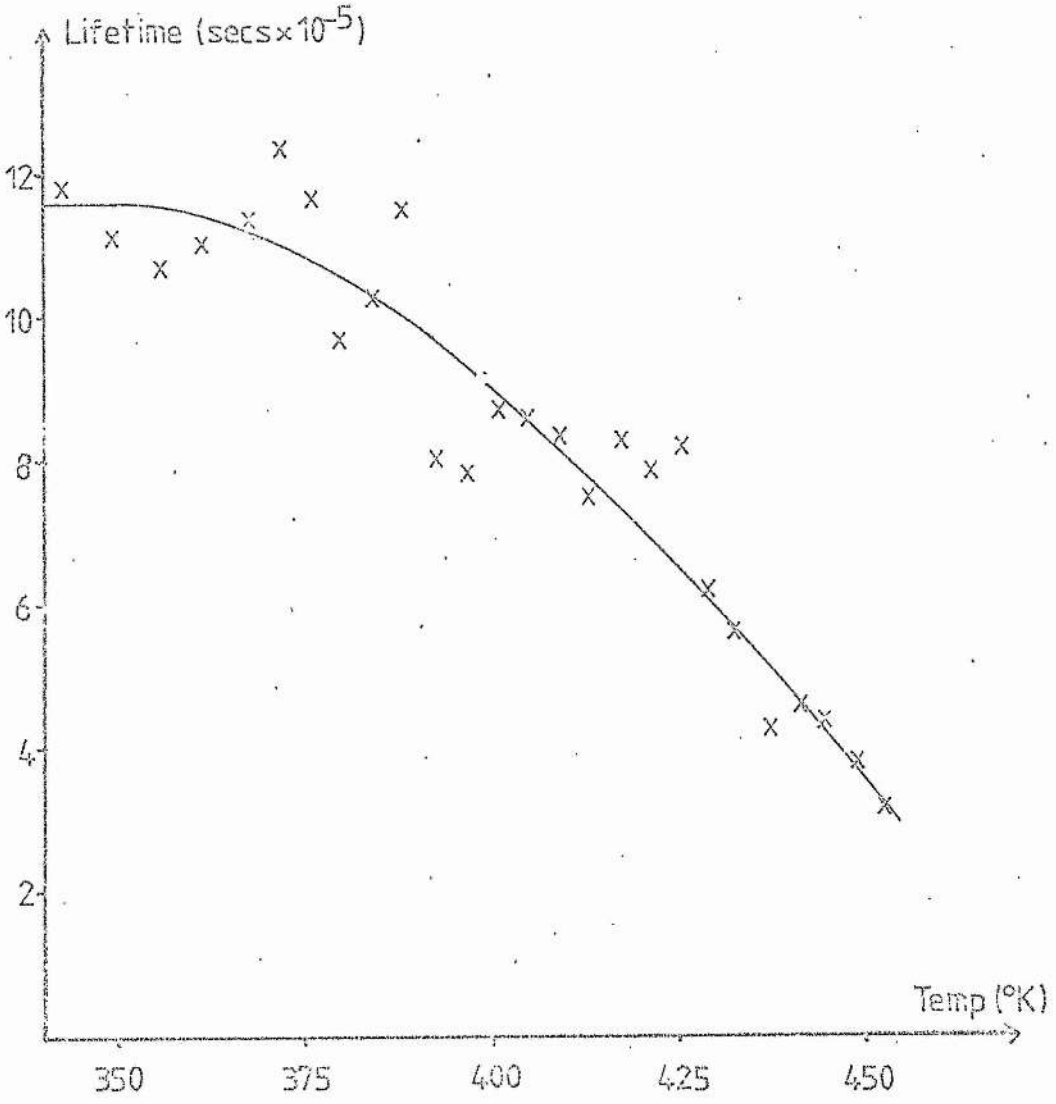

Fig [7-18]

Lifetime of the $^4T_1$ state of Mn in $ZnSe_xS_{1-x}Mn$ as a function of temperature.

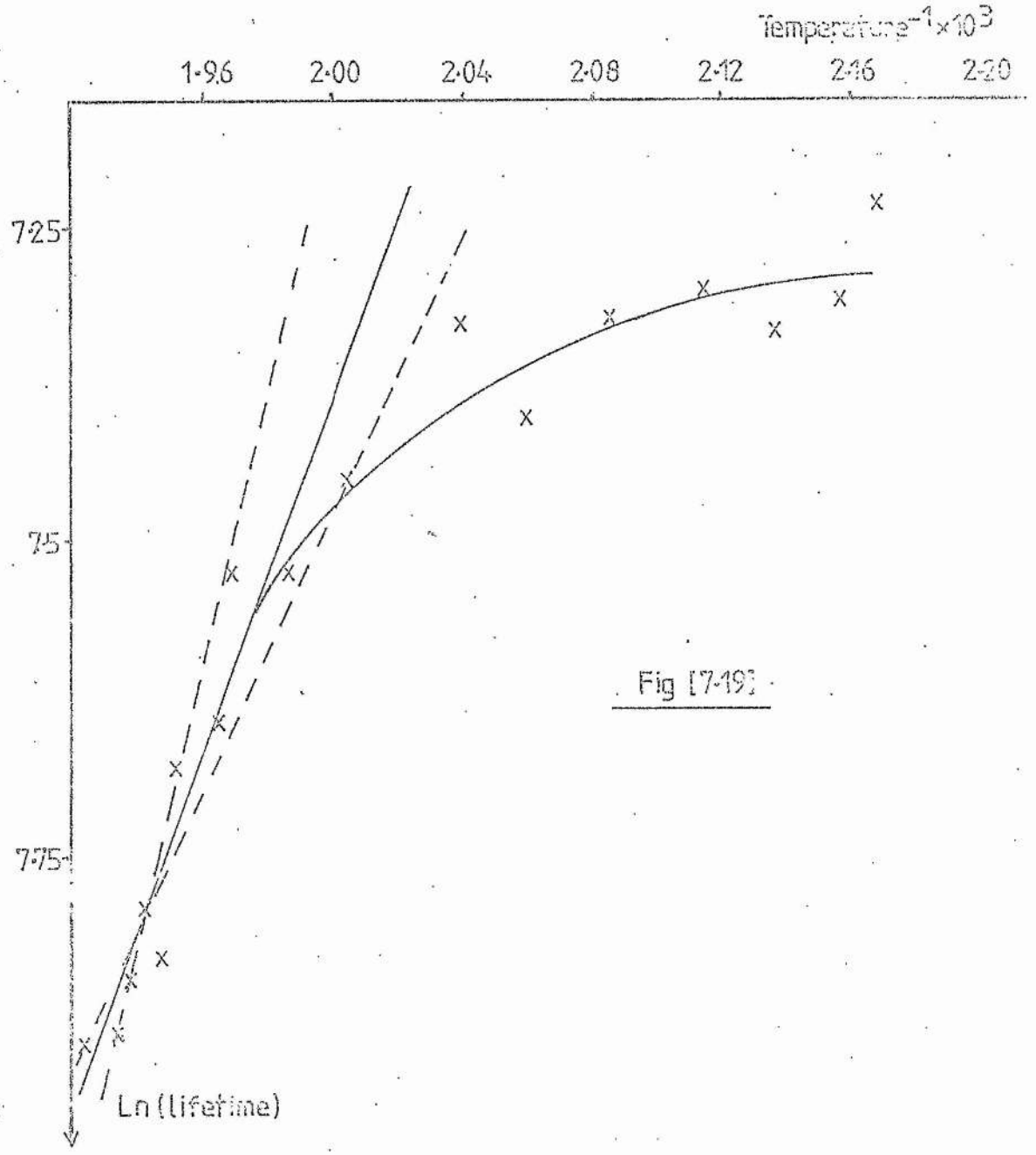

Fig [7-19]

Ln (lifetime) of the $^4T_1$ state of Mn in ZnS:Mn as a function of reciprocal temperature

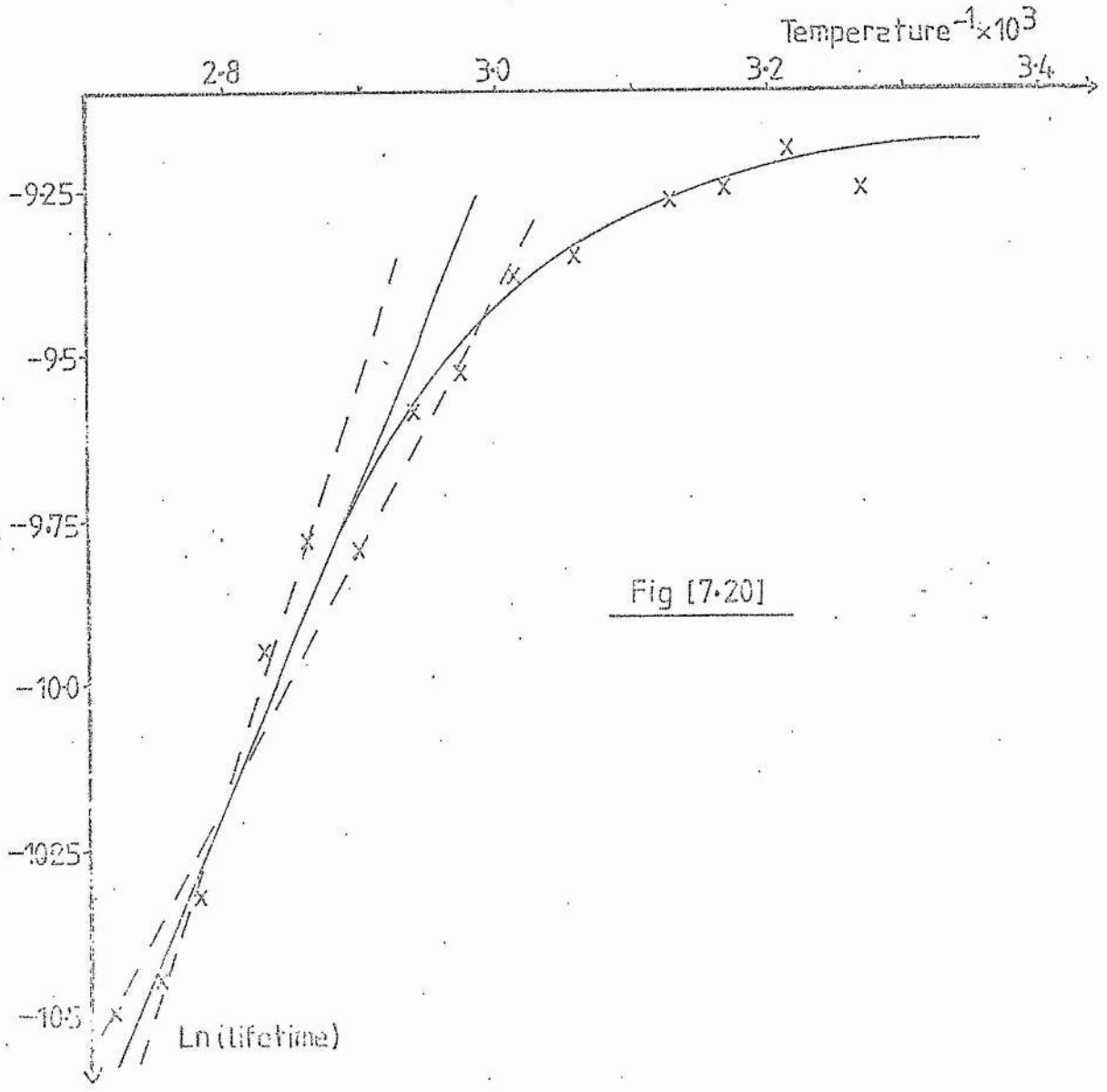

Fig [7·20]

Ln(lifetime) of the $^4T_1$ state of Mn in ZnSe:Mn as a function of reciprocal temperature

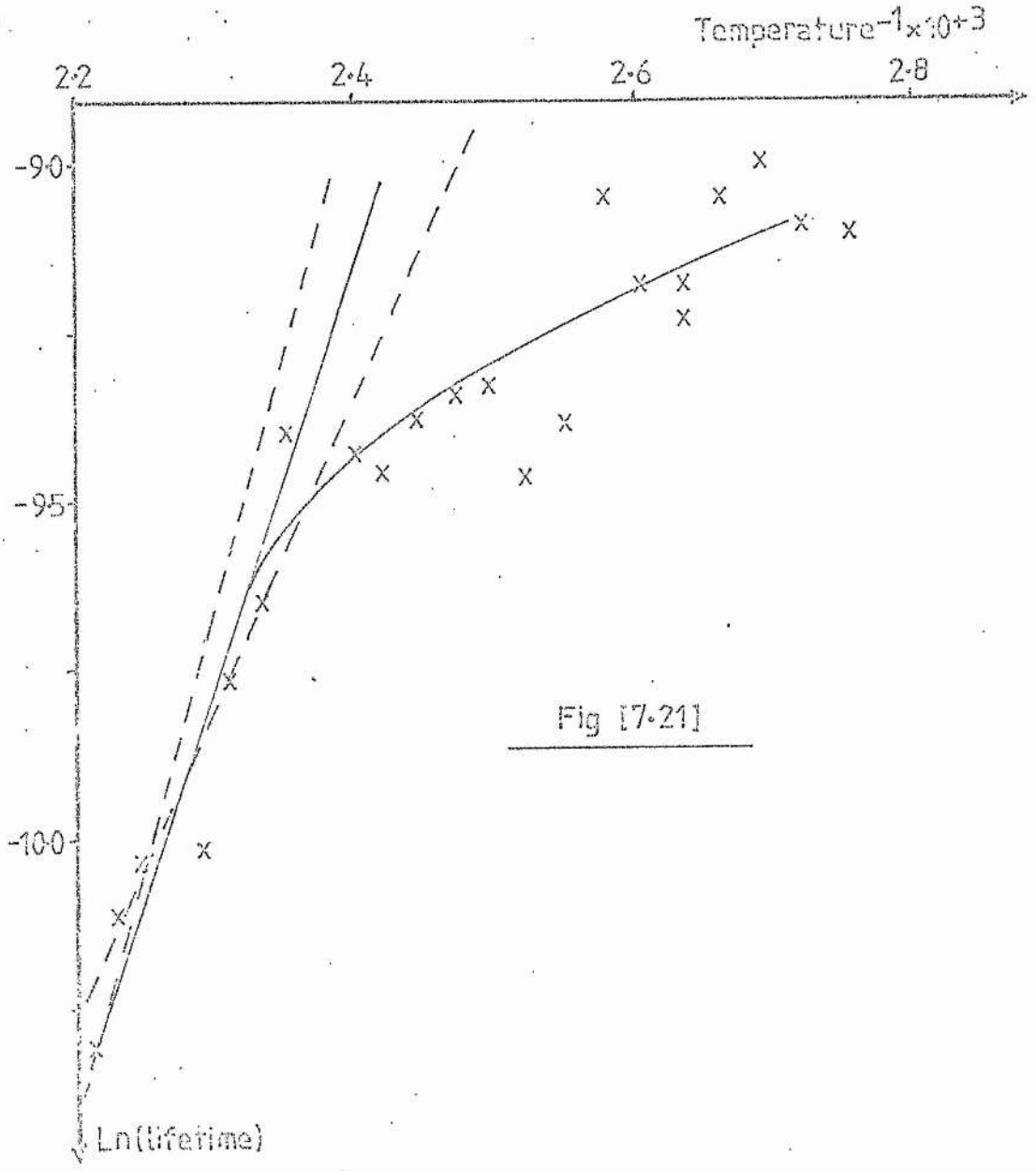

Fig [7·21]

Ln(lifetime) of the $^4T_1$ state of Mn in $ZnSe_xS_{1-x}$:Mn as a function of reciprocal temperature

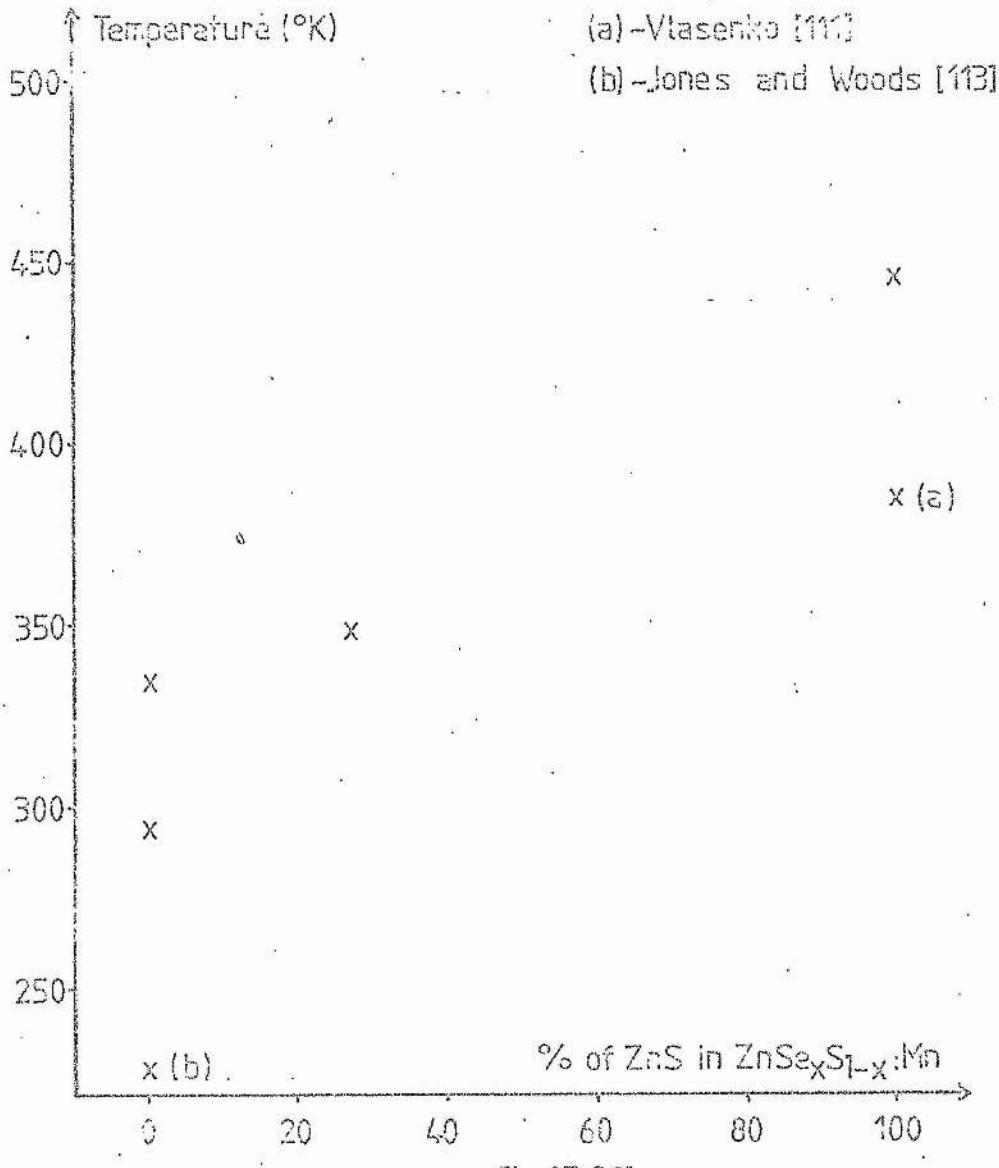

Fig [7·22]

Thermal quenching temperature (see text) as a function of material composition

CHAPTER 8

Concluding Remarks

In Ch.6 it was demonstrated that there is a very complex interplay of effects giving rise to observable quantities. The number of approximations which has to be made in order to explain some of the behaviour is quite appreciable. There is certainly a need for some more complicated calculations which will allow simultaneous treatment of the spin-orbit interaction and the Jahn-Teller effect. Such a calculation should also include the effects of covalent admixtures of ligand wavefunctions into those of the central ion, rather than simply treating a single spin-orbit coupling constant as a parameter.

It is probably a consequence of the accurate experimental technique, that a new broadening mechanism for zero phonon lines has been identified. There are few, if any, reports of zero-phonon line investigations in which both the resolution of the optical system, and control of temperature were simultaneously achieved at such low temperatures. Similar investigations into other materials, where one of the states involved in a transition lies very close in energy to others, may yield further evidence of the Orbach mechanism. Certainly, it should always be considered when dealing with the thermal behaviour of zero-phonon lines, since there is no reason to suggest that it is not as common in these studies, as in spin-lattice relaxation ones. It should also be noted that some of the commonly-used techniques for determining broadening mechanisms yield too many adjustable parameters for the confident fitting of experimental data. As a

general rule, it would appear to be obvious that the minimum number of adjustable parameters be used, assuming that the broadening mechanism invoked is appropriate.

The discussion in Ch 6 on the $^6A_1 \rightarrow {}^4E$ transition, where it was established that there is a great deal of similarity between ZnSe:Mn and ZnS:Mn is one instance of an approach to solid state physics which may bear fruit in the future. This is to characterise compounds by their chemical constituents and to look for trends in material properties based on the chemical families of the constituent elements. This approach has been suggested elsewhere[139]. In this context it would be very interesting to investigate the properties of ZnTe:Mn, and compare this (more covalent) system with ZnS:Mn and ZnSe:Mn, examining especially those properties such as spin-orbit interaction which are to some extent dependent on the admixture of the ligand wavefunctions into the central ion ones.

This effect of increasing covalency was used to account also for the lifetime of the $^4T_1$ state of Mn in ZnSe:Mn having a much shorter lifetime than the same state in ZnS:Mn examination of this state in ZnTe:Mn should, if the covalent argument is appropriate, show an even shorter lifetime.

In terms of analysing material properties with regard to device performance, the results of chapter seven would indicate that the properties of mixed-crystal systems should be investigated more fully. It may then be possible to produce materials with any desired lifetime between 0.1 and 1 mS simply by altering the composition of the mixed crystal. On the other hand, if high temperature performance is required, then mixed-crystal systems might prove to be better than

ZnSe:Mn. Certainly there is a case for examining the properties of $ZnSe_xS_{1-x}$:Mn syscems in order to determine the trend of properties such as quenching temperature and lifetimes with respect to the two endpoint materials.

REFERENCES

1. W. Kohn, Solid State Physics 5 257 (1957).
2. S. Sugano, T. Tanabe and H. Kamimura, "Multiplets of Transition - Metal Ions in Crystals", Academic Press (1970).
3. C.J. Ballhausen, "Introduction to Ligand Field Theory," McGraw-Hill (1962).
4. J.S. Griffith, "The Theory of Transition Metal Ions" Cambridge University Press (1964).
5. H.A. Bethe, Ann. Physik 3, 133 (1929).
6. J.C. Phillips, Phys. Rev. 166 832 (1968).
7. J.W. Allen, Proc. Int. Conf. Physics of Semiconductors p 781 Paris (1964).
8. F.D.M. Haldane and P.W. Anderson, Phys. Rev. 13, B2553 (1976).
9. T.A. Koopmans, Physica 1 104 (1933).
10. J.C. Slater, "Quantum Theory of Matter", McGraw-Hill (1951).
11. M. Born and K. Huang,"Dynamical Theory of Crystal Lattices", Oxford University Press (1954).
12. C.C. Klick and J.H. Schulman, Solid State Physics 5 (1957).
13. A.E. Hughes, J. Phys. 28, Colloque C4, pC4-55 (1967).
14. C.C. Klick, D.A. Patterson and R.S. Knox, Phys Rev 133, A1717 (1964).
15. M. Lax, J Chem Phys 20 1752 (1952).
16. K. Huang and A. Rhys, Proc Roy Soc A204 406 (1950)
17. D.E. McCumber, Phys Rev 135 A1676 (1964).
18. M.Mostoller, B.N. Ganguly and R.F. Wood,Phys Rev 4, B2015 (1971).

19. K.K. Rebane, "Impurity Spectra ofSolids" Plenum Press (1970).

20. M.D. Sturge, Solid State Physics 20 92 (1967).

21. R. Englman, "The Jahn-Teller Effect in Molecules and Crystals", Wiley (1972).

22. H.C. Longuet-Huggins, Advan. Spectry. 2, 429 (1961).

23. A.M. Stoneham, "Theory of Defects in Solids" Oxford University Press (1975).

24. H.A. Jahn and E. Teller, Proc Roy Soc A161 220 (1937).

25. H.A. Jahn, Proc Roy Soc A164 117 (1938).

26. W.L. Clinton and B. Rice, J. Chem. Phys. 30 542 (1959).

27. R.P. Feynmann, Phys. Rev. 56, 340 (1939).

28. H. Hellmann, "Quantenchemie", Deuticke, Liepzig (1937).

29. R.S. Mulliken, Phys. Rev. 43, 279 (1933).

30. M.C.M. O'Brien, J. Phys. C :Sol St Phys 5 2045 (1972).

31. J.C. Sloncewski, Phys Rev 131 1596 (1963).

32. J.R. Fletcher, J Phys C:Sol St Phys 5 852 (1972).

33. M.C.M. O'Brien, Phys Rev 187 407 (1969).

34. M.C.M. O'Brien, J. Phys C Sol St Phys 4 2524 (1971).

35. A.D. Liehr, J Phys Chem 67 pp 389 and 471 (1963).

36. U. Öpik and M.H. L. Pryce, Proc Roy Soc A238 425 (1957) and A244 1 (1958).

37. A.M. Stoneham and M. Lannco, J. Phys Chem Solids 30, 1769 (1969).

38. F.S. Ham, Phys Rev 138 A1727 (1965).

39. R.C. O'Rourke, Phys Rev 91 265 (1953).

40. S.I. Pekar

41. E.O. Kane, Phys Rev 119 40 (1960).

42. D.B. Fitchen, "Physics of Color Centres", ed W.B. Fowler, Academic Press (1968).

43. M.N. Sapozhnikov, Phys Stat Sol (b) 75 11 (1976).

44. T.H. Kiel, Phys Rev 140 A601 (1965).

45. J.J. Markham, Rev Mod Phys 31 956 (1959).

46. D.E. McCumber, J. Math. Phys 5 221 (1964).

47. A.A. Maradudin, Solid State Physics 18, 273 (1966).

48. M.C.M. O'Brien, Proc Phys Soc 86, 847 (1965).

49. D.E. McCumber, J Math Phys 5 508 (1964).

50. Y.E. Perlin, Sov Phys Sol St 10 1531 (1969).

51. Y.B. Rozenfield, B.G. Vekhter and B.S. Tsukerblat, Sov Phys JETP 28 1195 (1969).

52. N. Bloembergen, E.M. Purcell and R.V. Pound, Phys Rev 73 679 (1948).

53. D.E. McCumber, Phys Rev 133 A163 (1964).

54. D.E. McCumber and M.D. Sturge, J App Phys 34 1682 (1963).

55. J.M. Ziman, Proc Roy Soc A226 436 (1954).

56. T.H. Kiel, Phys Rev 126 1292 (1962).

57. W.M. Yen, W.C. Scott and A.L. Schawlow, Phys Rev 136 A271 (1964).

58. J.H. Van Vleck, Phys Rev 57 426 (1940).

59. W.C. Scott, Stanford University M.L. Report No 1390 (1965).

60. R Orbach, Proc Roy Soc A264 458 (1961).

61. C.B.P. Finn, R. Orbach and W.P. Wolf, Proc Phys Soc 77 261 (1961).

62. C.P. Poole and H.A. Farach, "Relaxation in Magnetic Resonance", Academic Press (1971).

63. W. Heitler, "Quantum Theory of Radiation", Oxford University Press (1954).

64. D.E. McCumber, Phys Rev 130 2271 (1963).

65. R. Orbach, "Proceedings of the Scottish Universities Summer School", ter Haar (ed), (1961).

66. A.C.G. Mitchell and M.W. Zemansky, "Resonance Radiation and Excited Atoms", Cambridge University Press (1934).

67. M.A. Krivoglaz, Sov Phys Sol St 6 1340 (1964).

68. A.F. Lubchenko and I.I. Fischuk, Sov Phys Dokl 18 493 (1974).

69. M. Mostoller, B.A. Henderson, W.A. Sibley and R.F. Wood, Phys Rev 4B 2667 (1971).

70. A.M. Stoneham, Rev Mod Phys 41 82 (1969).

71. G.F. Imbusch, W.M. Yen, A.L. Schawlow, D.E. McCumber and M.D. Sturge, Phys Rev 133 A1029 (1964).

72. L.G. Suslina, D.L. Fedorov, S.G. Konnikov, F.F. Kodzhespirov, A.A.Andreev and E.G. Sharlai, Sov Phys Semicond 11 1132 (1977).

73. S. Larach, R.E. Schrader and C.F. Stocker, Phys Rev 108 587 (1957).

74. Handbook of Chemistry and Physics 46th ed The Chemical Rubber Co.

75. F.A. Rushworth and D.P. Tunstall, "Nuclear Magnetic Resonance"

76. G.W. Ludwig and H.H. Woodbury, Sol St Phys 13 223 (1962).

77. G.W. Ludwig and H.H. Woodbury, Phys Rev Lett 5 98 (1960).

78. R.S. Title, Phys Rev. 131 2503 (1963).

79. B.C. Cavenett, Proc Phys Soc 84 1 (1964).

80. D.W. Langer and H.J. Richter, Phys Rev 146 554 (1966).

81. L.E. Orgel, J Chem Phys 23 1004 (1955).

82. S. Sugano and Y. Tanabe, J Phys Soc Japan 9 753; 766 (1954).

83. J.T. Vallin, G.A. Slack, S. Roberts and A.E. Hughes, Phys Rev B2 4313 (1970).

84. G.A. Slack, F.S. Ham and R.M. Chrenko, Phys Rev 152 376 (1976).

85. D. Posener, Australian J Phys 12 184 (1959).

86. M. Danos and S. Geschwind, Phys Rev 91 1159 (1953).

87. M. Born, "Optik", J Springer (Berlin)(1933).

88. J. Schneider, S.R. Sircar and A. Rauber, Z Naturforsch 18a 980 (1963).

89. P. Koidl, Phys Stat Sol b 74 477 (1976).

90. D. Fournier, A.C. Boccara and J.C. Rivoal, J Phys C Sol St Phys 10, 113 (1977).

91. R. Parrot, C. Naud, C. Porte, D. Fournier, A.C. Boccara and J.C. Rivoal, Phys Rev B17 1057 (1978).

92. J.T. Vallin and G.D. Watkins, Phys Rev B9 2051 (1974).

93. J. Owen and J.H.M. Thornley, Rep Prog Phys 29 827 (1966).

94. D. Langer and S. Ibuki, Phys Rev 138 A809 (1965).

95. M. Zigone, R. Beserman and B. Lambert, J Lum 9 45 (1974).

96. B. Lambert, T. Buch and A. Geoffrey, Phys Rev B8 863 (1973).

97. R. Parrot, C. Naud and F. Gendron Phys Rev B13 3748 (1976).

98. R. Parrot and D. Curie, J Lum 12/13 811 (1976).

99. B. Nygren, J.T. Vallin and G.A. Slack, Sol Stat Comm 11, 35 (1972).

100. E.I. Peripelitsa, Sov Phys Sol St 17 1660 (1976).

101. L.D. Merkle, R.C. Powell and T.M. Wilson, J Phys C Sol St Phys 11 3103 (1978).

102. J.T. Gourley, Phys Rev B5 22 (1971).

103. Y.P. Gnatenko and A.K. Rozhko, JETP Lett, 24 107 (1976).

104. R. Boyn, Phys Stat Sol (b) 72 173 (1975).

105. Q. Kim, R.C. Powell, M. Mostoller and T.M. Wilson, Phys Rev B12 5627 (1975).

106. C. Blanchard, A. Landi, R. Parrot, C. Naud and R. Romestain, Phys Lett 44A 17 (1973).

107. C. Blanchard and R. Parrot, Sol Stat Comm 10 413 (1972).

108. R. Parrot and C. Blanchard, Phys Rev B6 3992 (1972).

109. S. Koide and M.H.L. Pryce, Phil Mag 3 607 (1958).

110. R.R. Sharma, T.P. Das and R. Orbach, Phys Rev 149 257 (1966).

111. N.A. Vlasenko, Opt andSpect 8 445 (1960).

112. G.F.J. Garlick and M.H.F. Wilkins, Proc Roy Soc A184 408 (1945).

113. G. Jones and J. Woods, J. App Phys 6 1640 (1973).

114. D. Curie, Luminescence in Crystals, Methuen and Co (1963).

115. N. Robertson and L. Friedman, Phil Mag 33 753 (1976).

116. C.W. Struck and W.H. Fonger, J Lum 10 1 (1975).

117. A.P. Radlinski, Phys Stat Sol (b) 86 41 (1978).

118. S. Braun, H.G. Grimmeiss and J.W. Allen, Phys Stat Sol 14 527 (1972).

119. C. Ovren, PhD Thesis, Lund.

120. J.M. Langer, T. Langer, G.L. Pearson and B Krukowska - Fulde, Phys Stat Sol (a) 25 K61 (1974).

121. H.E. Gumlich, R.L. Pfrogner, J.C. Shaffer and F.E. Williams, J. Chem Phys 44 3929 (1966).

122. G.L. House and H.G. Drickamer, J Chem Phys 67 3230 (1977).

123. J.W. Allen and G.L. Pearson, Stanford University Technical Report No 5115-1 (1967).

124. M. Frackowiak, E. Chimczak, M. Kozielski, J. Kruszyna and A. Kuleczka, J Lum 14 243 (1976).

125. H.G. Grimmeiss, C. Ovren and J.W. Allen, J App Phys 47 1103, (1976).

126. V.L. Levshin and V.F. Tunitskaya, Opt and Spect 9 118 (1960).

127. L. Ley, R.A. Pollack, F.R. McFeely, S.P. Kowalczyk and D.A. Shirley, Phys Rev B9 600 (1974).

128. C.J. Vesely, R.L. Hengehold and D.W. Langer, Phys Rev B5 2296 (1972).

129. P.J. Dean, Topics in Applied Physics 17 ed. J.I. Pankove Springer-Verlag (1977).

130. E. Walentynowicz, E. Chimczak and W. Gordon, J Lum 17 109 (1978).

131. D.S. McClure, J Chem Phys 39 2850 (1963).

132. W. Busse, H.E. Gumlich, B. Meissner and D. Theis, J Lum 12/13 693 (1976).

133. N.A. Vlasenko, S.A. Zynio and Y.V. Koptyko, Phys Stat Sol (a) 29, 671 (1975)

134. B. Selle, Phys Stat Sol 5 649 (1964).

135. M.M. Kreitman and D.L. Barnet, J Chem Phys 43 364 (1965).

136. R.E. Behringer, J Chem Phys 29 537 (1958).

137. Y.S. Park and B.K. Shin, Topics in Applied Physics 17 ed J.I. Pankove, Springer-Verlag (1977).

138. T. Inoguchi and S. Mito, Topics in Applied Physics 17 ed J.I. Pankove, Springer-Verlag (1977).

139. J.C. Phillips, "Bands and Bands in Semiconductors" Academic Press (1973).